TÉCNICO LISBOA

Asteroseismology of a Massive Pre-White Dwarf - Structural and Evolutionary Impact of Neutrino Cooling

Fernando Fonseca Vieira de Lima

Thesis to obtain the Master of Science Degree in

Engineering Physics

Supervisors: Prof. Ilídio Pereira Lopes

Examination Committee

Chairperson: Prof. José Pizarro de Sande e Lemos
Supervisor: Prof. Ilídio Pereira Lopes
Member of the Committee: Dr. Koraljka Mužić

December 2020

Acknowledgments

I would like to start by acknowledging the person who possibly most contributed to the completion of this thesis, my supervisor prof. Ilídio Lopes, who always showed unending support and belief in me, provided invaluable insight that was crucial for the construction of this document, and most importantly, was always available at all times, whether it was work related or not. On this note, I also express my sincerest thanks to CENTRA and COSTAR, and all the people that are part of this unit and that in some way or another, gave their part in the construction of this document. I also want to mention the authors of MESA and GYRE, whose work is the entire foundation for what was done in this thesis.

I would also like to give my endless gratitude to a number of friends without whom I would never be able to accomplish all the achievements that led to this work. I want to thank them for all the wonderful experiences, past, present and surely future, and I hope they know how much I value the fact that they stuck with me.

Most importantly, I want to express my wholeheartedly gratitude to my family, for the immeasurable patience and support that they have shown me. To my grandparents, I'm eternally grateful for all the encouragement and I would like for you to know that you are the main reason for my success. Finally, a big "thank you" to my sister, for teaching me some of the most important lessons of my life, I could never learn them by myself.

Resumo

A emissão de neutrinos é o processo dominante no que toca à perda de energia em estrelas pre-anãs brancas, e apesar de haver consenso relativamente à física que está por detrás deste efeito de arrefecimento, os baixos valores de secções eficazes de interação destas partículas representam uma barreira no que toca a testar experimentalmente e corroborar as implicações deste fenómeno num laboratório terrestre.

Neste trabalho, fazemos uso de código numérico de ponta para modelar estrelas a partir da ZAMS (Sequência Principal de Idade Zero) com massas compreendidas entre $9M_{\odot}$ e $11M_{\odot}$ e com evolução até à sequência de arrefecimento das anãs brancas, obtendo também os correspondentes espetros de pulsação. Tomando atenção particular ao domínio de luminosidade compreendido entre $L/L_{\odot} = 4$ to $L/L_{\odot} = 2$, onde a emissão de neutrinos é o processo de perda de energia dominante, estudamos o impacto de diferentes taxas de emissão de neutrinos de natureza não nuclear no espetro de períodos dos modos de pulsação, bem como as consequências deste impacto na estrela a nível fenomenológico e estrutural.

Identificamos também um novo fenómeno que consiste numa deslocação do padrão da separação de período em modos com ordem radial elevada, consequência das alterações nas taxas de emissão de neutrinos, enquanto que o padrão relativo aos modos com ordem radial baixa permanece inalterado. Este resultado, bem como o estudo realizado nesta tese, representa uma ferramenta instrumental no que toca ao estudo da estrutura interna de anãs brancas pulsantes, as quais se espera serem observadas na futura missão PLATO.

Palavras Chave

Asterosismologia; Estrelas; Anã Branca; Pulsação Estelar;

Abstract

Neutrino emission is the most dominant process in what concerns energy loss for pre-white dwarf stars, and while there is consensus on the physics that is behind this cooling effect, the small interaction cross section of these particles makes it hard to experimentally test and corroborate the implications of this phenomena on a terrestrial laboratory.

We make use of state of the art numerical code to model stars beginning in the ZAMS with masses ranging from $9M_{\odot}$ to $11M_{\odot}$ and evolving up to the white dwarf cooling sequence, and obtain their correspondent asteroseismic spectrum. Taking particular attention to the luminosity range from $L/L_{\odot} = 4$ to $L/L_{\odot} = 2$, where neutrino emission is the dominant energy loss mechanism, we study the impact of different non nuclear neutrino emission rates on the period spectrum of the g-modes, as well as the consequences of this impact on the star at a chemical and structural level.

We identify a novel phenomena where a shift in the pattern of the period separation of higher order radial modes seems to take place when the neutrino emission rates are altered, whereas the pattern relative to lower order radial modes remains unchanged. This particular result, along with the study performed in this thesis, represents a powerful tool to study the internal structure of pulsating white dwarfs, expected to be observed by the forthcoming PLATO mission.

Keywords

Asteroseismology; Stars; White Dwarf; Stellar Pulsation;

Contents

List of Figures

List of Tables

Acronyms

AGB Asymptotic Giant Branch

CNO Carbon-Nitrogen-Oxygen

COROT Convection, Rotation and planetary Transits

DR2 Data Release 2

HR Hertzsprung–Russell

MESA Modules for Experiments in Stellar Astrophysics

PLATO PLAnetary Transits and Oscillations of stars

pp proton-proton

RGB Red Giant Branch

SDSS Sloan Digital Sky Survey

SGB Sub Giant Branch

WD White Dwarf

ZAMS Zero Age Main Sequence

1

Introduction

Contents

1.1 Motivation

White dwarfs are objects that represent the final evolutionary stage of most stars, and are characterized by their extremely high density and intrinsic low luminosity. Their status as the end product of most stars makes them important subjects of study and observation, since their current population contain information concerning general stellar evolution.

The discovery of white dwarfs dates back to 1914 [7], with the detection of a star located well below the main sequence in the HR diagram, characterized by a very small radius, comparable to that of the Earth, and later determined to have a mass comparable to that of the Sun. The introduction of this new spectral class of high density stars became of considerable importance, soon turning into one of the first tests of quantum theory of matter, as the high densities of these stars could only be explained by a quantum degeneracy pressure effect of the electrons in their core [8].

Nowadays, among the many utilities that come from the study of these objects, the white dwarf luminosity function [9, 10] represents one of the most important tools in what concerns not only the advances in this area [11, 12], but also contributions to several other topics such as the history of our Galaxy and certain constraints on its age [13, 14], photometric calibration [15], the theory of hot dense plasmas [16] and even the study of fundamental interactions in physics, since white dwarf stars represent quality astroparticle physics laboratories [17].

A particularly interesting trait of white dwarf evolution is the fact that as these objects cool, they cross several pulsation instability phases, one such phase corresponding to the GW Vir stage (or DOV stage). Stars at this stage have a characteristic chemical composition, lacking the typical hydrogen envelope that most white dwarfs have, and present higher temperature and luminosity than most white dwarfs, such that in this sense, they might as well be considered pre-white dwarfs.

Perhaps most importantly, these stars are known pulsating objects, presenting measurable buoyancy induced luminosity fluctuations with periods that reach up to thousands of seconds. It then becomes indispensable to approach the study of these stars with the use of asteroseismology, a recent branch of astrophysics that concerns the study of oscillatory stellar objects, providing several mathematical tools that allow for a detailed probing and analysis of the interior of stars.

To this context, one of the most interesting aspects of this GW Vir stage is that it corresponds to a very short-lived stage where the primary cooling mechanism is the emission of non nuclear neutrinos. The production of neutrinos inside stars is a well known process that may occur as a consequence of several different reactions [18, 19], and while there's consensus in what concerns the prevalence of neutrino cooling during this stage of evolution of white dwarf stars, it is a difficult task to replicate and experimentally test this phenomena in the laboratory, mainly due to the small interaction cross section of these particles [20], which in turn, makes it hard to verify certain predictions regarding their impact on the overall behaviour of this cooling stage, whether it be at a structural or at a phenomenological

level. On the other hand, asteroseismology has been a consistent tool in what concerns the study of an array of topics regarding stellar structure and evolution, and naturally encapsulates the main aspects to consider when trying to approach the subject of the impact of neutrino cooling, effectively working as a metaphorical laboratory that allows for the verification of this neutrino print.

It's also worth mentioning that calculation of neutrino emission rates in white dwarfs and pre-white dwarfs are based on the standard theory of leptonic interaction which contains several construction flaws, particularly in what concerns the inclusion of neutrinos, which are predicted to be left-handed particles with no renormalizable mass term [21]. This has since been proven incorrect with the introduction of neutrino flavor oscillation [22]. Nonetheless, stellar emission rates of these particles are computed making use of the interactions present in the standard electroweak Hamiltonian, being subject to the constraints established by this theory, and hence the measurement of the effects of altered neutrino rates and consequent neutrino interactions in these stars may represent an independent test of the coupling of neutrinos in the leptonic processes of the standard model.

1.2 Objectives

The focus of this work will be to study the impact of neutrino emission as a star evolves through the GW Vir stage. To this end, we make use of state of the art numerical models that contain detailed information regarding the structural and phenomenological properties of these type of stars, and whose neutrino emission rates we can manipulate in order to infer direct or indirect consequences of their effect.

At a first stage, we intend to study the structural ramification of altering neutrino rates, whether it be through the response of certain global quantities to different rates, or by analyzing how the chemical composition in the interior of the star behaves in these same circumstances. We then intend to inspect how the pulsation spectrum of our models is impacted by these varying rates, making use of several diagnostic quantities that concern the propagation and overall behavior of each mode.

In order to more effectively accomplish the goals of this study, we target stars with mass values which are considerably higher than the average. As mentioned above, non nuclear neutrino emission is the predominant effect in what concerns the cooling of stars at this stage of evolution, with most of the energy loss being done through the plasma-neutrino process [23], but in the case of massive stars, neutrino bremsstrahlung must also be taken into consideration [2, 24]. This attribute, along with several other important factors, make massive white dwarfs great subjects of study in what concerns the influence of neutrino emission along their evolution. In particular, mass-radius relations for massive white dwarfs seem to show a notable dependence on the neutrino luminosity [25], and even beyond that, these stars seem to be the ones which exhibit the most sensible temperature decay response to the neutrino luminosity in all the mass range of these kind of stars [1], as can be seen in figure 1.1.

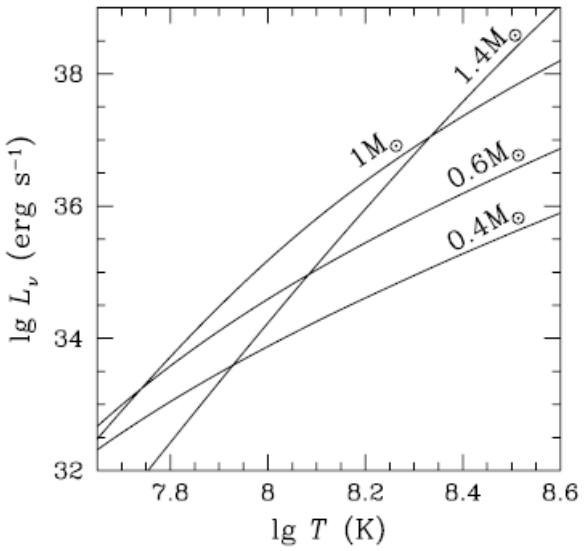

Figure 1.1: Neutrino luminosity L_ν as a function of stellar core temperature T for white dwarfs with masses $M = 0.4, 0.6, 1$ and $1.4 M_\odot$ [1]

Finally, it is important to mention that with the advent of mission PLATO [26], to be launched in 2025, the understanding of the underlying effects of certain phenomena on the measurable quantities of stars is of utmost importance, and hence, with neutrino emission being the controlling process in what concerns the cooling of stars at this stage of evolution, we intend with the work developed in this thesis to provide novel information that will contribute to the increase in documentation of these kind of stars, particularly since "PLATO 2.0 will be the very first mission to bring WD seismology in the space era, (...)" [26].

1.3 Organization of the Document

We now describe the configuration of this document. In this chapter, a brief motivation containing a small historical perspective of white dwarfs, along with the most important aspects of the stars that will be studied is presented.

In chapter 2, the theoretical basis needed for the work developed in this thesis is presented, containing the main aspects of stellar evolution that result in the formation of a white dwarf, the main processes involved in the production and emission of neutrinos inside of stars and the basic mathematical description of stellar oscillations.

In chapter 3, we present information concerning the state of the art which motivates the subject of this thesis, including some details concerning massive white dwarfs and some aspects of white dwarf asteroseismology.

In chapter 4, we give an overview of the code used in order to model the stars in study, we make an analysis of the different neutrino emission sources present and we study the impact of altering these rates on a phenomenological and structural level, as well as the influence it has on the period spectra of these models.

In chapter 5, we focus the study of the impact of these neutrino rates on the propagation of the pulsation modes inside of the star, defining an auxiliary sensitivity function to quantify the analysis. We also address a novel effect that results on a shift of the modes that are trapped as a consequence of the altered neutrino rates.

Finally, in chapter 6 we discuss our conclusions and address future prospects of this work.

2

Theoretical Background

Contents

This chapter contains the theoretical basis needed for the work present on this thesis, being divided in the three major topics that are necessary for the study being done. The first topic, present in 2.1, consists on the main aspects of stellar evolution, including all the evolutionary stages and processes that are comprised in the transition of a typical main sequence star into a white dwarf, and the subsequent cooling branch of the latter. Additionally, a brief description of the mathematical details behind the equations of stellar structure and evolution is also presented. The second topic, present in 2.2, concerns the main processes involved in the production and emission of neutrinos inside of stars. The third topic, present in 2.3, encompasses the basic mathematical description of stellar oscillations.

2.1 Stellar Evolution and White Dwarf Cooling Sequence

2.1.1 History of White Dwarf Evolution

White dwarfs are very dense stellar core remnants, presumably the final evolutionary stage of more than 97% of all stars [2]. Resulting from low- and intermediate-mass hydrogen burning stars, these objects have reached a phase of their evolutionary process in which nuclear burning has ceased to be a significant energy source. Since no other energy source of the star is relevant enough to compensate for the continuously radiated (stored) thermal energy, it will begin to cool, becoming dimmer with passing time.

In order to comprehend this evolutionary process that leads to the formation of a white dwarf, which is schematically depicted in figure 2.1 by the HR diagram of a typical $3.5M_{\odot}$ initial mass main sequence star, we must first understand the previous history of the stars that originate these remnants, starting from their Zero Age Main Sequence (ZAMS) stage and up to the white dwarf cooling branch itself.

2.1.1.A White Dwarf Progenitors

The formation of a typical main sequence star is preceded by the collapse of a gas cloud in the inter-stellar medium, with a chemical composition consisting mostly of hydrogen and helium [27], and the subsequent ignition of hydrogen nuclear burning. It is when this hydrogen burning proto-star reaches hydrostatic equilibrium that it is considered a main sequence star.

Evolution in the main sequence is very intricate, with several important aspects to consider, but in the context of this work, it is enough to mention that this stage is mostly a hydrogen burning stage, with this process happening through either the proton-proton chain (pp-chain) reaction or the CNO cycle. The first of these processes is dominant for stars with masses less than $1.3M_{\odot}$ [28], and may be summarized by the following expression:

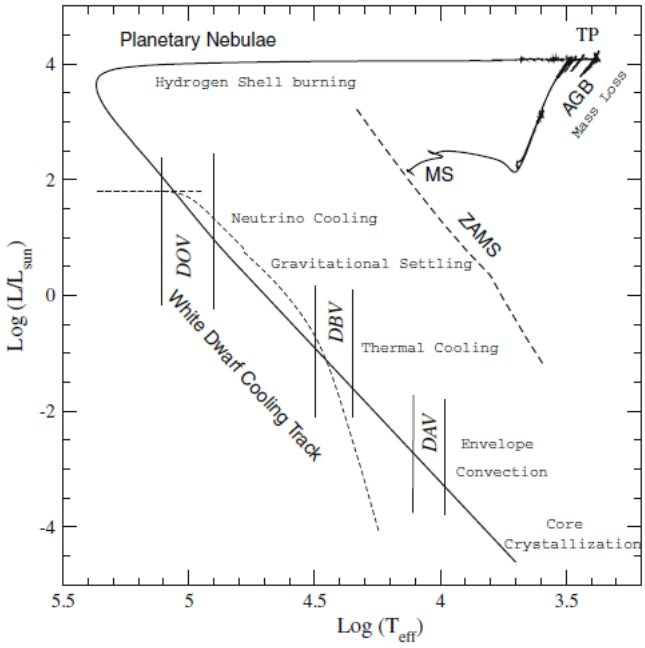

Figure 2.1: HR diagram for the evolution of a typical $3.5M_{\odot}$ star from the main sequence to the white dwarf cooling branch [2]

$$4\,{}^{1}_{1}\mathbf{H} \rightarrow {}^{4}_{2}\mathbf{He} + 2e^{+} + 2\nu_e + 2\gamma \tag{2.1}$$

Where e^{+} represents a positron, ν_e represents an electron neutrino and γ a gamma ray photon.

The CNO cycle is, in turn, dominant for stars with masses greater than $1.3M_{\odot}$ [28], and is a catalytic cycle composed of several reactions, all with the following end result:

$$4\,{}^{1}_{1}\mathbf{H} + 2e^{-} \rightarrow {}^{4}_{2}\mathbf{He} + 2\nu_e + 7\gamma \tag{2.2}$$

Where e^{-} is an electron. A star will remain on the main sequence while there is still hydrogen present in its core, so that nuclear burning is active. Once the hydrogen is depleted, the star will proceed to the next evolutionary stage, which in the case of the stars that we're studying, is usually the Sub Giant Branch (SGB) and Red Giant Branch (RGB) sequence. This is a consequence of the contraction of the core, triggered by the lack of hydrogen burning, which causes the release of gravitational energy to the outer regions, increasing the temperature of the shell. This in turn excites nuclear reactions in this region, increasing the luminosity and consequently the radiation pressure, which causes the envelope to expand and cool, meaning that the effective temperature of the star drops and the star enters the SGB. The expansion and drop in temperature of the envelope is accompanied by an increase of the opacity of the photosphere due to the presence of H^{-} ions. This in turn leads to the formation of a convective region near the surface, marking the transition to the RGB. Further detail about this description can be

found in [27].

Similarly to the main sequence, the RGB is a complex evolutionary stage with many important implications, but the most relevant event, in the scope of this work, happening at this stage is the ignition of helium burning in the core. In short, this event occurs when the growing temperature of the core reaches the required values to trigger the triple-alpha (3-α) process, originating carbon through the combination of the following reactions [28]:

$$\begin{aligned} {}^{4}_{2}\mathbf{He} + {}^{4}_{2}\mathbf{He} &\rightarrow {}^{8}_{4}\mathbf{Be} \\ {}^{8}_{4}\mathbf{Be} + {}^{4}_{2}\mathbf{He} &\rightarrow {}^{12}_{6}\mathbf{C} + 2\gamma \end{aligned} \tag{2.3}$$

Additionally, oxygen may also be created as a side effect through the following reaction:

$${}^{12}_{6}\mathbf{C} + {}^{4}_{2}\mathbf{He} \rightarrow {}^{16}_{8}\mathbf{O} + \gamma \tag{2.4}$$

It is then at this stage that the Carbon/Oxygen (C/O) composition, usually present in the core of white dwarfs, is built. It is then expected that a similar situation to that of the ending of the main sequence stage occurs, since helium burning is bound to cease. When this happens, the gravitational energy emitted from the core ignites the neighboring helium shell and the star enters the Asymptotic Giant Branch (AGB). Eventually, the outer hydrogen shell is ignited as well, while the helium shell falls off in what concerns energy output, but since the burning of the hydrogen of the outer shell results in helium that is deposited inwards, the helium shell will periodically reignite and generate intermittent helium shell flashes, also known as thermal pulses. In short, the net effect of these thermal pulses is an outward displacement of the outer shells and considerable mass loss, consequence of the ejection of most of the H-rich envelope, which can completely vanish if the star experiences some late thermal pulses as it is departing from the AGB [29].

When the mass fraction of the outer layers starts approaching certain lower limit values ($\sim 10^{-3} M_{\odot}$), a higher exposition of the core leads to a rapid increase in temperature at approximately constant luminosity, positioning the star in the planetary nebulae domain. Finally, at even lower mass fraction values of the outer envelope ($\sim 10^{-4} M_{\odot}$), nuclear energy generation becomes essentially null, and the star enters a phase of consistently decreasing luminosity with time, where it is effectively classified as pre-white dwarf [2].

2.1.1.B Neutrino Cooling and White Dwarf Cooling Branch

At this point, stars may already be treated as white dwarfs from a spectroscopic point of view. This means that they can be classified as DA and non-DA white dwarfs, depending on the main constituent

of their outer layers. DA white dwarfs represent the most abundant class, containing $\approx 85\%$ of all white dwarf stars [30], and it corresponds to such stars with hydrogen rich atmospheres, while non-DA white dwarfs correspond to these stars with hydrogen deficient atmospheres. This last class may be further subdivided according to their spectra and effective temperature, with DO white dwarfs presenting strong lines of HeII and with $45000K \leq T_{eff} \leq 200000K$, DB white dwarfs presenting strong HeI lines and with $11000K \leq T_{eff} \leq 30000K$ and DC, DQ and DZ presenting traces of carbon and metal in their spectra, and with $T_{eff} < 11000K$.

As the star is transitioning to the white dwarf cooling branch, reactions due to the CNO cycle are still occurring and they represent the largest contribution to the luminosity of the star. When nuclear reactions cease, the evolution is controlled by non nuclear neutrino losses, with these being created in the hotter, deep regions of the star, and due to their extremely small cross section, these leave the star without interacting. At this point, neutrino luminosity is up to five times the surface luminosity, and as a consequence, this phase has a small timescale in comparison with the timescale of the cooling branch. It is also in this stage that DOV and DBV (where the first two letters refer to the spectroscopic classification, and the V stands for "variable") are inserted, as can be seen by the thresholds presented in the cooling branch of the HR diagram present in figure 2.1. The processes responsible for the production of neutrinos are discussed in 2.2, but it is worth mentioning that plasma-neutrinos represent the main energy loss, with the possibility of a considerable contribution of neutrino bremsstrahlung at later stages of this neutrino dominated phase [31], noting that this last process implies a significant impact in the cooling of massive white dwarfs [24]. The majority of the work contained in this thesis will be focused on this stage of evolution, but for the sake of completeness, we further present a brief description of the events that follow after this neutrino dominated phase.

When neutrino rates are low enough so that the neutrino luminosity L_ν is negligible when compared with the surface luminosity L_{sur} (or total luminosity as depicted in HR diagrams), the released gravitational energy due to gravitational settling becomes relevant with $L_{sur} \approx L_{grav}$ and the star enters a stage where it satisfies most of the conditions established by the well known Mestel model [32]. In short, these conditions are the consideration of an isothermal core, the assumption that the energy transported throughout the envelope is done entirely by radiative processes and the usage of a non-degenerate, ideal gas, equation of state to describe said envelope. The use of these conditions to derive the expression that describes the cooling of the star at this stage, and the derivation itself, can be found in Mestel's original article [32], with the expression as follows:

$$t_{cool} = \frac{10^8}{A}\left(\frac{M/M_\odot}{L/L_\odot}\right)^{5/7} \tag{2.5}$$

Where A is the atomic weight of the ion species responsible for the luminosity process. This cooling time defined as $t_{cool} = t - t_0$, where t_0 is the time at which the star enters the white dwarf cooling branch,

may be computed at any present time t since both M and L are time dependent functions.

At lower luminosity values, around $log(L/L_{\odot}) \approx -3$, some conditions needed for the validity of Mestel's model fall off, namely the condition of energy transport in the outer layers, which is no longer exclusively done through radiative processes because of the setting of envelope convection, which will alter the rates at which energy flows from the inner regions to outer space [33]. Additionally, the consideration of Coulomb interactions in the core also become relevant in what concerns the energy output of the star [34], with the Coulomb coupling parameter $\Gamma = (Ze)^2/ak_BT$, where a is the interionic separation and k_B is the Boltzmann constant, being inversely proportional to temperature. Around this time, this coupling constant takes the value $\Gamma \approx 180$, which corresponds to the case where the short-range correlations experienced by the ions are so strong, that these begin to form a lattice structure, or in other words crystallize, suffering a first-order phase transition which is accompanied with a release of latent heat, enough to significantly alter the cooling rate of the star.

2.1.2 Equations of Stellar Evolution

The description that was made above presents an overview on the processes that occur as a star is formed and evolves, and allows for a qualitative understanding on the details that go into the history of a white dwarf. This evolution, however, is dictated by several physical principles that can be quantitatively assessed, and further organized into a set comprised of a number of equations containing this same number of unknown variables.

We then have a complete set of partial differential equations, determined under the assumption of spherical symmetry, known as the equations of stellar evolution, whose derivation can be found in [35]. The first of these equations concerns the mass conservation of a spherical shell, detailing a relation between its radius r and its mass m.

$$\frac{\partial r}{\partial m} = \frac{1}{4\pi r^2 \rho} \tag{2.6}$$

Where ρ is the density of the shell.

The second equation is also a conservation equation, this being the conservation of momentum. It serves as an hydrodynamic condition that defines the pressure in each layer of the star.

$$\frac{1}{4\pi r^2}\frac{\partial^2 r}{\partial t^2} = -\frac{\partial P}{\partial m} - \frac{Gm}{4\pi r^4} \tag{2.7}$$

In this equation, P is the pressure and G is the gravitational constant. An important form taken by this equation is that of the hydrostatic equilibrium condition, which is obtained when $\partial^2 r/\partial t^2 = 0$, meaning that a balance between pressure and gravity is obtained per unit volume of each shell.

Also part of the set, we have the equation of energy transport, which as the name suggests, conveys

information on how energy is transported at each layer of the star.

$$\frac{\partial T}{\partial m} = -\frac{GmT}{4\pi r^4 P}\nabla \tag{2.8}$$

Where T is the temperature and $\nabla \equiv \partial \ln T / \partial \ln P$ is a quantity whose value depends on how energy is transported. In the case where this happens through radiative processes, this expression takes the following form:

$$\nabla = \nabla_{rad} = \frac{3}{16\pi acG}\frac{\kappa l P}{mT^4} \tag{2.9}$$

Where $a = 7.57 \times 10^{-15}\ erg\ cm^{-3}\ K^{-4}$ is the radiation density constant that relates the energy density with temperature, c is the speed of light constant, l is the local luminosity and κ is the mean absorption coefficient that constrains the mean free path of a photon $l_{ph} = 1/(\kappa\rho)$ in the interior of the star.

An additional subset of equations that are part of our larger set is that of the chemical composition equations, which is comprised of I equations, each relative to one of the I nuclei that constitute the star. Each of these equations describes the evolution of the mass fraction χ_i of the i'th nucleus, taking the following form:

$$\frac{\partial \chi_i}{\partial t} = \frac{m_i}{\rho}\left(\sum_j r_{ji} - \sum_k r_{ik}\right) \qquad i = 1, ..., I \tag{2.10}$$

Where m_i is the mass of the i'th nucleus and r_{ji} is the number of reactions per unit time and unit volume that transform nuclei from type j to nuclei from type i.

Finally, and of most importance due to the context of this work, is the conservation of energy equation, which defines the local luminosity of a given shell:

$$\frac{\partial l}{\partial m} = \epsilon_n - \epsilon_\nu - \frac{\partial T}{\partial t} + \frac{\delta}{\rho}\frac{\partial P}{\partial t} \tag{2.11}$$

With $\delta \equiv (\partial \ln \rho / \partial \ln T)_P$, with the subscript meaning that the quantity is taken at constant pressure, and ϵ_n is the nuclear energy release per unit mass per second. The ϵ_ν term is of special interest in what concerns the rest of this work, since it represents the amount of energy released by unit mass per second due to neutrino emission. There are two types of neutrinos that contribute to this, depending on if they were created as a consequence of nuclear reactions or not. For this reason, we label the energy lost due to nuclear neutrinos as ϵ_{ν_n} and the energy due to non nuclear neutrinos as $\epsilon_{\widetilde{\nu}}$, such that:

$$\epsilon_\nu = \epsilon_{\nu_n} + \epsilon_{\widetilde{\nu}} \tag{2.12}$$

As mentioned previously, it is the process of non nuclear neutrino emission that dominates the cooling of stars during this DOV stage, and as can be seen by equation 2.11, this has a direct impact on the structure and evolution of the star, and hence the process that goes into the derivation of these emission rates represents a crucial point in the description of the energy reservoir of the star at this stage, seeing that changes in these rates represent differing results in what concerns the state of the star.

Equations 2.8 - 2.11 represent the equations of stellar evolution, which correspond to a complete set of partial differential equations that may be numerically solved, at any time, given the appropriate boundary conditions. The construction of these conditions is dependent on the model that is intended, and the process that goes into the formulation of these can be found in [35].

2.1.2.A MESA Evolution Code

The numerical process that is behind the solution of these equations may be developed in numerous ways given the existence of several state of the art stellar evolution codes that integrate this procedure. This in turn allows for the modelling of stars, as well as access to the global quantities that constitute this model, along several different evolutionary stages.

To this end, we make use of the MESA software [36], an open-source 1D stellar evolution package, composed of different modules constructed as Fortran 95 libraries with defined user interfaces to simplify independent use. In addition to solving the coupled equations of structure and composition which comprise the set of equations of stellar evolution, MESA contains modules that provide equation of state, opacities, nuclear reaction rates, element diffusion data and atmosphere boundary conditions, and allow for stellar modelling in a wide range of mass and at several stages of evolution, including tracks ranging from the ZAMS to the white dwarf branch, as is the case in this thesis. The main specifications that go into the modelling of the stars used in this work are described in 4.1.

2.2 Neutrino Processes in Stellar Interiors

Neutrino production inside stellar interiors is a known phenomena that may occur due to several different processes [18, 19] and results in the emission of these particles, which may represent a relevant energy loss in what concerns the energy balance of stars. Such is the case with white dwarfs, whose typical radii are far shorter than the mean free path of neutrinos, making it so that this could represent a source of energy loss during evolution.

There are several neutrino production processes, with them being divided into two categories, the first being ordinary beta processes, which are essentially processes where electrons or positrons are either captured or emitted by nucleons or nuclei. Some processes that fall in this category are interactions involving nuclei, such as electron decay, positron decay and electron capture; interactions with nucleons,

such as electron capture on free protons and positron capture on free neutrons; and the Urca process [37]. Relevant for this work, and containing some of the processes that we will cover more carefully are the leptonic processes. There are several processes that belong to this category, but only the ones that are prevalent during the pre-white dwarf neutrino cooling phase will be covered.

2.2.1 Photoneutrinos

This process is a consequence of Compton scattering, where the outgoing photon is replaced by a neutrino-antineutrino pair. This process is given by:

$$\gamma + e \rightarrow e + \nu + \bar{\nu} \tag{2.13}$$

We will follow the description of electroweak theory in order to compute the energy rate of this process in a completely ionized gas with temperature T and density ρ. To this end, we make use of the lowest order Feynman diagrams for this process, present in figure 2.2.

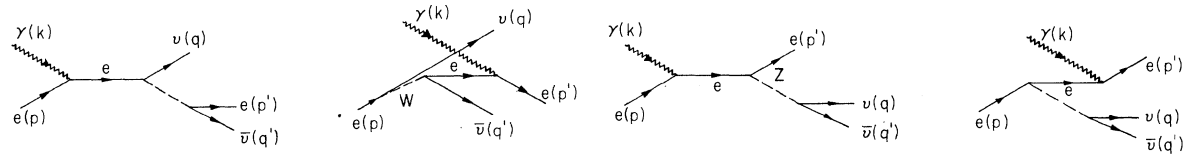

Figure 2.2: Lowest order Feynman diagrams for the photoneutrino production process [3]

Each of these diagrams contributes with a factor to the total matrix element for this process, which can be written as [3]:

$$\begin{aligned} M = &- \frac{ieg^2}{8m_W^2}\bar{u}_e(p')\gamma^a(C_V - C_A\gamma_5)\frac{\not{p} + \not{k} + m_e}{2p\cdot k + \omega_0^2}\not{\epsilon}u_e(p)\bar{u}_\nu(q)\gamma_a(1-\gamma^5)v_{\bar{\nu}}(q') \\ &- \frac{ieg^2}{8m_W^2}\bar{u}_e(p')\not{\epsilon}\frac{\not{p}' - \not{k} + m_e}{-2p'\cdot k + \omega_0^2}\gamma^a(C_V - C_A\gamma_5)u_e(p)\bar{u}_\nu(q)\gamma_a(1-\gamma^5)v_{\bar{\nu}}(q') \end{aligned} \tag{2.14}$$

With:

$$C_A = 1 - \frac{g'^2 + g^2}{2m_Z^2}\frac{m_W^2}{g^2} \qquad\qquad C_V = 1 + \frac{3g'^2 - g^2}{2m_Z^2}\frac{m_W^2}{g^2} \tag{2.15}$$

In these expressions, both g and g' are coupling constants, p, p', q, q' and k are the incoming electron, outgoing electron, outgoing neutrino, outgoing antineutrino and incoming photon momenta, respectively. u_e and $\bar{u}_e$ are the incoming and outgoing electron spinors, $\bar{u}_\nu$ and $v_{\bar{\nu}}$ are the outgoing neutrino and

antineutrino spinors. γ^a with $a \in \{0,1,2,3\}$ are the Dirac gamma matrices and γ_5 is the fifth gamma matrix. ω_0 is the oscillation frequency of the gas and m_e, m_W and m_Z are the electron, W-boson and Z-boson masses respectively.

The interaction cross section σ of this process can now be obtained by summing and averaging over the electron and neutrino spins, integrating over the neutrino momenta, and finally summing over the polarization of the photon, while the energy rate per unit volume and unit time of the process Q_{photo} can be obtained by integrating, over the number density of the particles involved, the product of this cross section with the energy of the neutrino pair. These computations, while straightforward, are very extensive, and so we refer to [19], where the main steps of these computations are described, with the end result:

$$Q_{photo} = \frac{1}{2}\left[(C_V^2 + C_A^2) + n(C_V'^2 + C_A'^2)\right] Q_{photo}^{+} - \frac{1}{2}\left[(C_V^2 - C_A^2) + n(C_V'^2 - C_A'^2)\right] Q_{photo}^{-} \tag{2.16}$$

Where n is the number of neutrino flavours other than the electron neutrinos, $C_A' = 1 - C_A$ and $C_V' = 1 - C_V$, and Q_{photo}^{+} and Q_{photo}^{-} correspond to the numerical energy rates relative to the process triggered by an electron or a positron respectively, present in [24].

2.2.2 Plasma Neutrinos

This process occurs when a photon, referred to as a plasmon in this situation, propagating inside an electron gas, spontaneously transforms into a neutrino-antineutrino pair. This process is given by:

$$plasmon \rightarrow \nu + \bar{\nu} \tag{2.17}$$

Following the same procedure as in the previous section, we present the lowest order Feynman diagrams for the decay of a plasmon in figure 2.3.

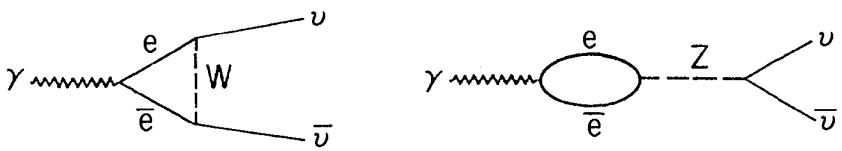

Figure 2.3: Lowest order Feynman diagrams for the decay of a plasmon [3]

The computation of the matrix element correspondent to these diagrams is not as straightforward as it was in the previous case, since it involves the computation of the Green's function for the propagation of an electron in a sea of particles, as well as the consideration of both longitudinal and transverse components of the vector potential of the plasmon. The mathematical details involved in this procedure

are detailed in [3, 38], and the resultant energy rate is, as presented in [24]:

$$Q_{plasma} = (C_V^2 + nC_V'^2)Q_V \tag{2.18}$$

With:

$$Q_V = Q_L + Q_T \tag{2.19}$$

Where Q_L and Q_T correspond to the numerical energy rates relative to the longitudinal and transverse components contribution respectively, present in [39].

2.2.3 Bremsstrahlung Neutrinos

This process refers to a modification of the regular bremsstrahlung process and consists on the braking or acceleration of charged particles in the interior of a star, resulting in the emission of a neutrino-antineutrino pair instead of a photon. In a white dwarf, where the charged particles that generate this process are electrons, this process is given by:

$$e^- + (Z, A) \rightarrow e^- + (Z, A) + \nu + \bar{\nu} \tag{2.20}$$

Where (Z, A) corresponds to a fixed nucleus that is responsible for the generation of the Coulomb field that is responsible for braking or accelerating the electron. The Feynman diagrams describing this process are represented in figure 2.4, while the total matrix element relative to these is [4]:

$$M = -\frac{Ze^2G_f}{4}\frac{f(|\vec{k}|)^2}{[|\vec{k}|^2\epsilon(|\vec{k}|)]^2}\bar{u}_e(p')\gamma^a(C_V - C_A\gamma^5)\frac{1}{\not{p} + \not{k} - m_e}\gamma_0 u_e(p)\bar{u}_\nu(q)\gamma_a(1-\gamma^5)v_{\bar{\nu}}(q') \tag{2.21}$$

$$-\frac{Ze^2G_f}{4}\frac{f(|\vec{k}|)^2}{[|\vec{k}|^2\epsilon(|\vec{k}|)]^2}\bar{u}_e(p')\gamma_0\frac{1}{\not{p} - \not{k} - m_e}\gamma^a(C_V - C_A\gamma^5)u_e(p)\bar{u}_\nu(q)\gamma_a(1-\gamma^5)v_{\bar{\nu}}(q') \tag{2.22}$$

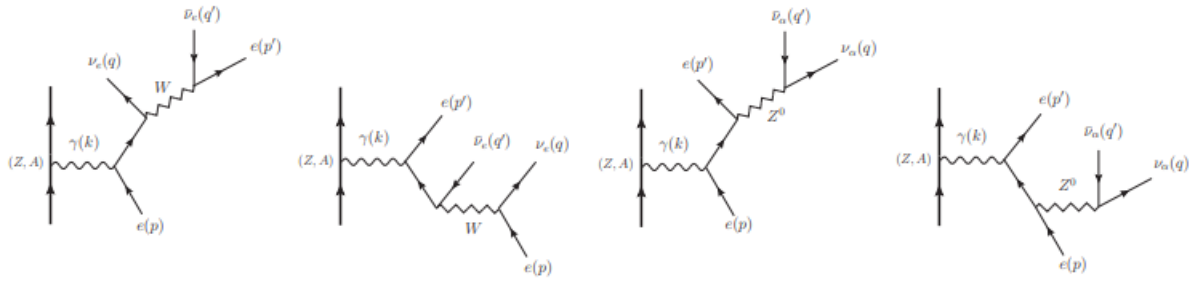

Figure 2.4: Lowest order Feynman diagrams for the neutrino bremsstrahlung effect [4]

In equation 2.22, $\epsilon(|\vec{k}|)$ is the static dielectric function that accounts for electron screening, $f(|\vec{k}|)$ is the form factor corresponding to a uniform charge distribution within the charge radius r_c for the nucleus (Z, A) and G_f is the Fermi coupling constant.

Once again, the procedure for obtaining the energy rate is the same as the one used in the previous subsections, the mathematical details of this procedure being described in [40], resulting in the following expression:

$$Q_{brem} = a_{en}(Z^2/A)\rho\Big\{\frac{1}{2}\left[(C_V^2 + C_A^2) + n({C'_V}^2 + {C'_A}^2)F_{gas} - \frac{1}{2}\left[(C_V^2 - C_A^2) + n({C'_V}^2 - {C'_A}^2)\right]G_{gas}\Big\} \tag{2.23}$$

Where a_{en}, F_{gas} and G_{gas} are temperature dependent numerical values, whose expressions are present in [24].

2.3 Stellar Pulsation Theory

Variable stars are, as the name suggests, stars whose brightness as measured on Earth fluctuates with time, either due to a non-constant luminosity of the star itself - Intrinsic variable star; or due to changes in the amount of light that reaches Earth, consequence of external objects such as nearby orbiting companions in case of binary systems - Extrinsic variable stars.

In the case of intrinsic variables, many factors may contribute to the variation in their luminosity, and further classifications based on the underlying effect exist. One such example of this are the pulsating intrinsic variables, whose name comes from the fact that their radius undergoes alternating expansions and contractions, caused due to a non-equilibrium state between pressure and gravity in the star [41].

2.3.1 Linear Adiabatic Equations of Stellar Pulsation

In order to formally assess these stellar pulsations in a theoretical fashion, certain considerations are needed, with the most important being the assumption that the star is a continuous spherical gas cloud, and its properties may be specified as functions of position $\vec{r}$ and time t. When describing the properties of the star, $\vec{r}$ may refer to a an independent quantity as observed from a stationary frame, or it can refer to a time dependent quantity with a reference value $\vec{r}_0$, described in a frame where which follows the motion, so that $\vec{r} \equiv \vec{r}(\vec{r}_0, t)$. These descriptions are known as the Eulerian and Lagrangian descriptions respectively, and are related to each other when analyzing the time derivative of a certain quantity A, through the following expression:

$$\frac{dA}{dt} = \left(\frac{\partial A}{\partial t}\right)_{\vec{r}} + \vec{\nabla} A \cdot \frac{d\vec{r}}{dt} = \left(\frac{\partial A}{\partial t}\right) + \vec{v} \cdot \vec{\nabla} A \tag{2.24}$$

Where d/dt refers to the time derivative in the frame following the motion, while $\partial/\partial t$ is the time derivative at a fixed point.

Additionally, the star must obey certain fundamental equations. The first equation is the continuity equation, which states that the rate of a change in mass of a certain volume of the star must equal the mass flux across that volume:

$$\frac{\partial \rho}{\partial t} + \vec{\nabla} \cdot (\rho \vec{v}) = 0 \tag{2.25}$$

The second equation is the momentum conservation equation, which describes the motion of the object, taking into account the forces acting it:

$$\rho \frac{d\vec{v}}{dt} = -\vec{\nabla} p + \rho \vec{f} \tag{2.26}$$

Where p is the pressure on the surface of the body and $\vec{f}$ represents any other external forces, per unit mass. One such force that must be considered is the force per unit mass from gravity, given by $\vec{g} = -\vec{\nabla}\Phi$, written as the gradient of the gravitational potential Φ. This potential must satisfy the third equation of the set, this being the Poisson equation:

$$\nabla^2 \Phi = 4\pi G \rho \tag{2.27}$$

Finally, the last equation contains the information regarding the energy balance of the gas, which must follow the first law of thermodynamics, and can be written as:

$$\frac{dq}{dt} = \frac{dE}{dt} + \frac{p}{\rho^2}\frac{d\rho}{dt} = \frac{1}{\rho(\Gamma_3 - 1)}\left(\frac{dp}{dt} - \frac{\Gamma_1 p}{\rho}\frac{d\rho}{dt}\right) \tag{2.28}$$

With the following adiabatic exponents:

$$\Gamma_1 = \left(\frac{\partial \ln p}{\partial \ln \rho}\right)_{ad} \qquad \Gamma_3 - 1 = \left(\frac{\partial \ln T}{\partial \ln \rho}\right)_{ad} \tag{2.29}$$

The information concerning the last step shown in equation 2.28 with the addition of the adiabatic exponents can be found in [42].

In order to linearize this set of equations, a perturbative analysis is employed, where the relevant quantities in the equations are perturbed around their equilibrium position. This may be done using the Eulerian description, where a perturbed scalar quantity f is written as:

$$f(\vec{r},t) = f_0(\vec{r}) + f'(\vec{r},t) \tag{2.30}$$

Where f' is the function that describes the Eulerian perturbation.

This can also be done making use of the Lagrangian description, noting that a perturbation in the path of the particle that is being followed reads as $\vec{r} = \vec{r}_0 + \delta\vec{r}$, hence $\vec{v} = \partial\delta\vec{r}/\partial t$. In this situation, we write the perturbation as:

$$f(\vec{r} + \delta\vec{r}) = f_0(\vec{r}_0) + \delta f(\vec{r}) \tag{2.31}$$

Where δf is the function that describes the Lagrangian perturbation.

Both perturbations are then related through the following expression:

$$\delta f(\vec{r}) = f'(\vec{r}_0) + \delta\vec{r}\cdot\vec{\nabla} f_0 \tag{2.32}$$

The linearization of the set of equations can then be done by replacing ρ, p, Φ and v by their appropriate perturbed forms, neglecting any terms that are higher than first order in the perturbations. Additionally, we employ the well known adiabatic approximation [43], which further simplifies the expression 2.28 by allowing to set $dq/dt = 0$. This leaves us with the linearized set:

$$\rho' + \vec{\nabla}\cdot(\rho_0\delta\vec{r}) = 0 \tag{2.33}$$

$$\rho_0\frac{d^2\delta\vec{r}}{dt^2} = -\vec{\nabla}p' + \rho_0\vec{g}' + \rho'\vec{g}_0 \tag{2.34}$$

$$\nabla^2\Phi' = 4\pi G\rho' \tag{2.35}$$

$$p' + \delta\vec{r}\cdot\vec{\nabla}p_0 = \frac{\Gamma_{1,0}p_0}{\rho_0}(\rho' + \delta\vec{r}\cdot\vec{\nabla}\rho_0) \tag{2.36}$$

It's important to note that this linearization is done considering a spherically symmetric equilibrium, and for this reason, it is adequate to specify the equations in a spherical coordinate system (r,θ,ϕ). In these coordinates, the displacement $\delta\vec{r}$ is written as:

$$\delta\vec{r} = \xi_r\vec{e}_r + \xi_\theta\vec{e}_\theta + \xi_\phi\vec{e}_\phi = \xi_r\vec{e}_r + \vec{\xi}_h \tag{2.37}$$

Additionally, the symmetry of the equilibrium implies that it is not dependent on θ and ϕ, and hence the solution is separable in these coordinates, presenting a radial component $\widetilde{F}$, and an angular component

$f(\theta, \phi)$, which, through some manipulation of the equations, and considering a time dependence of $e^{-i\omega t}$, can be shown to require the form:

$$F(r, \theta, \phi, t) = \widetilde{F}(r) f(\theta, \phi) e^{-i\omega t} = \sqrt{4\pi} R(r) (-1)^m c_{l,m} P_l^m(\cos\theta) e^{im\phi} e^{-i\omega t}$$
$$= \sqrt{4\pi} R(r) Y_l^m(\theta, \phi) e^{-i\omega t} \tag{2.38}$$

Here, Y_l^m is a spherical harmonic function, with angular degree l and azimuthal order m, and $c_{l,m}$ is a normalization factor, dependent on these quantities. Using this ansatz on our set of equations, and with some further extensive manipulation [43], we can rewrite them, now as differential equations for the amplitude functions of the perturbations, which are labeled, for consistency, as the primed variables in the equations.

The adiabatic condition 2.36, used for the simplification of the other equations, is rewritten as:

$$\rho' = \frac{\rho}{\Gamma_1 p} p' + \rho \xi_r \left(\frac{1}{\Gamma_1 p} \frac{dp}{dr} - \frac{1}{\rho} \frac{d\rho}{dr} \right) \tag{2.39}$$

As for equations 2.33-2.35, these become:

$$\frac{d\xi_r}{dr} = -\left(\frac{2}{r} + \frac{1}{\Gamma_1 p} \frac{dp}{dr} \right) \xi_r + \frac{1}{\rho c^2} \left(\frac{L_l^2}{\omega^2} - 1 \right) p' + \frac{l(l+1)}{\omega^2 r^2} \Phi' \tag{2.40}$$

$$\frac{dp'}{dr} = \rho(\omega^2 - N^2) \xi_r + \frac{1}{\Gamma_1 p} \frac{dp}{dr} p' - \rho \frac{d\Phi'}{dr} \tag{2.41}$$

$$\frac{1}{r^2} \frac{d}{dr} \left(r^2 \frac{d\Phi'}{dr} \right) = 4\pi G \left(\frac{p'}{c^2} + \frac{\rho \xi_r}{g} N^2 \right) + \frac{l(l+1)}{r^2} \Phi' \tag{2.42}$$

Where $c^2 = \Gamma_1 p / \rho$. Additionally, two other important quantities are defined, with:

$$N^2 = g \left(\frac{1}{\Gamma_1 p} \frac{dp}{dr} - \frac{1}{\rho} \frac{d\rho}{dr} \right) \tag{2.43}$$

This quantity is known as the Brunt-Väisälä frequency, and it is the relevant quantity in what concerns the spectrum of low frequency modes excited by buoyancy, as will be seen further.

Furthermore:

$$L_l^2 = l(l+1) \frac{c_s^2}{r^2} \tag{2.44}$$

This is the Lamb frequency, and is the quantity that governs the spectrum of high frequency modes, excited by pressure.

These equations, 2.40-2.42, form a fourth-order system of ordinary differential equations, with the

four dependent variables ξ_r, p', Φ' and $d\Phi'/dr$, thus constituting a complete set of differential equations that can be solved with the appropriate boundary conditions, which may be found, for instance, in [44], known as the linear adiabatic equations of stellar pulsation.

2.3.2 Asymptotic Theory and Cowling Approximation

One very useful approximation that can be used to simplify our set of linear adiabatic equations of stellar pulsation, used extensively in order to analyse the behavior of the oscillations, is known as the Cowling approximation [45], and it essentially consists on neglecting the perturbation of the gravitational potential, such that $\Phi' = 0$. The mathematical details that are behind the validity of this approximation can be found, for example, in [46].

With the use of this approximation, the order of the equation system of stellar oscillations is reduced by two, and due to the form of our newer system, some properties of the solutions that represent the pulsations can be inferred. With the additional consideration of high radial order modes, i.e. $k >> l$ where k is the radial order, our original set of equations is reduced to:

$$\frac{d\xi_r}{dr} = \frac{1}{\rho c^2}\left(\frac{L_l^2}{\omega^2} - 1\right) p' \tag{2.45}$$

$$\frac{dp'}{dr} = \rho(\omega^2 - N^2)\xi_r \tag{2.46}$$

Which can be further combined into a single second-order differential equation for ξ_r:

$$\frac{d^2\xi_r}{dr^2} = -K(r)^2\xi_r \tag{2.47}$$

Where:

$$K(r)^2 = \frac{\omega^2}{c^2}\left(\frac{N^2}{\omega^2} - 1\right)\left(\frac{L_l^2}{\omega^2} - 1\right) \tag{2.48}$$

By looking at the form of 2.47, we can see that the behavior of ξ_r depends on the sign of the squared wavenumber K^2, since the expression of the solution will either be, approximately, an oscillatory sinusoidal function if $K^2 > 0$, meaning that the wavenumber K is a real number, or an exponentially decreasing function of r if $K^2 < 0$, meaning that K is a purely imaginary number.

In order for the wavenumber to be real, we can define four inequalities, $\omega^2 > N^2, L_l^2$ and $\omega^2 < N^2, L_l^2$. Both these inequalities define two regions of propagation inside the star, also known as resonant cavities, which are called the p-region (associated with the first inequality) and the g-region (associated with the second inequality). If none of the inequalities is respected, then K is a purely imaginary number, meaning that the perturbation is in fact an evanescent wave whose amplitude decreases exponentially

along its path of propagation.

As the name of these cavities suggests, the p-region corresponds to the region of the star where acoustic waves propagate, leading to the formation of p-modes (pressure modes), these being higher frequency modes which are maintained as a consequence of pressure gradients working as restoring forces, and the g-region corresponds to the region where gravity waves propagate, leading to the formation of g-modes (gravity modes), with buoyancy serving as the restoring force in this case. Since these regions are dependent on the r coordinate, it is possible to admit situations where a wave of a certain frequency may propagate in the g-region at a certain radial domain of the star (for instance, the core), while it propagates in the p-region in another zone (for instance, the outer layers closer to the surface), which indicates that it contains a mixed character in what concerns the force that is responsible for its propagation, generating what is called a mixed mode. In order to provide a better insight into the propagation of these perturbations along a star, propagation diagrams are usually sketched, in which both N^2 and L_l^2 are plotted against a typical global quantity such as radius or mass (or a function of these), making it possible to visualize the regions of interest. Examples of typical propagation diagrams are presented in figure 2.5 [2]:

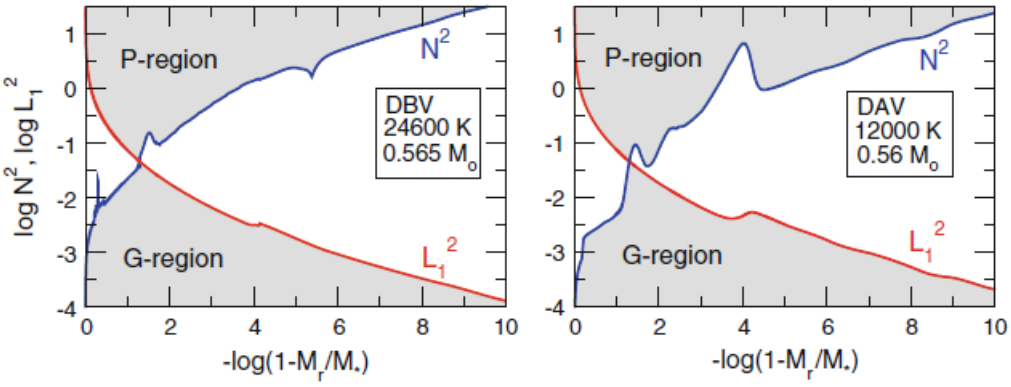

Figure 2.5: Propagation diagrams representative of a DBV star (left) and a DAV star (right) [2]

2.3.3 Dziembowski Variables

There are some helpful quantities of interest in regards to the study of the behavior of pulsation modes inside of the star if we consider a certain set of variables, known as the Dziembowski variables [47], when defining the equations of stellar pulsation.

$$y_1 = \frac{\xi_r}{r} \qquad y_2 = \frac{1}{gr}\left(\frac{p}{\rho} + \Phi'\right)$$
$$y_3 = \frac{1}{gr}\Phi' \qquad y_4 = \frac{1}{g}\frac{d\Phi'}{dr} \tag{2.49}$$

With the additional definition of a dimensionless frequency, as a function of the mode frequency σ_k:

$$\omega_k^2 = \frac{R^{*3}}{GM^*}\sigma_k^2 \tag{2.50}$$

If we now make use of equations 2.33-2.35 and the adiabatic condition 2.39, defining $x = r/R^*$ where R^* is the radius of the star, and once again considering perturbations of the form 2.38, we can write the following set of equations:

$$x\frac{dy_1}{dx} = (V_g - 3)y_1 + \left[\frac{l(l+1)}{C_1\omega^2} - V_g\right] y_2 + V_g y_3 \tag{2.51}$$

$$x\frac{dy_2}{dx} = (C_1\omega^2 - A^*)y_1 + (A^* - U + 1)y_2 - A^* y_3 \tag{2.52}$$

$$x\frac{dy_3}{dx} = (1 - U)y_3 + y_4 \tag{2.53}$$

$$x\frac{dy_4}{dx} = UA^* y_1 + UV_g y_2 + [l(l+1) - UV_g]\, y_3 - U y_4 \tag{2.54}$$

Where the following dimensionless coefficients were defined:

$$V_g = \frac{gr}{c^2} \qquad U = \frac{4\pi\rho r^3}{M_r}$$
$$C_1 = \left(\frac{r}{R^*}\right)^3 \left(\frac{M^*}{M_r}\right) \qquad A^* = \frac{r}{g}N^2 \tag{2.55}$$

Equations 2.51-2.52 represent an alternative fourth-order set of equations for linear adiabatic stellar oscillations, which is usually used due to the simplicity in expressing many relevant physical quantities as function of the Dziembowski variables. This set of equations may be solved with the use of appropriate boundary conditions [48].

At stellar center ($x = 0$):

$$y_1 C_1\omega^2 - l y_2 = 0 \qquad l y_3 - y_4 = 0 \tag{2.56}$$

At stellar surface ($x = 1$):

$$y_1 - y_2 + y_3 = 0 \qquad (l+1)y_3 + y_4 = 0 \tag{2.57}$$

2.3.3.A GYRE Oscillation Code

As with the case of the numerical implementation of the equations of stellar evolution, there is an ample amount of available code that integrate the adiabatic equations of stellar oscillation and allow for the acquisition of quality pulsation spectra, as well as relevant quantities that are common practice in contemporary asteroseismology.

With this intent, we make use of the GYRE oscillation code [49], an open-source stellar oscillation code that solves both the adiabatic and non-adiabatic equations of stellar pulsation making use of a new Magnus Multiple Shooting numerical scheme. Given an input stellar model at a certain temporal instant, GYRE computes the eigenfunctions and eigenfrequencies concerning the oscillation modes of that model, and outputs them, along with several relevant quantities to use in asteroseismic analysis, as a text file.

The selection of GYRE as the code to be used in this work is of utmost importance due to two particular characteristics of its architecture, the first being the fact that the construction of the equations is based on the procedure presented in this section, making use of the Dziembowski variables, and presenting the outputs of the simulation as a function of these. These outputs may be presented as summary files containing overall information of the entire spectra that was found, such as eigenfrequencies, radial orders and the nature of the modes, or detail files containing information concerning single modes, such as the eigenfunctions themselves. The second important characteristic of the GYRE code is that it is built such that it may receive output files of resulting MESA models as input for computation of the spectra, allowing for a smooth transition between the numerical computation of the stellar structure and evolution to the computation of the spectra. The specifications, required by GYRE to be present in the input files, that go into the computation itself, are detailed in 4.1.

3

Massive White Dwarfs and Asteroseismology

Contents

This chapter contains the relevant information concerning the state of the art which motivates the subject of this thesis. In 3.1, we review some aspects concerning massive white dwarfs. In 3.2 we discuss some particular aspects of asteroseismology when applied in order to study white dwarf stars, namely the interesting occurrence of mode trapping due to the non homogeneous constitution of these stars.

3.1 Massive White Dwarfs

As mentioned in 1.1, the study of the impact of neutrino emission in the cooling process of pre-white dwarf stars becomes substantially richer when a more massive subset of these star are considered, namely due to the fact that these seem to be the most responsive to variations in the emission of these particles [1, 25].

With this, we refer to an important consideration to take into account when studying the evolution and properties of white dwarfs, this being their mass distribution. These objects result from stars with masses up to $\approx 12M_{\odot}$ [50], with resulting masses theoretically reaching up to the Chandrasekhar mass limit [51, 52], with a value of $1.45M_{\odot}$ for a C/O core white dwarf. Recently, white dwarfs with masses reaching up to $1.33M_{\odot}$ have been catalogued through the data acquired by the SDSS [53], and candidates with even higher masses [6, 54], closing in on the limit were also identified after the Gaia Data Release (DR2) [55].

Recent studies resulting in mass distributions of select sets of white dwarfs [56, 57] all seem to agree on a main peak of stars centered at around $\approx 0.6M_{\odot}$, with existence of a secondary peak at higher mass values of around $\approx 0.8M_{\odot}$ [58], and further analyzing isolated massive white dwarfs above this mass value reveals that a peak at $\approx 1.04M_{\odot}$ [59] is present. There seems to be indeed a significant number of massive white dwarfs with masses $> 0.8M_{\odot}$, presenting fractions of around $\approx 8\%$ of all catalogued white dwarfs, either it be DA or DB [53].

It is clear to see that massive white dwarfs represent a considerable fraction of the total population of these kind of stars. Not only this, but several particularities characteristic of said massive objects make them interesting subjects of study. For instance, massive white dwarfs represent the only type of these objects where Debye cooling is present at observable luminosities, since crystallization of the core occurs at also high luminosities due to their higher densities [2, 60], hence making it so that these objects cool faster than their less massive counterparts as the luminosities decrease. Another feature of these objects is the fact that the temperature of their progenitors is presumably high enough to achieve stable carbon burning, making it so that O/Ne cores are possible [61], which is a relevant point to consider when studying the cooling of these massive stars, since the diffusion of this ^{22}Ne in the core may be responsible for the release of a non-negligible amount of gravitational potential energy that may impact

the cooling time of these objects [62].

3.2 White Dwarf Asteroseismology

The use of asteroseismology as a tool to infer about several quantities and properties of stars is a mainstay of modern astrophysics, and hence the inclusion of white dwarf stars in this discussion is natural.

In this particular case of white dwarfs, the development of this area is accompanied with the formulation of typical procedures to consider when an observational pulsation spectrum is available. Examples of these procedures are the determination of the stellar mass, which can be inferred by a dependence on the period spacing of the modes [63], mode identification through magnetic and rotational splitting [64], matching of pulsation models through period-to-period fits [65], among many others.

3.2.1 Asymptotic Period Spacing and Mode Trapping

DOV white dwarfs, as is the case with other classes of white dwarfs, are multiperiodic, low-amplitude g-mode pulsators, and hence, this work will be focused on the study of g-mode spectra of modelled pre-white dwarfs.

When dealing with a g-mode spectrum, it is usual to study the evolution of the period of the pulsation modes, since these correspond to lower frequency modes which present periods whose timescales may correspond to values that are sensible enough so that they are prone to being measured. One of the main characteristics of the period spectrum of chemically homogeneous stellar structures is that in the asymptotic limit ($k >> l$), every consecutive radial order modes (k) with the same harmonic degree (l) have the same period spacing $\Delta\Pi_l^a$ [66]:

$$\Delta\Pi_l^a = \Pi_{k+1l} - \Pi_{kl} = \frac{2\pi^2}{\sqrt{l(l+1)}} \left[\int_0^{R*} \frac{N(r)}{r} dr \right]^{-1} = constant \tag{3.1}$$

This is particularly interesting when considering the fact that typical models for GW Vir stars (and white dwarfs in general) present steep composition gradients which result in deviations from the behaviour established by equation 3.1, with the most evident cases, in the case of a GW Vir star (DOV), being the transition regions from the C/O core to the outer layers, and also the steep transition caused by the He envelope. From a pictorial point of view, chemical interfaces work as reflecting boundaries inside of the star, making it so that if the length between boundaries matches the wavelength of a certain mode, it is possible to trap this mode as a standing wave, forcing it to oscillate with higher amplitudes in this trapping region. Trapped modes have their nodes confined to a smaller region, effectively making their periods seem shorter, and disabling the validity of a constant period separation value. It becomes more

or less intuitive then to analyze the behavior of $\Delta\Pi_k$, which is usually done through diagrams which plot this quantity as a function of Π_k, revealing patterns that must deviate from the horizontal line established by the asymptotic limit of equation 3.1, with local minima presumably referring to modes that are being subject to this trapping effect, as seen in the upper panel of figure 3.1.

When analyzing these diagrams, there are three main features that are usually the main focal points in what concerns the study of the period separation and all are identifiable in the figure: (i) The first is known as the trapping cycle, as it refers to the number of modes between period spacing minima, and it is generally inversely proportional to the thickness of the outer layers where the mode is trapped [2]. (ii) There is also the trapping amplitude, which refers to, as the name suggests, as the amplitude of the period spacing relative to the asymptotic limit, or in other words, it represents the amount by which trapping alters the period spacing of the mode, this being generally proportional to thickness of the chemical transition layer. (iii) The last relevant feature is known as the trapping phase, which corresponds to the pattern generated by the period spacing as a function of the period, which usually moves with changing stellar temperature.

The manifestation of mode trapping is then extremely dependent on the depth of the chemical transition regions inside of the star, as can be seen by the following analytical approximation, taken from [67], which expresses the periods of trapped modes:

$$\Pi_i^2 = 4\pi^2\lambda_i^2 \left[\left(1 - \frac{r_c}{R^*}\right) l(l+1)\omega_0^2\right]^{-1} \qquad \omega_0 = \sqrt{\frac{GM^*}{R^{*3}}} \tag{3.2}$$

This expression refers to the trapped mode that contains i nodes between the surface and the chemical transition radius r_c, with λ_i being constants related with the roots of Bessel functions.

3.2.2 Oscillation Energy and Weight Function

Another very important flag in what concerns mode trapping is the behavior of the oscillation kinetic energy of modes, which can be written as a function of the Dziembowski variables defined in equation 2.49 as the following [44, 48]:

$$E_k = \frac{1}{2} GM^* R^{*2} \omega_k^2 \int_0^1 x^2 \rho \left[x^2 y_1^2 + x^2 \frac{l(l+1)}{(C_1\omega_k^2)^2} y_2^2\right] dx \tag{3.3}$$

It's clear to see in this expression that, aside from the factors, this kinetic energy is proportional to the integral of some of the squared eigenfunctions defined as the Dziembowski variables, weighted by the density along the star. This then leads to the inference that modes propagating in deeper regions of the star, where the density is high, will have larger kinetic energy values, even when they are induced by small perturbations, while in turn, modes that are trapped in the outer layers of the star due to the steep

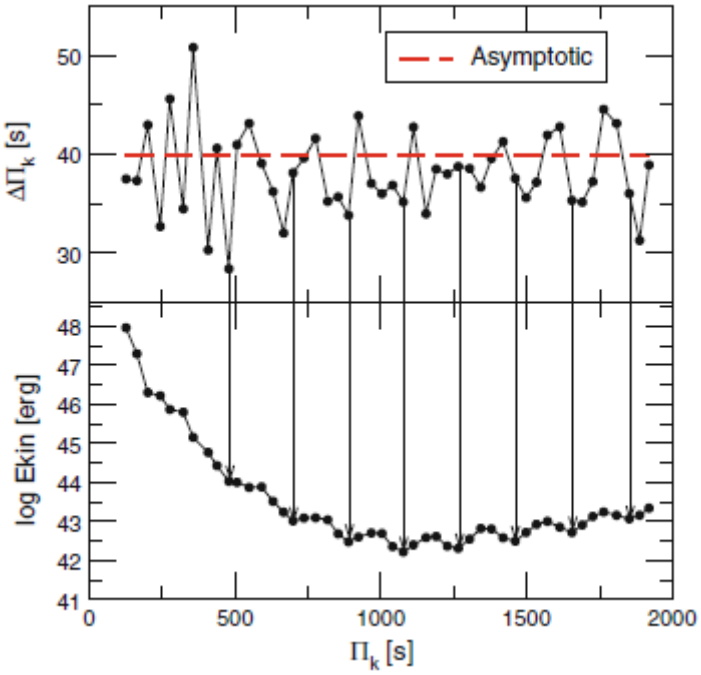

Figure 3.1: Period separation (upper panel) and oscillation kinetic energy (lower pannel) as a function of the pulsation periods for a typical DB white dwarf model [2].

He transition in the envelope will necessarily have small kinetic energy values. This makes it so that, similarly to the period spacing diagram, plots of the kinetic energy as a function o Π_k function as good indicators of trapped modes, since local minima of this function seems to indicate that a mode has less kinetic energy than it otherwise would have, were it not trapped, as can be seen in the lower panel of figure 3.1, which also enhances the idea that this energy analysis in conjunction with the period spacing diagram represents an effective method of identification of mode trapping.

To complement the study of the behavior of the perturbations inside of the star, while providing additional information regarding the period spectrum formation, it is usual to analyze another mathematical function, known as the mode weight function, which similarly to the kinetic energy, can also be written as a function of the Dziembowski variables [44, 48]:

$$W_k = (4\pi G R_*^2)\frac{r^2\rho^2}{R_*^2 U^2} * \left[A^* y_1^2 + V_g(y_2 - y_3)^2 - \frac{1}{U}(l(l+1)y_3 + y_4)^2\right] \tag{3.4}$$

Each mode runs through the star, presenting different amplitude values depending on the stellar structure and on how effective is the excitation mechanism. The relative values of weight functions serve as indicators on how the eigendunctions are settled along the star [5], and they may provide information regarding which regions of the stellar interior most contribute to the determination of the modes' periods.

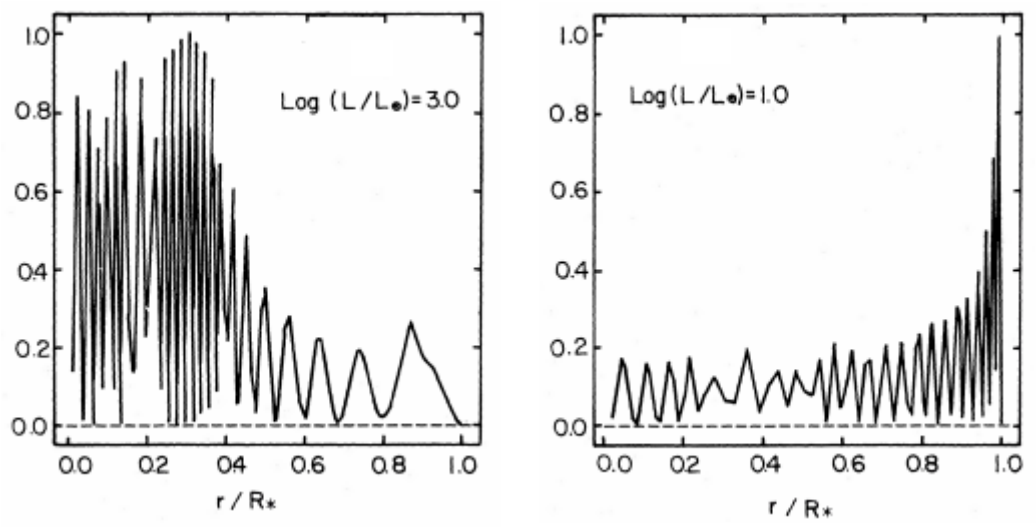

Figure 3.2: Weight function of a modelled $0.6M_{\odot}$ mass pre-white dwarf at two different stages of evolution, with left panel taken at $\log L/L_{\odot} = 3$ and the second panel taken at $\log L/L_{\odot} = 1$ [5]

Among other properties, the weight functions of g-modes are highly dependent on the polytrope index n, which is a good indicator of central condensation of the star. A pre-white dwarf can be more or less modelled as a $n = 3$ polytrope with significant central condensation and with g-modes being generated in core, which is where the weight function will assume its maximum values, but as central condensation decreases, this behavior will shift to the outer regions, making it so that at lower luminosities, the g-modes are mostly generated in the outer regions of the star [68]. This behavior can be seen in figure 3.2, where the normalized weight function of the g_{25} mode (meaning that $l = 1$ and $n = 25$) of a modelled $0.6M_{\odot}$ mass pre-white dwarf [5] is shown at two distinct points of evolution with different luminosity values, as labelled in each panel. In the first panel, as mentioned previously, central condensation is still significant enough so that the weight function is mainly centered in the core, but as the star evolves and luminosity drops, the peak of this weight function shifts outwards until it is established in the outer envelope of the star.

4

White Dwarf Stellar Evolution and Adiabatic Pulsational Analysis

Contents

In this chapter we begin by discussing, in 4.1, the code used in order to model different mass stars from the ZAMS up to the white dwarf cooling sequence, as well as to obtain appropriate g-modes spectra for each of these stars. In 4.2 we analyze the evolution of the neutrino emission rates as the star cools during this DOV stage, discussing the prevalence of each neutrino source, and finally in 4.3, by manually altering the neutrino rates of these models, we discuss the impact of neutrino cooling at a phenomenological and structural level, as well as the influence it has on the period spectra of these models.

4.1 Evolutionary Input Physics and Pre-White Dwarf Track

In order to study the signature of neutrino emission in massive white dwarfs, an appropriate model was used to replicate the evolution of these stars. This was done using the MESA code [36], version r10398, with evolutionary input closely following the description present in [69], which details the evolution of both H and He atmosphere massive white dwarfs, starting from the ZAMS and reaching up to the oldest stages of cooling, where luminosity values are as low as $L/L_{\odot} \approx 4$.

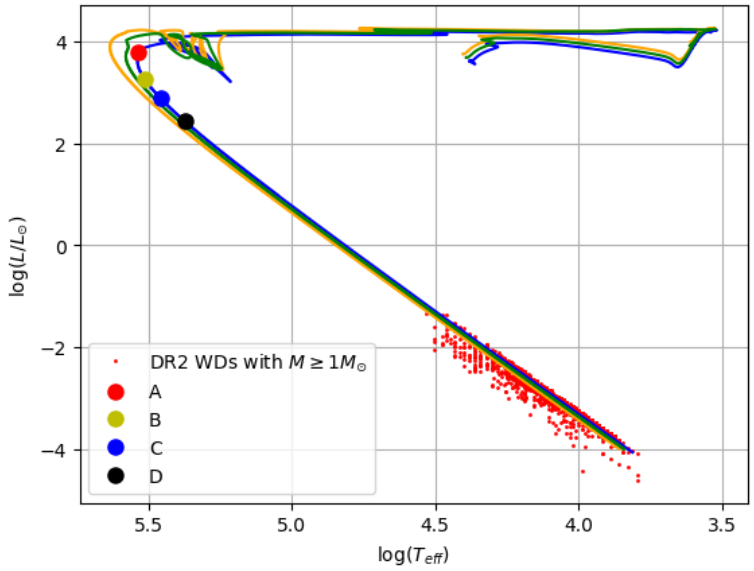

Figure 4.1: HR diagram containing the curves relative to the evolution of $9M_{\odot}$ (blue), $9.5M_{\odot}$ (green) and $10M_{\odot}$ (orange) initial mass stars from the ZAMS up to the white dwarf cooling sequence. Points A, B, C and D are benchmark evolutionary stages from the $9M_{\odot}$ initial mass star, chosen to study this region of evolution. Additionally, massive white dwarf candidates from GAIA [6] are shown at the end of the cooling sequences.

Our models consist of different evolutionary tracks, concerning stars beginning at the ZAMS with masses ranging from $9M_{\odot}$ to $11M_{\odot}$, resulting in white dwarfs with $1.02M_{\odot}$ to $1.22M_{\odot}$, chosen with the intent of covering a wide range in which typical massive white dwarfs are present. Regarding the

timezone in which we will focus our study, this being the initial track of the white dwarf cooling sequence, corresponding to an age range of $\log t[yrs] \approx 7.435 - 7.440$, the main input considerations are, as described in [69], the formulation of chemical diffusion and gravitational settling from [70], the absence of convection due to numerical instabilities, which has no impact on the cooling times relative to when convection is left active, and particularly does not affect the study of stellar pulsations and neutrino emission at this stage of the evolution, since at this stage (GW Vir stage), convection is yet to set in and pulsations are mainly excited by the $\kappa-$mechanism [71]. Lastly, the emission rates for plasmon, bremsstrahlung and several less important neutrino sources are taken from [24], whose derivations are briefly described in 2.2.

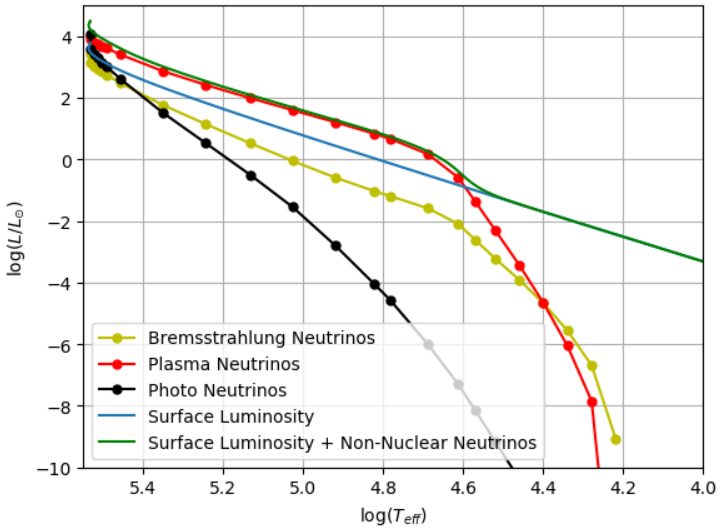

Figure 4.2: Weight of the several non-nuclear neutrino energy sinks for modelled $9M_{\odot}$ initial mass star, starting at the white dwarf cooling sequence.

Resulting HR diagrams from our models are shown in figure 4.1, as well as the benchmark profiles chosen for one of the models, to probe the region where neutrinos represent the largest energy sink. This figure also contains points relative to massive white dwarf candidates from GAIA, taken from [6], which fall on the ending phase of our models and seem to agree with the branches established by our models. The selection of these profiles is based on the information conveyed in figure 4.2, which allows to compare the impact of several different loss mechanisms with the surface luminosity of the star as a function of T_{eff}.

Regarding the seismology component of this work, the pulsation eigenmodes of our models were obtained making use of the GYRE oscillation code [49], version 5.1, using the MESA models as direct input and using the formulation of [72] in what concerns the boundary condition of the shooting method used in the search. An inverse frequency grid type (uniform in period) is also used in order to more easily scan for adiabatic g-modes.

4.2 Neutrino Emission Rates

The main purpose of this work is to study the impact that neutrino cooling has on the overall evolution of pre-white dwarf objects while neutrinos are still the most relevant energy sink. For this reason, and due to the numerical nature of the models, a similar prescription to that of [73] was used, in which the emission rates of non nuclear neutrinos, as seen in equation 2.12, was parameterized before the star enters the white dwarf cooling sequence. This parameterization takes the following form:

$$\epsilon_{\tilde{\nu}_m} = \gamma_m \epsilon_{\tilde{\nu}_0} \tag{4.1}$$

Where $\epsilon_{\tilde{\nu}_0}$ corresponds to the neutrino emission rate as predicted by standard leptonic theory. This then allows to compare models relative to the same star but with different neutrino emission rates and detect any changes which, as a result, will necessarily be a direct consequence of the neutrino effects on the cooling of the star.

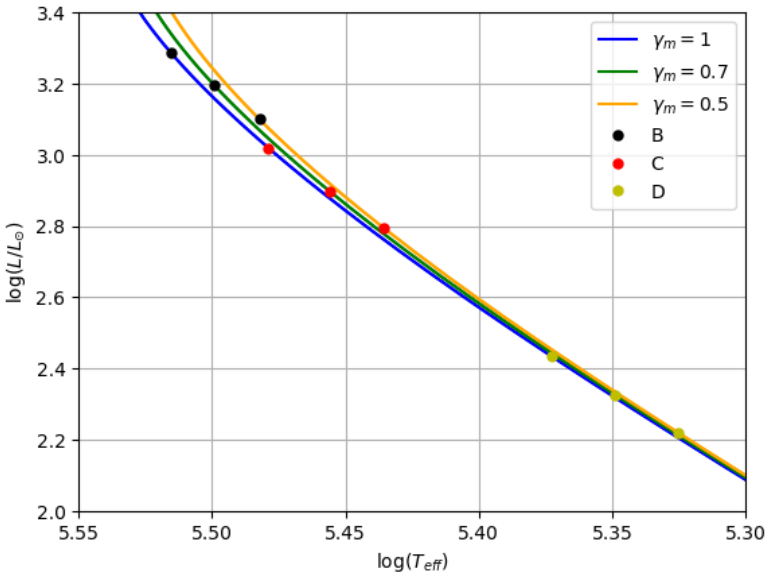

Figure 4.3: HR diagram containing the curves relative to the evolution of a $9M_\odot$ initial mass star, each with different initial neutrino emission rates, these being the unchanged rate of ϵ_{ν_0} (blue), $0.7\epsilon_{\nu_0}$ (green) and $0.5\epsilon_{\nu_0}$ (orange). Each curve contains their respective benchmark points A, B and C, where each set of points with the same color across all curves correspond to comparison evolutionary points.

Starting from the benchmark points shown in figure 4.1, we reproduce the same model, which in this case corresponds to the $9M_\odot$ initial mass model, up to the first of these points, this being profile A, and at this point, we set the neutrino emission rate factor γ_m, making it so that the evolutionary track is slightly changed from this point on. Figure 4.3 shows how the evolutionary track is altered by considering situations where at point A, the neutrino emission rates are set to 50% and 70% of the original rate, these being represented in orange and green respectively, relative to the model with unaltered rates,

represented in blue. As for the comparison points, which are also represented in the figure, where each set of points with the same color represent comparison points, these were selected such that the current neutrino rate of the unaltered model multiplied by the factor of the altered model, is equal to the current neutrino rate of the altered model, i.e., the neutrino emission rates of point B relative to the orange curve is, at that point, half of the neutrino emission rate of point B relative to the blue curve.

Table 4.1: Values of certain global quantities relative to the profiles chosen as comparison points in figure 4.3

Profile	$\log T_{eff}$	$\log L/L_{\odot}$	$R^*/R_{\odot}$	Age($t - t_A$) [yrs]
A	5.53	3.79	0.023	0
B_{100}	5.51	3.29	0.014	8055
B_{70}	5.50	3.20	0.013	10847
B_{50}	5.48	3.10	0.013	14572
C_{100}	5.48	3.01	0.012	13491
C_{70}	5.46	2.90	0.011	19031
C_{50}	5.44	2.79	0.011	25584
D_{100}	5.37	2.43	0.010	32655
D_{70}	5.35	2.33	0.010	43683
D_{50}	5.33	2.22	0.010	57250

Information concerning some relevant quantities of each comparison point shown in figure 4.3 is presented in table 4.1, where it is clear to see that throughout each set of comparison points chosen, the star does not present equal values for the global quantities, but it is interesting to notice that, in what concerns the age of the star relative to profile A, there seems to be an agreement between the proportions of this value along each set of comparison points and the respective neutrino rate factor, meaning for instance, that it took approximately twice as much time for the model with halved neutrino emission rates to reach B_{50} than it took for the model with unchanged rates to reach B_{100}. It's important to note that there is no mass column in this table, but this is only due to the fact that there is no mass loss along this evolutionary segment, meaning that the mass of the star is equal across all profiles and across all models, and its value is $M^*/M_{\odot} = 1.028$.

Furthermore, figure 4.4 shows how the main unaltered sources of neutrino emission change as the star evolves, both in terms of position in the star and intensity. As mentioned prior, plasma neutrinos are the dominant energy source during this pre-WD phase, and along with the energy due to bremsstrahlung neutrinos, which are also relevant when considering such high mass values, both make up for almost the totality of energy lost during this phase. From this figure, we notice how the production of these neutrinos moves outwards along the star as they decrease with time, and for this reason we don't extend the analysis to much later times relative to profile C, because it's clear to see that the neutrino emission rate dies off if we move ahead in time.

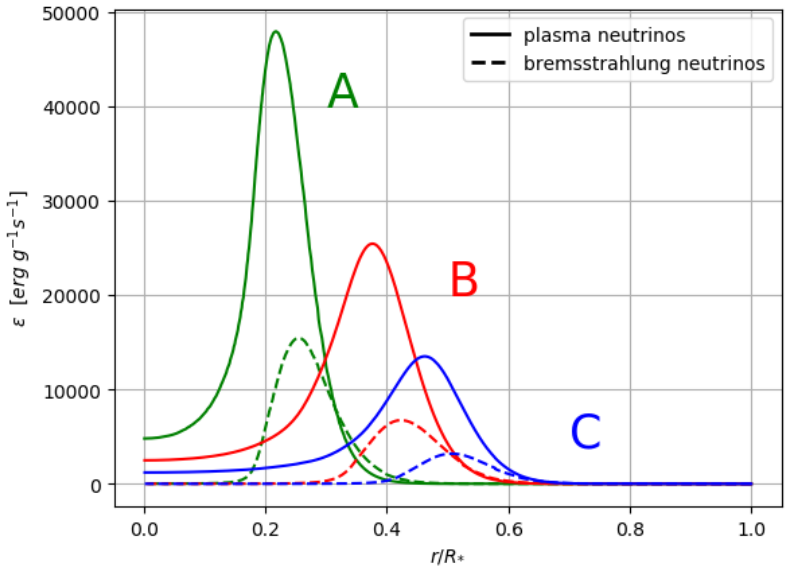

Figure 4.4: Neutrino emission rates relative to benchmark points A, B and C concerning the modelled $9M_{\odot}$ initial mass star with unchanged neutrino emission rates. Continuous lines refer to plasma neutrino emission rates while dashed lines refer to bremsstrahlung neutrino emission rates.

4.3 Nonradial Pulsation Spectrum of Massive Pre-White Dwarf

We now proceed with the analysis of the impact of altered neutrino rates on the structure and evolution of the model. We begin by discussing some of the properties that are usually relevant in typical spectra of massive (and overall) white dwarf pulsation. To this end, we can start by analyzing the evolution of propagation diagrams along the region in study.

The first row of Figure 4.5 shows exactly how this takes place, containing, from left to right, the corresponding diagrams relative to the profiles A, B and C present in Figure 4.1, concerning a $9M_{\odot}$ initial mass star and evolving into a $1.02M_{\odot}$ white dwarf. In this figure, both the propagation diagrams and the chemical profiles contain information regarding the star as it would normally evolve, and the case where neutrino emission rates were set to half (orange curve in figure 4.3), with this being represented with dashed lines. The situation corresponding to the rate reducing factor of 0.7 is not represented in these diagrams in order to keep the figure visually clear, but the shape of the lines concerning this case is evident, as this represents a midway point between the two cases that are shown.

Profile A, which is the common point between the cases, depicts the star right before T_{eff} achieves its maximum value, being at $T_{eff} = 341491K$ and with $\log(L/L_{\odot}) = 3.79$, and for this reason, it presents some similarities with typical red giants diagrams, which correspond to a previous stage of evolution in the lifetime of this star. In this regard, it can be seen that the central values of N^2 are comparable to the outer values, and some dips in this frequency structure allow for the presence of some mixed modes. This trait vanishes as the star keeps evolving through this neutrino phase, with N^2 increasing

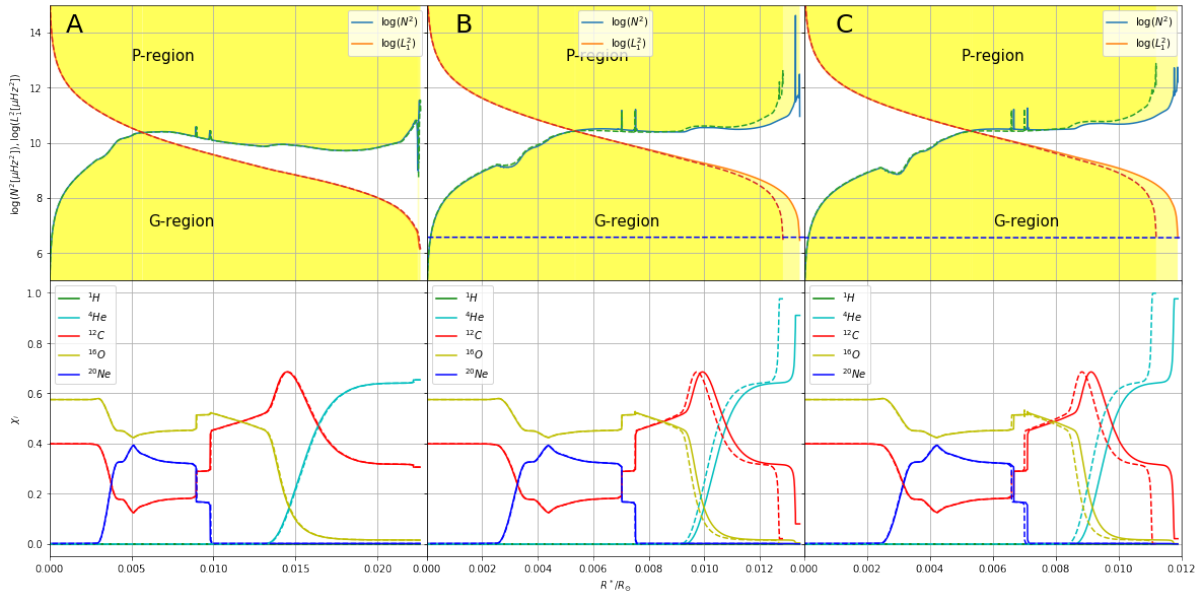

Figure 4.5: Propagation diagrams (first row) and chemical profiles (second row) of $9M_{\odot}$ initial mass star models. Continuous lines refer to the model where neutrino emission rates are unchanged and dashed lines refer to the case where neutrino emission rates are halved. A, B and C labels are representative of the benchmark points chosen for each model

in value in the outer regions of the star, making it so that there is a wider gap between the G- and P-regions and no mixed modes seem to be possible. The propagation diagrams relative to profiles B and C clearly illustrate this point, with the correspondent chemical profiles revealing that this is accompanied with a settling of several layers in the star, with the outer carbon layer being the most evident. It is then interesting to compare the situation between the case where neutrinos are unaltered and the case where their rate is set to half. As seen in the figure, there's a clear agreement between the abundance curves at the inner regions of the star, but the outer layers seem to have a small departure from one another as the evolution goes on, as can be seen by the helium and carbon curves, indicating that the effects of gravitational settling are stronger when neutrino emission is halved, which is in agreement with the fact that the model with halved neutrino takes approximately double the time to reach point B when compared with the model where rates are unchanged.

As mentioned prior, GW Vir stars are known to pulsate with low amplitude g-modes, and for that reason, the focus of the seismologic analysis in this work is done according to the eigenmodes present in the G-region of the evolving propagation diagram of the star. We instill particular attention to the blue dashed line present in the propagation diagrams of B and C, which corresponds to the frequency of the mode g_{60} (radial order $k = 60$ and angular degree $l = 1$), which we choose as a reference mode due to the fact that it is one of the lowest radial order g-modes that is allowed to propagate up to the surface during most of the time range on which our study is focused on, and theoretically, would be one of the easiest to detect.

Nonetheless, it's still relevant to acknowledge the general evolution of the g-mode spectrum, since typical measured periods of modes for (non-massive) GW Vir stars are considerably smaller than the period of this g_{60} mode. Figure 4.6 shows the evolution of the period Π for $k = 20$, 25, 30, 35, 40, 45, 50, 55 and 60 radial order g-modes for both models, with continuous lines being relative to the model with unchanged rates and dashed lines relative to the model with halved rates. The period evolution behavior is as expected when compared to other studies on a similar topic [48] (where non-massive GW Vir stars are being considered), starting with a decrease in periods while the star approaches maximum effective temperature due to rapid contraction of its layers, followed by a steady increase as the temperature and luminosity both drop.

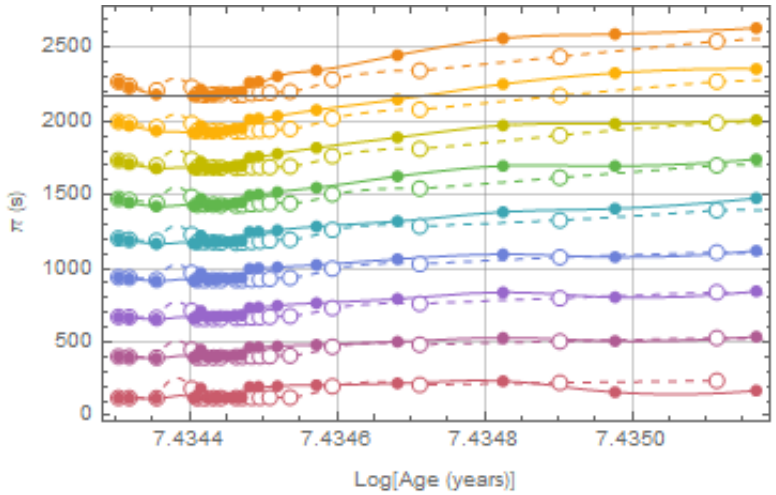

Figure 4.6: Evolution of the period Π for $k = 20$, 25, 30, 35, 40, 45, 50, 55 and 60 radial order g-modes. The continuous lines refer to the model with unchanged neutrino rates and the dashed lines refer to model with halved rates. The color scheme was chosen in order to easily distinguish the curves for each mode, and each color corresponds to the same radial order mode. The points were connected through the use of a Spline2 interpolation.

The general behavior of this evolution is similar in both cases, but it is clear to see that at later, equal times, the period of the modes concerning the model with halved rates are smaller than those of the model with unaltered rates, with this being more and more noticeable as the radial order increases. This seems to be a consequence of the fact that the period evolution of the modes is directly affected by the neutrino emission rates, making it so that modes concerning the model with halved rates take approximately twice as much time in order to acquire a certain period value, meaning that the periods of the modes in each model are approximately the same at the comparison points defined in figure 4.3. To illustrate this point, we present in figure 4.7 the evolution of the deviation between the period the g_{50} mode of the model with unchanged rates, taken at $t_{C_{100}}$ (time of the model with unchanged rates at profile C), and the period of this same mode relative to the model with halved rates, as a function $t_{50}/t_{C_{100}}$.

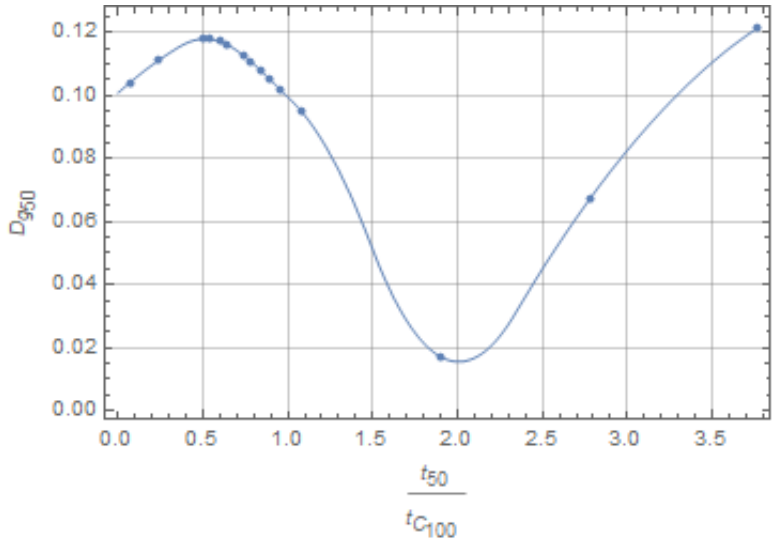

Figure 4.7: Deviation between the period the g_{50} mode of the model with unchanged rates, taken at $t_{C_{100}}$, and the period of this same mode relative to the model with halved rates, as a function $t_{50}/t_{C_{100}}$. The points were connected through the use of a Spline2 interpolation.

Where we define the deviation $D_{g_{50}}$ as:

$$D_{g_{50}} = \frac{\pi_{g_{50}}(t_{50}) - \pi_{g_{50}}(t_{C_{100}})}{\pi_{g_{50}}(t_{C_{100}})} \tag{4.2}$$

In this expression, $\pi_{g_{50}}(t_{50})$ represents the period of g_{50} as a function time t_{50} concerning the model with halved rates, and $\pi_{g_{50}}(t_{C_{100}})$ represents the period of this same mode taken at $t_{C_{100}}$. Indeed this figure reveals that the minimum deviation occurs at $t_{50}/t_{C_{100}} \approx 2$, indicating that the periods of this mode seems to match between models at approximately this point, in agreement with our previous statement.

5

Asteroseismology: Probing Neutrino Emission and Trapping Phase Shift

Contents

In this chapter we proceed with the discussion of the impact of altered neutrino rates as the star cools, with special attention to the propagation of the pulsation modes inside of the star, doing so in 5.1 by making use of the weight functions that describe their behavior in stellar interiors. In 5.2 we define a neutrino sensitivity function in order to more quantitatively assess the effects that neutrinos have on these weight functions and on which modes the impact is more prevalent, and finally in 5.3 we tie this subject to a novel effect that results on a shift of the radial order of the modes that are trapped as a consequence of the altered neutrino rates.

5.1 Neutrino Impact on the Weight Function

While in the last section we were able to study the overall progression of the g-mode spectra as the star evolves, no information regarding the behavior of the modes inside the star was inferred. To that end, a more helpful procedure would be an analysis of the evolution of the weight functions of the modes, which give information concerning the running of the mode inside of the star.

As mentioned previously in section 3.2, the typical behavior expected from these type of stars [5] consists on an initial weight confined to the inner regions of the star, mostly the core, followed by an uniformization of the envelope of the function caused due to the decrease of the weight values in the interior and simultaneous increase of this function in the outer layers of the star, as a consequence of the decrease in central condensation as the star evolves, making it look like the mode travels outwards in intensity as the star cools. Indeed this behaviour can be mostly verified, as can be seen in Figure 5.1, where this outward motion of the weight function seems to be present when the radial order of the mode is not too small. In this figure, we can see the evolution of the normalized weight function concerning different radial order modes, these being $k = 1, 5, 10, 20, 40$ and 60 for our $9M_{\odot}$ initial mass star with unchanged neutrino rates, and it's clear that the described behaviour starts taking place at around $k = 10$, with modes below this radial order showing a less defined pattern, partly due to the lesser amount of nodes intrinsic to lower radial orders, consequence of the dependence of the weight function on the eigenfunctions defined by the Dziembowski variables, as can be seen in equation 3.4.

It is worth mentioning that the dependence of the eigenfunctions and of the variables defined in equation 2.55 on quantities such as the Brunt-Väisälä frequency N^2 makes it so that some unusual discontinuities spikes occur on the weight function, to match the spikes that are present in N^2 and are visible in the propagation diagrams of figure 4.5. The existence of these spikes and further implications will be addressed ahead, since at this point, the overall behavior of the weight functions is not at all altered because of them.

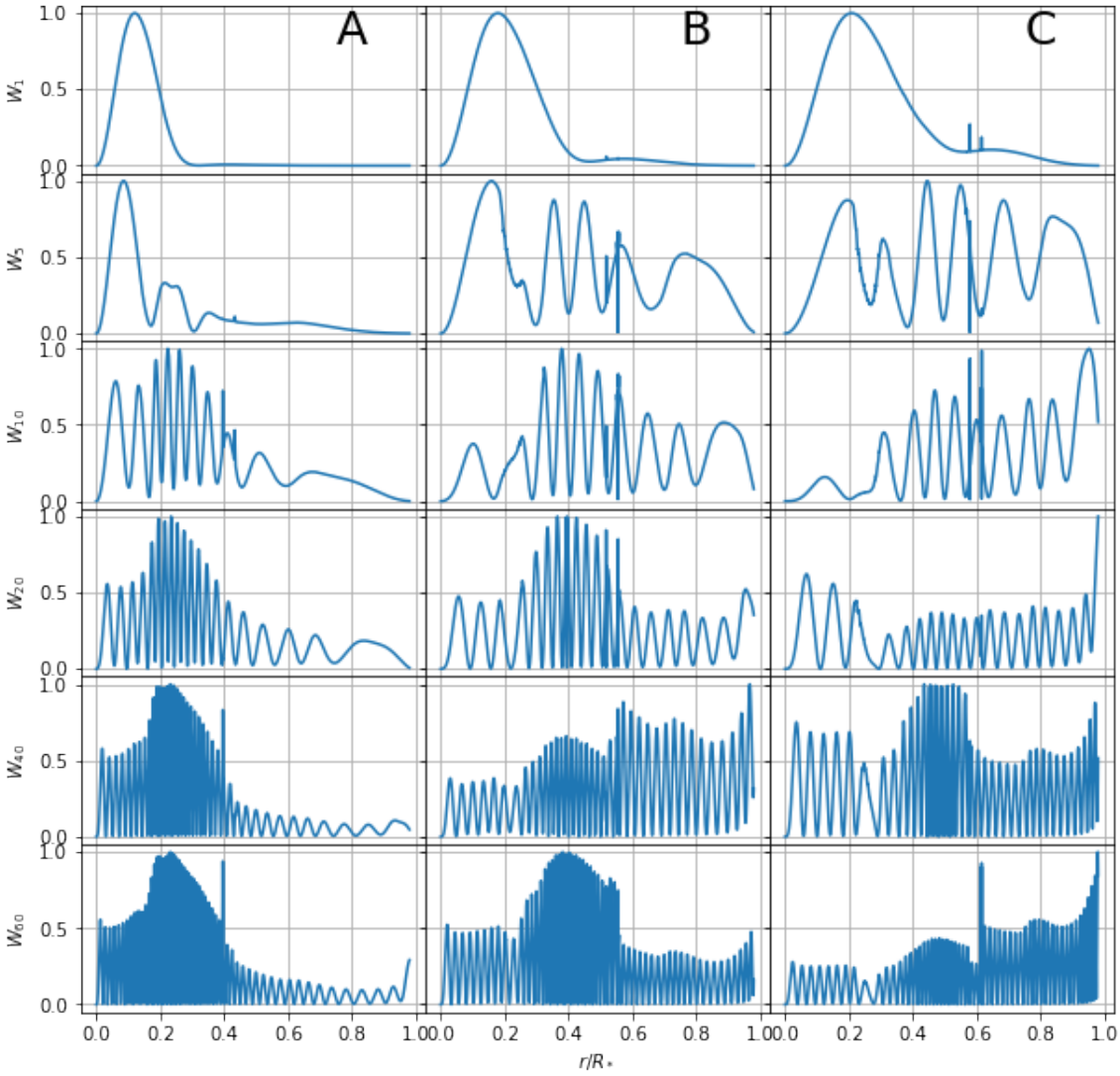

Figure 5.1: Weight functions of several radial order modes at different evolutionary points of modelled $9M_\odot$ initial mass star with unchanged neutrino emission rates. A, B and C labels apply to each column and are representative of the benchmark points chosen for this model.

It is interesting to notice that this outward displacement effect is very identical to the outward displacement of the neutrino emission rate curves seen in figure 4.4, which might imply the existence of a relation between neutrino emission and mode formation. We may assess this possibility in more detail by analyzing figure 5.2, where we plot the weight function of our previously selected reference mode g_{60} at several stages of evolution of the star, with the first row corresponding to the case where the neutrino emission rates are unchanged, and the second row to the case where neutrino emission rates were halved. The lines present in each panel correspond to the plasma (orange) and bremsstrahlung (green) neutrino emission rates associated to that profile, with all cases being normalized to the maximum value of the first panel of the correspondent row.

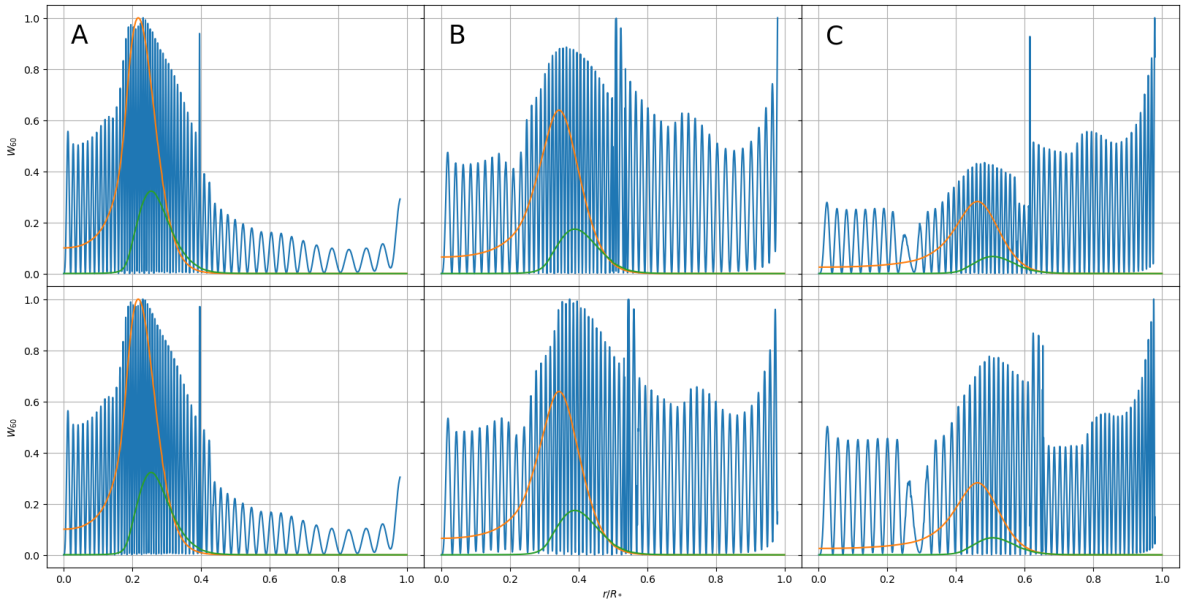

Figure 5.2: Weight functions of g_{60} mode at different evolutionary points of modelled $9M_{\odot}$ initial mass star with unchanged neutrino emission rates (first row) and halved neutrino emission rates (second row), as well as plasma (orange) and bremsstrahlung (green) neutrino emission rates normalized to highest value of correspondent row. A, B and C labels are representative of the benchmark points chosen for each model.

Indeed the normalized neutrino curve seems to resemble this prevalent peak in the weight function, both in shape and position, as they move outwards and decrease along this cooling period. Both these peaks seem to follow the small region just outside the C/O core where there's a drop in oxygen and carbon, and an increase in neon, which corresponds to the region where off-center carbon ignition occurred [74], and hence represents the hottest region of the star during this neutrino dominated period. This attribute more or less explains why the neutrino emission rates are prevalent in this area, since it is the region that most easily excites the pair production from plasmons, but no evident connection between this neutrino production area and the peak in the weight function can be deducted.

5.2 Neutrino Sensitivity Function

Even though the behavior of the weight functions relative to the models in comparison in figure 5.2 is similar, it is worth mentioning that the values of the normalized weight function along the stellar interior corresponding to the model with halved rates, as the star evolves from point A, seem to be higher than the ones relative to the model with unchanged rates in the chosen comparison points, which at the very minimum, seems to imply that the rate of neutrino emission seems to have an impact on the regions that most contribute for the formation of modes inside of the star.

In order to quantify this relation, so that a more concrete analysis of this overall effect can be done,

even for different radial order modes, we define the following neutrino sensitivity function S_{ν_k}:

$$S_{\nu_k}(r,t) = \frac{\int_0^r 4\pi r'^2 \rho(r',t)\epsilon_\nu(r',t)W_k(r',t)dr'}{L_\nu(r,t)} \tag{5.1}$$

This function is taken at a certain temporal point of the evolution, with ϵ_ν being the rate of non-nuclear neutrinos along the star at this temporal point, W_k being the normalized weight function of the g_k mode also at this point, and $L_\nu = \int_0^{R*} 4\pi r^2 \rho(r)\epsilon_\nu(r)dr$ being the non-nuclear neutrino luminosity, which essentially corresponds to the integral in the numerator of equation 5.1 without the weight function, meaning that this sensitivity function will only present values between 0 and 1. This function is designed with the intent of verifying how sensible the g-modes are in what pertains to the decaying neutrino rates as the evolution proceeds, and hence why the numerator of this expression is chosen as a "weighted" version of the neutrino luminosity function, directly relating these two quantities across the entire stellar structure. Looking at the shape of both functions in each panel of figure 5.2, it is expected that this sensitivity assumes a similar behavior to that of a step function, with a very steep increase characterized by an inflexion point right where both peaks assume their maximum value, making it so that, as time progresses, this inflexion point moves outwards and the upper threshold decreases, assuming that the peak of the weight function ceases to be the overall highest value of this function as it happens in the first row of the figure.

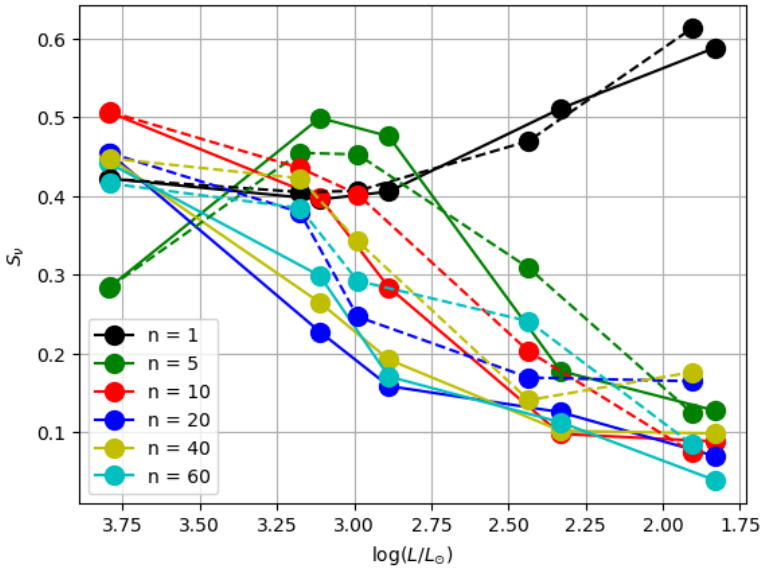

Figure 5.3: Evolution of the sensitivity function given in equation 5.1 for different radial order g-modes for modelled $9M_\odot$ initial mass star. Continuous lines refer to the model where neutrino emission rates are unchanged and dashed lines refer to the case where neutrino emission rates are halved.

It is of interest to analyze how the sensitivity function of different modes behave as the star evolves, and specially how it compares between the cases with different neutrino emission rates. Figure 5.3

contains several points concerning the maximum value (upper threshold) of the sensitivity function of different radial order g-modes at several stages of the neutrino cooling process as a function of the surface luminosity. Points connected by a continuous line represent modes concerning the model where neutrino rates are unaltered, while points connected by dashed lines represent modes concerning the model where rates were halved.

It is clear to see that in most cases, regardless of the fact that the rates of neutrino emission were changed or not, there is a common behavior in which the sensitivity seems to decrease with time, which agrees with the fact that the peak of the weight function decreases with time relative to the absolute maximum of this function. This behavior however seems to only be established when we consider modes with $k \geq 10$, since modes such as g_1 and g_5 seem to respond in a different manner, presenting increasing sensibilities at certain stages. This seems to agree with the previously mentioned fact that modes with lower radial orders, specifically $k < 10$, have weight functions with a considerably different shape than the others, partly due to having a lesser amount of nodes, but mostly due to how their envelopes are more evenly distributed along the star, not showing many evident peaks as is the case with the envelopes of weight functions of higher radial order modes. Nonetheless, the existence of fewer nodes in the weight functions of these lower radial order modes makes it so that, if any of the peaks of this function fully encapsulates the peak of the neutrino emission rate, then the integral present in S_{ν_k} will increase relative to the case where a similar valued oscillatory weight function takes the same position. This trait explains the increases that might be present in the evolution of the sensitivity function of lower radial order modes.

Another interesting subject regarding this figure is how the functions concerning the altered and non-altered neutrino emission rates compare to each other. This, once again, seems to have a certain dependence on the radial order of the modes that are being considered, and while the number of points available should be increased in order to study this feature in more detail, it is more or less apparent that higher radial order modes seem to be the ones that are more sensible to changes in the rates of neutrino emission. Indeed when comparing the values of this function relative to a single mode in the case where neutrino rates are unchanged to the values of the function relative to this same mode but with the rates halved, it is indisputable that they do not match for any mode, even taking into account the small sampling size that is being used. However, it is also clear that this mismatch is much more evident as the radial order of the mode that is being considered increases, with a noticeable gap between the continuous and the dashed line forming at around $k = 10$ and seemingly increasing as we consider higher k values. This gap forms as a consequence of the fact that the sensitivity values are higher along the evolution of the star when the rates halved, which is a direct consequence of the differences between the weight functions present in the upper and lower panels of the last two columns. As discussed in the beginning of this subsection, in the case where neutrino production is halved, this being the second

row, the maximum values of the peak's envelope that is being considered are considerably higher after normalization than those of the first row. As a consequence of this fact, the area below the smaller width peaks that are encapsulated by the envelope and also encapsulated by the neutrino emission peak, or in other words, the integral of the product of these two functions, is higher, which is easily understandable when noticing that these peaks "close" slower as they grow into their maximum value due to having a higher value to grow into when compared to the case where the rates are unchanged. This effect becomes more and more drastic as we increase the radial order of the mode, which indicates that the amplitudes of the weight functions of these modes are the most affected by changes in the rates of neutrino emission as the star cools. As a consequence, and returning to our first assessment regarding the differences between the weight functions of our models, this implies that the neutrino emission rates seem to mostly influence some of the regions that contribute for the generation of higher radial order modes.

5.3 Trapping Phase Shift due to Neutrinos

The analysis performed making use of the sensitivity function suggests that the rate of neutrino emission at a certain point of evolution of a pre-white dwarf has a direct influence on the pulsation modes of the star. This inference regarding the sensitivity of pulsation modes was done through a graphical analysis of a function that suggests, but does not imply correlation. It is then instructive to further extend the exploration of the impact of neutrino emission to defining and measurable properties of pulsation modes. To this end, we will study the evolution of the period separation pattern during this phase, which is shown in figure 5.4, where each panel corresponds to one of the previously mentioned profiles in what concerns the model where neutrino emission rates are unchanged. In this figure, points connected by a continuous (blue) line once again refer to this model, whereas points connected by a dashed black line correspond to the model where rates were halved. For further auxiliary purposes, the last panel also contains information concerning the model with a neutrino emission rate of 70% relative to the model with unchanged rates, this being represented by points connected by a dashed orange line. Additionally, the dashed, horizontal red line corresponds to the period spacing asymptotic limit, given by equation 3.1, concerning the model with unchanged rates, noting that while the asymptotic value relative to the model with halved rates is not represented, it practically matches the previous case.

At first glance, it is evident that neither of the patterns correspond to the behavior established by the asymptotic limit, which is to be expected due to the fact that our models contain several composition gradients that, as mentioned previously, may work as reflecting boundaries for certain modes, which makes it so that various resonant cavities may be identified throughout the star, these being evident by looking at the chemical profiles of figure 4.5. The direct consequences of these cavities is that modes

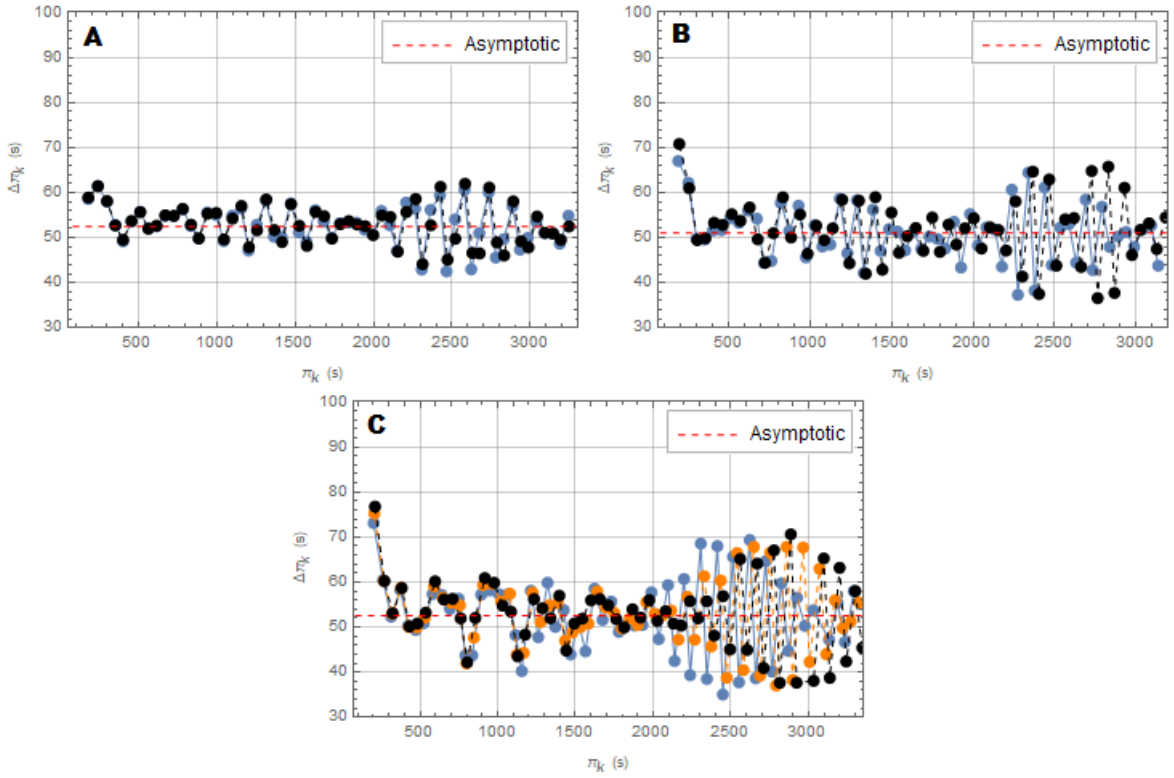

Figure 5.4: Evolution of the period separation $\Delta\Pi_l^a$ of the g-mode spectrum for modelled $9M_\odot$ initial mass star. Once again, continuous blue lines refer to the model where neutrino emission rates are unchanged, black dashed lines refer to the case where neutrino emission rates are halved, orange dashed lines refer to the case where neutrino emission rates were set to 70% and the A, B and C labels are representative of the benchmark points chosen for the models. The red, horizontal dashed line in each panel corresponds to the value of the period separation in the asymptotic limit given in equation 3.1 concerning the model with unchanged rates.

with wavelengths identical to their sizes might get trapped inside, in return presenting changes in their periods, which may then be mirrored onto the values of the period separation, since the distance relative to the periods of adjacent modes in radial order (which coincidentally, might also have their own periods altered due to this same effect) is altered as well. This creates a situation where $\Delta\Pi_l^a$ for a certain k mode becomes higher or smaller in value, and deviates from the expected behavior, hence creating the maxima and minima that can be observed in the period separation patterns of our figure. This trapping occurrence is of particular interest in what concerns predicting what modes might be impossible to measure even though they are excited, since they may be enclosed in the resonant cavities inside of the star, this being done with a correct identification of the extrema in the pattern and the respective mode and cavity that is causing them.

That being said, there is an interesting feature that can be identified in this figure once a comparison between the patterns generated by our two models is done, and that is the progressive shift of the rightmost part of the pattern corresponding to the model with halved neutrino emission rates relative to

the model with unchanged rates, as both evolve. As can be seen on the first panel, both patterns seem to match entirely, which is expected since profile A correspond to the point of evolution where the rates of the second model were set to half, effectively working as the initial point of the cooling phase in study, but as we look further in time, there seems to be a slight localized displacement of the dashed pattern to the right, relative to the continuous pattern. This displacement begins to be noticeable at stages close to the temporal point where profile B is located, where from figure 4.4, plasma-neutrino rates are of around $\epsilon_{\tilde{\nu}_p} \approx 25000\ erg \cdot g^{-1} \cdot s^{-1}$, and half of that value in the case of the second model, and it seems to be completely established at the evolutionary point represented by profile C, where the rates are now close to half than the ones in B, and neutrinos start to become less and less relevant moving forward.

It is important to mention that this clear pattern that is being shifted contains several local minima and maxima of the period separation, which suggests that the modes relative to these points are being subject to trapping. This is further enhanced by performing a similar procedure to the one presented in figure 3.1 and noting that local minima in $\Delta\Pi_l^a$ correspond to local minima in the oscillation kinetic energy, which can be obtained with the use of equation 3.3. This can be seen in figure 5.5, where both these quantities, relative to the model with unchanged rates, are plotted in part of the period domain containing the pattern that is being shifted.

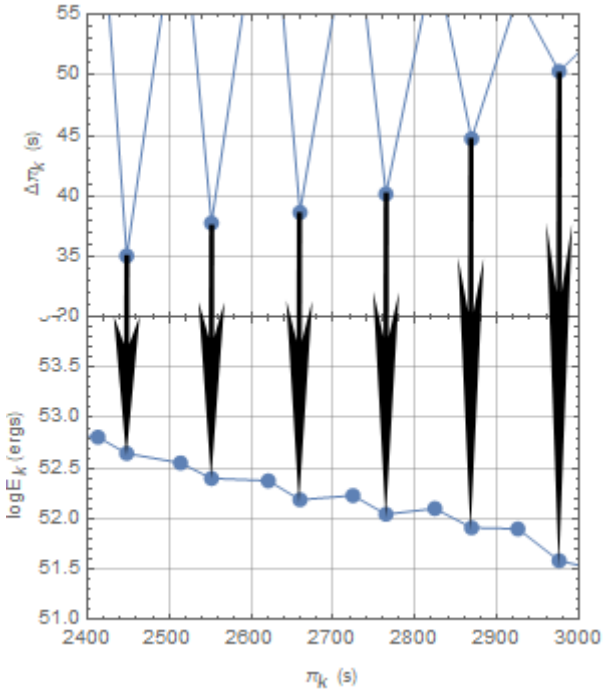

Figure 5.5: Segment of the evolution of the period separation $\Delta\Pi_l^a$ (upper panel) and oscillation kinetic energy E_{kin} (lower pannel) as a function of the pulsation periods relative to profile C of our modelled $9M_\odot$ initial mass star. Minima in each panel correspondent to the same period are connected by an arrow and represent to modes that are being subject to trapping.

Another interesting trait from this result is that this displacement appears to occur only when considering higher period modes, starting at around $\Pi_k \approx 1700s$, which interestingly correspond to higher radial order modes, with $k \gtrapprox 30$, meaning that the direct or indirect effects of altering the neutrino rates of the star seem to have an impact on these modes while leaving lower order modes unaltered, which agrees with our previous assessment that higher radial order modes are more sensible to changes in the rates of neutrino emission.

This pattern shift seems to be a consequence of various factors in which neutrino emission seems to be a relevant factor, namely the propagation regions for g-modes inside the star, as well as the chemical profiles. Indeed when looking at figure 4.5, there is a clear displacement of the outer chemical transition interfaces between both models, which also seems to become more evident as time progresses. This feature makes us refer to equation 3.2, which shows the dependence between the periods of trapped modes and the radius of these transition regions r_c, with these being effectively different when looking at the outer layers of both models, but maintaining the same values when considering the inner regions. This in turn makes it so that the trapping effect occurring at the outer regions of the model with halved neutrino emission rates suffers a shift in what concerns the periods of the modes that are being subject to this effect, relative to the model where neutrino emission rates are unchanged, while the periods of modes that are trapped in the innermost regions of the star are unaltered.

We may quantitatively assess this effect by using equation 3.2 to write an appropriate expression that allows for the comparison of the periods of trapped modes in the case where neutrino emission rates are unchanged, which we label as Π_{100} with the periods relative to the case where rates are halved, labelled as Π_{50}:

$$\left(\frac{\Pi_{50}}{\Pi_{100}}\right) = \sqrt{\frac{\left[\left(1-\frac{r_{c_{100}}}{R^*_{100}}\right)\frac{M^*_{100}}{{R^*_{100}}^3}\right]}{\left[\left(1-\frac{r_{c_{50}}}{R^*_{50}}\right)\frac{M^*_{50}}{{R^*_{50}}^3}\right]}} \tag{5.2}$$

This expression eliminates the original dependence on λ_i since it intends to compare the modes that are subject to trapping as a consequence of a chemical interface r_c and contain the same amount of nodes between this interface and the surface, even though the interface is shifted between models.

It is now necessary to define the values of r_c relative to the interfaces that might be the reason for the trapping. In 3.2.1, we mention how generally, this effect is a consequence of steep chemical interfaces in the interior of the star, such as the inner transitions from the core to outer layer, or even the steep transition to the He envelope. A useful diagnostic of what chemical interfaces might be relevant in what concerns this effect is the Brunt-Väisälä frequency N^2, since its dependence on $d\rho/dr$ will reveal some spikes in this structure as a consequence of discontinuities in density, which is a typical trait of chemical transition regions. With this in mind, and focusing on profile C, three different transition regions were selected for each model with their r_c being represented by the colored vertical lines in figure 5.6, with

continuous and dashed representing the model with unchanged rates and the model with halved rates respectively.

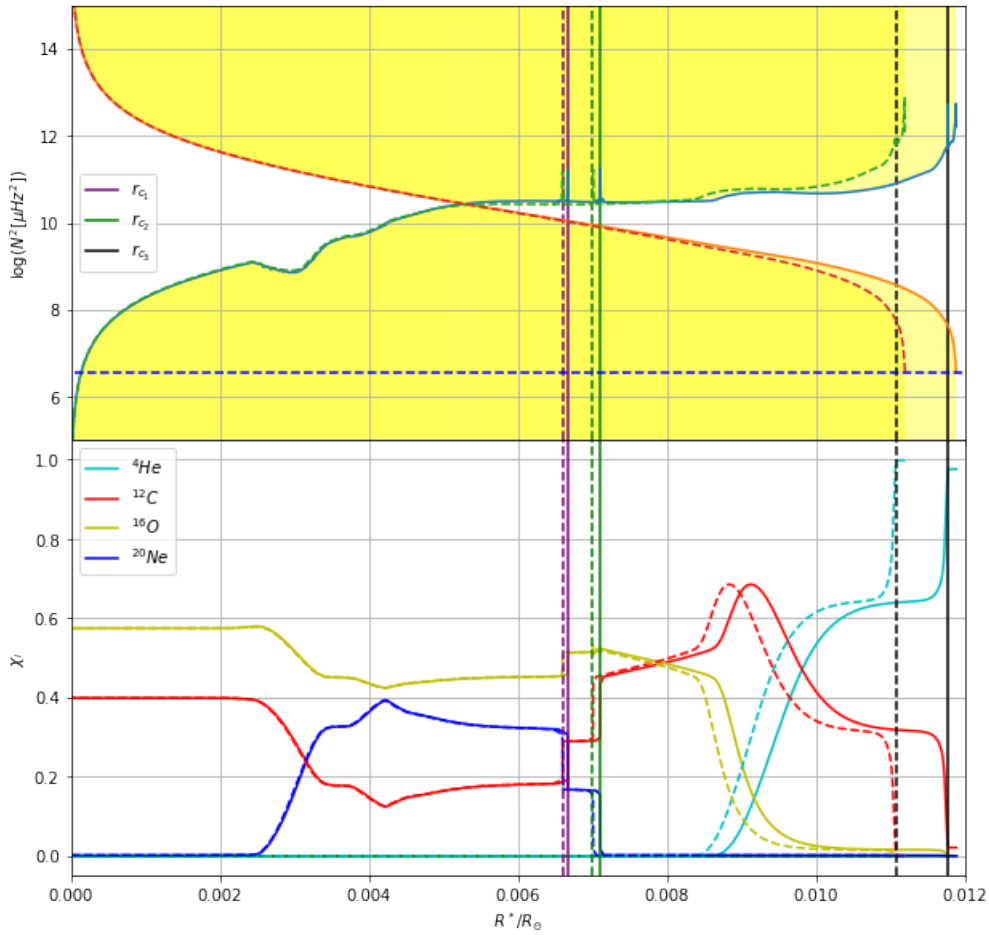

Figure 5.6: Propagation diagrams (first row) and chemical profiles (second row) relative to profile C of $9M_\odot$ initial mass star models. Continuous lines refer to the model where neutrino emission rates are unchanged and dashed lines refer to the case where neutrino emission rates are halved. A, B and C labels are representative of the benchmark points chosen for each model. The coloured vertical lines correspond to the r_c of the steep chemical interfaces that might be responsible for mode trapping, and are identified according to the label in figure

Table 5.1: Values of all the r_c represented as dashed lines in figure 5.6 and correspondent values of equation 5.2 for these transition regions.

i	$r_{c_i;50}/R_\odot$	$r_{c_i;100}/R_\odot$	$(\Pi_{50}/\Pi_{100})_{r_{c_i}}$
1	0.0066	0.0067	0.945
2	0.0070	0.0071	0.946
3	0.1112	0.1175	1.194

Additionally, table 5.1 contains the values of all the r_c defined in figure 5.6, as well as the values given by equation 5.2 relative to these transition regions. Each of these values corresponds to ratio between

the periods of modes trapped in the correspondent transition layer in the model where neutrino emission rates are halved and the model where these rates are unchanged. This seems to indicate that the shift of the rightmost pattern must be caused by the outermost transition region due to the He envelope, since the value for this ratio seems to correspond to the same ratio between the periods in which this pattern is present for each model. As for what modes are the ones being affected, the propagation diagrams seem to show that the region of the star in which g-modes propagate grows with increasing radial order, with modes starting at approximately $k \gtrapprox 30$ in radial order reaching this layer, meaning that this predicted shift of trapped modes' periods should only be noticeable for higher radial order modes, which agrees with the results shown in figure 5.4.

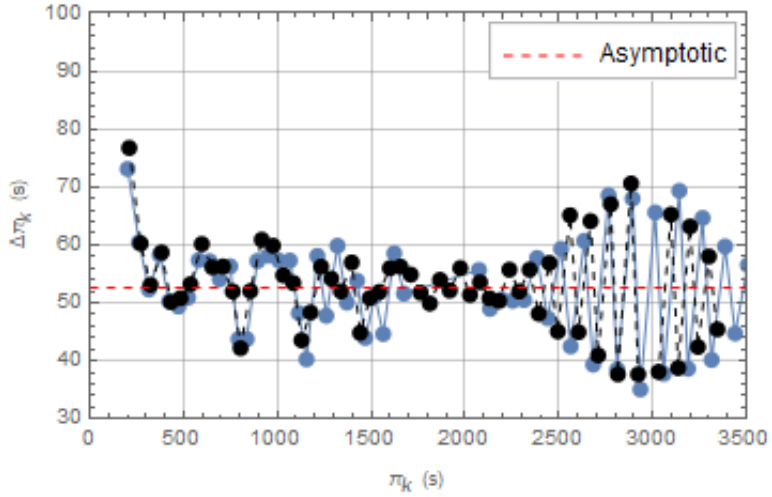

Figure 5.7: Evolution of the period separation $\Delta\Pi_l^a$ of the g-mode spectrum for modelled $9M_\odot$ initial mass star, with periods of trapping pattern relative to the model with unchanged rates corrected by the appropriate factor given by equation 5.2 for the He transition region. Continuous blue lines refer to the model where neutrino emission rates are unchanged and black dashed lines refer to the case where neutrino emission rates are halved.

If we indeed shift the the periods of the model with unchanged neutrino rates in which this pattern seems to occur (starting at $\Pi_{30} \approx 1700s$) by the equation 5.2 factor correspondent to this layer, we see that the patterns of both models almost coincide as can be seen in figure 5.7, which is a strong evidence to support the claims that indeed this trapping is being caused by the outer He layer, and that this trapping effect is dependent on neutrino emission rates of the star, which indirectly alter the periods of the modes that are being subject to this effect.

6

Conclusion

Contents

6.1 Conclusions

This thesis focused on an overall analysis of the evolution of massive pre-white dwarfs at the GW Vir (DOV) stage, as well as the behavior of the pulsation spectrum of these stars during this stage, but most importantly, it contemplates an effective method to address the effect that the prime cooling mechanism along this evolutionary stage, this being non nuclear neutrino emission, has on not only the structural and phenomenological behavior of these stars, but also on the propagation of pulsation modes inside the star and their measurable properties.

The topic of neutrinos as the largest energy sink during this early white dwarf stage is extensively documented and agreed upon, but the exotic nature of these particles represents a barrier in what concerns the experimental development of this subject. On the other hand, the small duration of this short lived GW Vir stage when compared to the overall evolutionary timescale of white dwarfs imposes a restriction in what concerns the quantity of observational data regarding the pulsation spectrum of these kind of stars. The usage of asteroseismology as a tool for probing the interiors of stars, coupled with state of the art numerical models that simulate the structural and evolutionary behavior of these stars in detail, allows to tie both these ends to the best of our abilities and in turn provide crucial information that might contribute to the loosening of these aforementioned restrictions.

6.2 Achievements

The main intent of the work developed in this thesis was to verify that indeed the emission of non nuclear neutrinos has a significant impact on the pulsation spectrum of white dwarfs. To this point, not only did we verify the evolution of the star is sensitive to the emission rate of these particles at a structural level, as seen by the displacement of the outer chemical layers when comparing models with different emission rates, but most importantly, the part of the spectrum concerning higher radial order modes, specifically with $k \gtrapprox 30$, also shows a significant response in what concerns altering the emission rates of these particles.

We verified that the behavior of the modes in the interior of our model stars seems to follow a pattern in line with the emission rates, making use of the weight function of individual modes, and further noticed how altering these rates seems to impact the relative values of this weight function inside of the stars, with an evident discrepancy growing as the radial order grows, as quantified by our neutrino sensitivity function.

We further extended our study of the impact of neutrinos to typically measurable quantities of these kind of stars by comparing the period separation and kinetic energy of our distinct neutrino rates models, and verifying the onset of a displacement of the pattern of the period separation relative to higher radial order modes, with $k \gtrapprox 30$, in agreement with the assessment that may be infered by our previous

results that these are the modes most sensible to the emission rates of neutrinos. We verified that this pattern was being caused due to trapping of these modes, and concluded that the pattern shift was a consequence of the displacement of the He envelope transition layer between models with different rates, effectively presenting a method of deducing that this layer is responsible for the trapping of high order radial modes during this evolutionary stage, and most importantly establishing, as a complement of the analysis of the sensitivity function, that changing neutrino emission rates impact the propagation and overall behavior of these same modes.

6.3 Future Work

The continuous advances concerning the identification and the acquisition of information of a tremendous amount of celestial objects is undeniable, as evidenced by the numerous missions carried out to this purpose, and it immensely improves the quality of work in the field of asteroseismology. In particular, the satellite missions COROT [75] and Kepler [76] were responsible for surveying an impressive amount of stars, in which considerable numbers of main-sequence stars, red giants and white-dwarfs were identified to present stellar oscillations. The Gaia [77] space mission only further increased these numbers, and moreover, it is expected that the PLATO [26] mission will be launched in 2025, contributing to the potential of yet again extending the number of observed pulsating stars, in which white dwarfs and pre-white dwarfs are included. The increase in documentation concerning typical pulsation properties in these kind of stars, which is scarce, would allow for an increase in quality of the numerical models that are used currently to simulate and study these stars. In the specific case of the work developed in this thesis, an ample measurement of several g-mode spectra relative to these kind of stars at different stages of evolution would allow for a better understanding of the impact of neutrino emission during this stage, as possibly allow for a more complete description of effects such as the one studied in this work.

Nonetheless, while our study of the impact of neutrino emission rates on the evolution and spectra of pre-white dwarfs was focused on a small subset consisting on the massive portion of these stars with He atmospheres, there is no constraint in what concerns chemical composition nor mass that prevents this procedure to be applied. A similar analysis to this one on a larger set of pre-white dwarfs represents an interesting prospect which may contribute to a more complete description of the impact of neutrino cooling on evolution, either it be by furthering the insight of the effects studied in this thesis, or by finding and understanding new ones.

Bibliography

[1] E. M. Kantor and M. E. Gusakov, "The neutrino emission due to plasmon decay and neutrino luminosity of white dwarfs," *Monthly Notices of the Royal Astronomical Society*, vol. 381, no. 4, p. 1702–1710, Nov 2007. [Online]. Available: http://dx.doi.org/10.1111/j.1365-2966.2007.12342.x

[2] L. G. Althaus, A. H. Córsico, J. Isern, and E. García-Berro, "Evolutionary and pulsational properties of white dwarf stars," *The Astronomy and Astrophysics Review*, vol. 18, no. 4, p. 471–566, Aug 2010. [Online]. Available: http://dx.doi.org/10.1007/s00159-010-0033-1

[3] D. A. Dicus, "Stellar energy-loss rates in a convergent theory of weak and electromagnetic interactions," *Phys. Rev. D*, vol. 6, pp. 941–949, Aug 1972. [Online]. Available: https://link.aps.org/doi/10.1103/PhysRevD.6.941%7D

[4] G. Guo and Y.-Z. Qian, "Spectra and rates of bremsstrahlung neutrino emission in stars," *Physical Review D*, vol. 94, no. 4, Aug 2016. [Online]. Available: http://dx.doi.org/10.1103/PhysRevD.94.043005

[5] S. D. Kawaler, D. E. Winget, and C. J. Hansen, "Evolution of the pulsation properties of hot pre-white dwarf stars." , vol. 295, pp. 547–560, Aug. 1985.

[6] F. M. Jiménez-Esteban, S. Torres, A. Rebassa-Mansergas, G. Skorobogatov, E. Solano, C. Cantero, and C. Rodrigo, "A white dwarf catalogue from Gaia-DR2 and the Virtual Observatory," *Monthly Notices of the Royal Astronomical Society*, vol. 480, no. 4, pp. 4505–4518, 08 2018. [Online]. Available: https://doi.org/10.1093/mnras/sty2120

[7] H. N. Russell, "Relations Between the Spectra and Other Characteristics of the Stars," *Popular Astronomy*, vol. 22, pp. 275–294, May 1914.

[8] R. H. Fowler, "On dense matter," , vol. 87, pp. 114–122, Dec. 1926.

[9] E. García–Berro and T. D. Oswalt, "The white dwarf luminosity function," *New Astronomy Reviews*, vol. 72-74, p. 1–22, Jun 2016. [Online]. Available: http://dx.doi.org/10.1016/j.newar.2016.08.001

[10] H. C. Harris, J. A. Munn, M. Kilic, J. Liebert, K. A. Williams, T. von Hippel, S. E. Levine, D. G. Monet, D. J. Eisenstein, S. J. Kleinman, T. S. Metcalfe, A. Nitta, D. E. Winget, J. Brinkmann, M. Fukugita, G. R. Knapp, R. H. Lupton, J. A. Smith, and D. P. Schneider, "The white dwarf luminosity function from sloan digital sky survey imaging data," *The Astronomical Journal*, vol. 131, no. 1, pp. 571–581, jan 2006. [Online]. Available: https://doi.org/10.1086%2F497966

[11] R. A. Mendez and M. T. Ruiz, "The luminosity function of magnitude and proper-motion–selected samples: The case of white dwarfs," *The Astrophysical Journal*, vol. 547, no. 1, pp. 252–263, jan 2001. [Online]. Available: https://doi.org/10.1086%2F318359

[12] B. M. Hansen and J. Liebert, "Cool white dwarfs," *Annual Review of Astronomy and Astrophysics*, vol. 41, no. 1, pp. 465–515, 2003. [Online]. Available: https://doi.org/10.1146/annurev.astro.41.081401.155117

[13] H.-R. Noh and J. Scalo, "History of the Milky Way Star Formation Rate from the White Dwarf Luminosity Function," *apj*, vol. 352, p. 605, Apr. 1990.

[14] M. A. Wood, "Constraints on the Age and Evolution of the Galaxy from the White Dwarf Luminosity Function," *apj*, vol. 386, p. 539, Feb. 1992.

[15] J. B. Holberg and P. Bergeron, "Calibration of synthetic photometry using DA white dwarfs," *The Astronomical Journal*, vol. 132, no. 3, pp. 1221–1233, aug 2006. [Online]. Available: https://doi.org/10.1086%2F505938

[16] J. Isern, R. Mochkovitch, E. Garcia-Berro, and M. Hernanz, "The physics of crystallizing white dwarfs," *The Astrophysical Journal*, vol. 485, no. 1, pp. 308–312, aug 1997. [Online]. Available: https://doi.org/10.1086%2F304425

[17] G. Raffelt, *Stars as Laboratories for Fundamental Physics: The Astrophysics of Neutrinos, Axions, and Other Weakly Interacting Particles*, ser. Theoretical Astrophysics. University of Chicago Press, 1996. [Online]. Available: https://books.google.pt/books?id=6esnbt7BfIwC

[18] Z. Barkat, "Neutrino processes in stellar interiors." *araa*, vol. 13, pp. 45–68, Jan. 1975.

[19] H. Munakata, Y. Kohyama, and N. Itoh, "Neutrino Energy Loss in Stellar Interiors," *apj*, vol. 296, p. 197, Sep. 1985.

[20] B. M. S. Hansen, H. Richer, J. Kalirai, R. Goldsbury, S. Frewen, and J. Heyl, "CONSTRAINING NEUTRINO COOLING USING THE HOT WHITE DWARF LUMINOSITY FUNCTION IN THE GLOBULAR CLUSTER 47 TUCANAE," *The Astrophysical Journal*, vol. 809, no. 2, p. 141, aug 2015. [Online]. Available: https://doi.org/10.1088%2F0004-637x%2F809%2F2%2F141

[21] M. E. Peskin and D. V. Schroeder, *An introduction to quantum field theory*. Boulder, CO: Westview, 1995, includes exercises. [Online]. Available: https://cds.cern.ch/record/257493

[22] Z. Maki, M. Nakagawa, and S. Sakata, "Remarks on the Unified Model of Elementary Particles," *Progress of Theoretical Physics*, vol. 28, no. 5, pp. 870–880, 11 1962. [Online]. Available: https://doi.org/10.1143/PTP.28.870

[23] M. Haft, G. Raffelt, and A. Weiss, "Standard and nonstandard plasma neutrino emission revisited," *The Astrophysical Journal*, vol. 425, p. 222, Apr 1994. [Online]. Available: http://dx.doi.org/10.1086/173978

[24] N. Itoh, H. Hayashi, A. Nishikawa, and Y. Kohyama, "Neutrino Energy Loss in Stellar Interiors. VII. Pair, Photo-, Plasma, Bremsstrahlung, and Recombination Neutrino Processes," *apjs*, vol. 102, p. 411, Feb. 1996.

[25] L. G. Althaus, E. García-Berro, J. Isern, and A. H. Córsico, "Mass-radius relations for massive white dwarf stars," *Astronomy Astrophysics*, vol. 441, no. 2, p. 689–694, Sep 2005. [Online]. Available: http://dx.doi.org/10.1051/0004-6361:20052996

[26] H. Rauer, C. Catala, C. Aerts, T. Appourchaux, W. Benz, A. Brandeker, J. Christensen-Dalsgaard, M. Deleuil, L. Gizon, M.-J. Goupil, and et al., "The plato 2.0 mission," *Experimental Astronomy*, vol. 38, no. 1-2, p. 249–330, Sep 2014. [Online]. Available: http://dx.doi.org/10.1007/s10686-014-9383-4

[27] B. Carroll and D. Ostlie, *An Introduction to Modern Astrophysics*, 09 2017.

[28] M. Salaris and S. Cassisi, *Evolution of Stars and Stellar Populations*, 2005.

[29] K. Werner and F. Herwig, "The elemental abundances in bare planetary nebula central stars and the shell burning in agb stars," *Publications of the Astronomical Society of the Pacific*, vol. 118, no. 840, p. 183–204, Feb 2006. [Online]. Available: http://dx.doi.org/10.1086/500443

[30] D. J. Eisenstein, J. Liebert, H. C. Harris, S. J. Kleinman, A. Nitta, N. Silvestri, S. A. Anderson, J. C. Barentine, H. J. Brewington, J. Brinkmann, M. Harvanek, J. Krzesiński, J. Eric H. Neilsen, D. Long, D. P. Schneider, and S. A. Snedden, "A catalog of spectroscopically confirmed white dwarfs from the sloan digital sky survey data release 4," *The Astrophysical Journal Supplement Series*, vol. 167, no. 1, pp. 40–58, nov 2006. [Online]. Available: https://doi.org/10.1086%2F507110

[31] D. Q. Lamb and H. M. van Horn, "Evolution of crystallizing pure ^{12}C white dwarfs." *apj*, vol. 200, pp. 306–323, Sep. 1975.

[32] L. Mestel, “On the Theory of White Dwarf Stars: I. The Energy Sources of White Dwarfs,” *Monthly Notices of the Royal Astronomical Society*, vol. 112, no. 6, pp. 583–597, 12 1952. [Online]. Available: https://doi.org/10.1093/mnras/112.6.583

[33] F. D’Antona and I. Mazzitelli, “Cooling of white dwarfs,” *Annual Review of Astronomy and Astrophysics*, vol. 28, no. 1, pp. 139–181, 1990. [Online]. Available: https://doi.org/10.1146/annurev.aa.28.090190.001035

[34] E. E. Salpeter, “Energy and Pressure of a Zero-Temperature Plasma.” , vol. 134, p. 669, Nov. 1961.

[35] R. Kippenhahn and A. Weigert, *Stellar Structure and Evolution*, 1990.

[36] B. Paxton, L. Bildsten, A. Dotter, F. Herwig, P. Lesaffre, and F. Timmes, “Modules for experiments in stellar astrophysics (mesa),” *The Astrophysical Journal Supplement Series*, vol. 192, no. 1, p. 3, Dec 2010. [Online]. Available: http://dx.doi.org/10.1088/0067-0049/192/1/3

[37] G. Gamow and M. Schoenberg, “Neutrino theory of stellar collapse,” *Phys. Rev.*, vol. 59, pp. 539–547, Apr 1941. [Online]. Available: https://link.aps.org/doi/10.1103/PhysRev.59.539%7D

[38] J. B. Adams, M. A. Ruderman, and C. H. Woo, “Neutrino pair emission by a stellar plasma,” *Phys. Rev.*, vol. 129, pp. 1383–1390, Feb 1963. [Online]. Available: https://link.aps.org/doi/10.1103/PhysRev.129.1383

[39] Y. Kohyama, N. Itoh, A. Obama, and H. Hayashi, “Neutrino Energy Loss in Stellar Interiors. VI. Axial Vector Contribution to the Plasma Neutrino Energy-Loss Rate for Strongly Degenerate Electrons,” , vol. 431, p. 761, Aug. 1994.

[40] G. G. Festa and M. A. Ruderman, “Neutrino-pair bremsstrahlung from a degenerate electron gas,” *Phys. Rev.*, vol. 180, pp. 1227–1231, Apr 1969. [Online]. Available: https://link.aps.org/doi/10.1103/PhysRev.180.1227

[41] J. P. Cox, “Pulsating stars,” *Reports on Progress in Physics*, vol. 37, no. 5, pp. 563–698, may 1974. [Online]. Available: https://doi.org/10.1088%2F0034-4885%2F37%2F5%2F001

[42] A. Weiss, W. Hillebrandt, H.-C. Thomas, and H. Ritter, “Cox and giuli’s principles of stellar structure,” *Cox and Giuli’s Principles of Stellar Structure, by A. Weiss, W. Hillebrandt, H-C. Thomas, H. Ritter. Cambridge, UK: Princeton Publishing Associates Ltd, 2004.*, vol. -1, 01 2004.

[43] C. Aerts, J. Christensen-Dalsgaard, and D. Kurtz, *Asteroseismology*, ser. Astronomy and Astrophysics Library. Springer Netherlands, 2010. [Online]. Available: https://books.google.pt/books?id=N8pswDrdSyUC

[44] W. Unno, Y. Osaki, H. Ando, and H. Shibahashi, “Nonradial oscillations of stars,” *University of Tokyo press*, 1979.

[45] T. G. Cowling, “The Non-radial Oscillations of Polytropic Stars,” *Monthly Notices of the Royal Astronomical Society*, vol. 101, no. 8, pp. 367–375, 12 1941. [Online]. Available: https://doi.org/10.1093/mnras/101.8.367

[46] J. Christensen-Dalsgaard, “Solar Models with Enhanced Energy Transport in the Core,” , vol. 385, p. 354, Jan. 1992.

[47] W. A. Dziembowski, “Nonradial Oscillations of Evolved Stars. I. Quasiadiabatic Approximation,” , vol. 21, pp. 289–306, Jan. 1971.

[48] Córsico, A. H. and Althaus, L. G., “Asteroseismic inferences on gw virginis variable stars in the frame of new pg 1159 evolutionary models,” *A&A*, vol. 454, no. 3, pp. 863–881, 2006. [Online]. Available: https://doi.org/10.1051/0004-6361:20054199

[49] R. H. D. Townsend and S. A. Teitler, “gyre: an open-source stellar oscillation code based on a new Magnus Multiple Shooting scheme,” *Monthly Notices of the Royal Astronomical Society*, vol. 435, no. 4, pp. 3406–3418, 09 2013. [Online]. Available: https://doi.org/10.1093/mnras/stt1533

[50] C. L. Doherty, P. Gil-Pons, L. Siess, J. C. Lattanzio, and H. H. B. Lau, “Super- and massive AGB stars – IV. Final fates – initial-to-final mass relation,” *Monthly Notices of the Royal Astronomical Society*, vol. 446, no. 3, pp. 2599–2612, 11 2014. [Online]. Available: https://doi.org/10.1093/mnras/stu2180

[51] S. Chandrasekhar and E. A. Milne, “The Highly Collapsed Configurations of a Stellar Mass,” *Monthly Notices of the Royal Astronomical Society*, vol. 91, no. 5, pp. 456–466, 03 1931. [Online]. Available: https://doi.org/10.1093/mnras/91.5.456

[52] S. Chandrasekhar, “The Highly Collapsed Configurations of a Stellar Mass. (Second Paper.),” *Monthly Notices of the Royal Astronomical Society*, vol. 95, no. 3, pp. 207–225, 01 1935. [Online]. Available: https://doi.org/10.1093/mnras/95.3.207

[53] S. O. Kepler, S. J. Kleinman, A. Nitta, D. Koester, B. G. Castanheira, O. Giovannini, A. F. M. Costa, and L. Althaus, “White dwarf mass distribution in the SDSS,” *Monthly Notices of the Royal Astronomical Society*, vol. 375, no. 4, pp. 1315–1324, 02 2007. [Online]. Available: https://doi.org/10.1111/j.1365-2966.2006.11388.x

[54] N. P. Gentile Fusillo, P.-E. Tremblay, B. T. Gänsicke, C. J. Manser, T. Cunningham, E. Cukanovaite, M. Hollands, T. Marsh, R. Raddi, S. Jordan, and et al., “Agaiadata release 2 catalogue of white

dwarfs and a comparison with sdss," *Monthly Notices of the Royal Astronomical Society*, vol. 482, no. 4, p. 4570–4591, Nov 2018. [Online]. Available: http://dx.doi.org/10.1093/mnras/sty3016

[55] T. Prusti, J. de Bruijne, A. Brown, A. Vallenari, C. Babusiaux, C. Bailer-Jones, U. Bastian, M. Biermann, D. Evans, L. Eyer, F. Jansen, C. Jordi, S. Klioner, U. Lammers, L. Lindegren, X. Luri, F. Mignard, D. Milligan, C. Panem, and S. Zschocke, "The gaia mission," *Astronomy & Astrophysics*, vol. 595, 09 2016.

[56] J. Liebert, P. Bergeron, and J. B. Holberg, "The Formation Rate and Mass and Luminosity Functions of DA White Dwarfs from the Palomar Green Survey," *apjs*, vol. 156, no. 1, pp. 47–68, Jan. 2005.

[57] S. J. Kleinman, S. O. Kepler, D. Koester, I. Pelisoli, V. Peçanha, A. Nitta, J. E. S. Costa, J. Krzesinski, P. Dufour, F. R. Lachapelle, P. Bergeron, C.-W. Yip, H. C. Harris, D. J. Eisenstein, L. Althaus, and A. Córsico, "SDSS DR7 White Dwarf Catalog," *apjs*, vol. 204, no. 1, p. 5, Jan. 2013.

[58] S. O. Kepler, I. Pelisoli, D. Koester, G. Ourique, S. J. Kleinman, A. D. Romero, A. Nitta, D. J. Eisenstein, J. E. S. Costa, B. Külebi, S. Jordan, P. Dufour, P. Giommi, and A. Rebassa-Mansergas, "New white dwarf stars in the Sloan Digital Sky Survey Data Release 10," *Monthly Notices of the Royal Astronomical Society*, vol. 446, no. 4, pp. 4078–4087, 12 2014. [Online]. Available: https://doi.org/10.1093/mnras/stu2388

[59] Nalezyty, M. and Madej, J., "A catalogue of isolated massive white dwarfs * - mass distribution of massive stars," *A&A*, vol. 420, no. 2, pp. 507–513, 2004. [Online]. Available: https://doi.org/10.1051/0004-6361:20040123

[60] F. D'Antona and I. Mazzitelli, "Cooling of white dwarfs." *araa*, vol. 28, pp. 139–181, Jan. 1990.

[61] E. Garcia-Berro, J. Isern, and M. Hernanz, "The cooling of oxygen-neon white dwarfs," *mnras*, vol. 289, no. 4, pp. 973–978, Aug. 1997.

[62] C. Deloye and L. Bildsten, "Gravitational settling of 22ne in liquid white dwarf interiors: Cooling and seismological effects," *Astrophysical Journal - ASTROPHYS J*, vol. 580, pp. 1077–1090, 12 2002.

[63] S. D. Kawaler, "The stellar seismology of hot white dwarfs and planetary nebula nuclei," in *IAU Colloq. 95: Second Conference on Faint Blue Stars*, A. G. D. Philip, D. S. Hayes, and J. W. Liebert, Eds., Jan. 1987, pp. 297–307.

[64] S. Charpinet, G. Fontaine, and P. Brassard, "Seismic evidence for the loss of stellar angular momentum before the white-dwarf stage," *Nature*, vol. 461, pp. 501–3, 09 2009.

[65] A. Córsico, M. Bertolami, L. Althaus, G. Vauclair, and K. Werner, "Asteroseismological constraints on the coolest gw virginis variable star (pg 1159-type) pg 0122+200," *http://dx.doi.org/10.1051/0004-6361:20078145*, vol. 475, 11 2007.

[66] M. Tassoul, “Asymptotic approximations for stellar nonradial pulsations,” *The Astrophysical Journal Supplement Series*, vol. 43, pp. 469–490, 07 1980.

[67] S. D. Kawaler and P. A. Bradley, “Precision Asteroseismology of Pulsating PG 1159 Stars,” , vol. 427, p. 415, May 1994.

[68] D. C. Schwank, “Epstein Weight Functions for Non-Radial Oscillations of Polytropes,” , vol. 43, no. 2, pp. 459–468, Sep. 1976.

[69] G. R. Lauffer, A. D. Romero, and S. O. Kepler, “New full evolutionary sequences of h- and he-atmosphere massive white dwarf stars using mesa,” *Monthly Notices of the Royal Astronomical Society*, vol. 480, no. 2, p. 1547–1562, Aug 2018. [Online]. Available: http://dx.doi.org/10.1093/mnras/sty1925

[70] J. M. Burgers, *Flow Equations for Composite Gases*, 1969.

[71] Saio, H., “Pulsations in white dwarfs: Selected topics,” *EPJ Web of Conferences*, vol. 43, p. 05005, 2013. [Online]. Available: https://doi.org/10.1051/epjconf/20134305005

[72] J. Christensen-Dalsgaard, “Adipls—the aarhus adiabatic oscillation package,” *Astrophysics and Space Science*, vol. 316, no. 1-4, p. 113–120, Jan 2008. [Online]. Available: http://dx.doi.org/10.1007/s10509-007-9689-z

[73] M. S. O’Brien and S. D. Kawaler, “The predicted signature of neutrino emission in observations of pulsating pre–white dwarf stars,” *The Astrophysical Journal*, vol. 539, no. 1, pp. 372–378, aug 2000. [Online]. Available: https://doi.org/10.1086/309216

[74] Siess, L., “Evolution of massive agb stars - i. carbon burning phase,” *A&A*, vol. 448, no. 2, pp. 717–729, 2006. [Online]. Available: https://doi.org/10.1051/0004-6361:20053043

[75] M. Auvergne, P. Bodin, L. Boisnard, J.-T. Buey, S. Chaintreuil, G. Epstein, M. Jouret, T. Lam-Trong, P. Levacher, A. Magnan, and et al., “The corot satellite in flight: description and performance,” *Astronomy and Astrophysics*, vol. 506, no. 1, p. 411–424, Mar 2009. [Online]. Available: http://dx.doi.org/10.1051/0004-6361/200810860

[76] L. Molnár, R. Szabó, and E. Plachy, “Variable stars with the kepler space telescope,” 2016.

[77] T. Prusti, J. H. J. de Bruijne, A. G. A. Brown, A. Vallenari, C. Babusiaux, C. A. L. Bailer-Jones, U. Bastian, M. Biermann, D. W. Evans, and et al., “Thegaiamission,” *Astronomy and Astrophysics*, vol. 595, p. A1, Nov 2016. [Online]. Available: http://dx.doi.org/10.1051/0004-6361/201629272

A

Article

We present in this appendix the scientific article that resulted from the work developed in this thesis.

MNRAS **000**, 1–11 () Preprint 23 January 2021 Compiled using MNRAS LATEX style file v3.0

Asteroseismology of a Massive Pre-White Dwarf - Structural and Evolutionary Impact of Neutrino Cooling

Fernando Lima,[1]★ Ilídio Lopes,[1]
[1]*CENTRA, Instituto Superior Técnico, University of Lisbon, Lisbon, Portugal*

ABSTRACT

Neutrino emission is the most dominant process in what concerns energy loss for pre-white dwarf stars, and while there is consensus on the physics that is behind this cooling effect, the small interaction cross section of these particles makes it hard to experimentally test and corroborate the implications of this phenomena on a terrestrial laboratory. We make use of state of the art numerical code to model stars beginning in the ZAMS with masses ranging from $9M_{\odot}$ to $11M_{\odot}$ and evolving up to the white dwarf cooling sequence, and obtain their correspondent asteroseismic spectrum. Taking particular attention to the luminosity range of $L/L_{\odot} = 4$ to $L/L_{\odot} = 2$, where neutrino emission is the dominant energy loss mechanism, we study the impact of different non nuclear neutrino emission rates on the period spectrum of the g-modes, as well as the consequences of this impact on the star at a chemical and structural level. We identify a novel phenomena where a shift in the pattern of the period separation of higher order radial modes seems to take place when the neutrino emission rates are altered, whereas the pattern relative to lower order radial modes remains unchanged.

Key words: Asteroseismology – Stars – White dwarfs

1 INTRODUCTION

White dwarfs are very dense stellar core remnants, presumably the final evolutionary stage of more than 97% of all stars. Resulting from low- and intermediate-mass hydrogen burning stars, these objects have reached a phase of their evolutionary process in which nuclear burning has ceased to be a significant energy source. Since no other energy source of the star is relevant enough to compensate for the continuously radiated (stored) thermal energy, it will begin to cool, becoming dimmer with passing time.

Among the many utilities that come from the study of these objects, the white dwarf luminosity function (García–Berro & Oswalt (2016); Harris et al. (2006)) represents one of the most important tools in what concerns not only the advances in this area (Mendez & Ruiz (2001); Hansen & Liebert (2003)), but also contributions to several other topics such as the history of our Galaxy and certain constraints on its age (Noh & Scalo (1990); Wood (1992)), photometric calibration (Holberg & Bergeron (2006)), the theory of hot dense plasmas (Isern et al. (1997)) and even the study of fundamental interactions in physics, since white dwarf stars represent quality astroparticle physics laboratories (Raffelt (1996)).

From a spectroscopic point of view, these objects can be classified as DA and non-DA white dwarfs, depending on the main constituent of their outer layers. DA white dwarfs represent the most abundant class, containing ≈ 85% of all white dwarf stars (Eisenstein et al. (2006)), and it corresponds to such stars with hydrogen rich atmospheres, while non-DA white dwarfs correspond to these stars with hydrogen deficient atmospheres. This last class may be further subdivided according to their spectra and effective temperature, with DO white dwarfs presenting strong lines of HeII and with $45000K \leq T_{eff} \leq 200000K$, DB white dwarfs presenting strong HeI lines and with $11000K \leq T_{eff} \leq 30000K$ and DC, DQ and DZ presenting traces of carbon and metal in their spectra, and with $T_{eff} < 11000K$.

2 NEUTRINO PHYSICS

The cooling of white dwarfs along their evolution is one of the main subjects of study in what concerns these stars, and any HR diagram containing the evolution of one of these objects indeed shows a characteristic evolutionary branch known as the cooling curve. Several analytical descriptions of this evolutionary branch are presently available or currently on the works, with the first and simplest being the Mestel model (Mestel (1952)), which indeed captures the essential features of this cooling sequence, but it is derived with few and simple assumptions that do not include the many processes are known to occur along this path (D'Antona & Mazzitelli (1990a); Garcia-Berro et al. (1997); Jr & MacDonald (1985)). One such process that has a significant impact at certain stages of this branch is the emission of neutrinos.

Neutrino production inside stellar interiors is a known phenomena that may occur due to several different processes (Barkat (1975); Munakata et al. (1985)) and results in the emission of these particles, which may represent a relevant energy sink in what concerns the energy balance of stars. Such is the case with white dwarfs, whose typical radii are far shorter than the mean free path of neutrinos, making it so that this could represent a source of energy loss during evolution. In a typical white dwarf, when nuclear burning ceases, the

★ E-mail: fernando.lima@tecnico.ulisboa.pt

timescales of the surface luminosity drop and the central temperature drop differ, with the latter occurring over a longer period, which is a consequence of the large ratio between neutrino emission and the aforementioned surface luminosity (D'Antona & Mazzitelli (1990b)), with this being the case during a significant amount of time during the evolution along the cooling curve, extending up to timescales of around $t \approx 10^7$ years (Althaus et al. (2010)). Since this neutrino dominated phase corresponds to the beginning of the cooling process, it is common to refer to these stars as pre-white dwarfs, noting that the spectroscopic classification of these objects is valid anyways. A very interesting class of variable stars that fall into this category are the well-known GW Vir stars, which are essentially variable DO white dwarfs (also known as DOV's) whose pulsations are gravity driven with typically low amplitudes. As already mentioned, stars at this stage have a characteristic chemical composition, lacking the typical hydrogen envelope that most white dwarfs have, and present higher temperature and luminosity than most white dwarfs, such that in this sense, they might effectively be considered pre-white dwarfs.

Among the many processes that are responsible for the production and subsequent release of non nuclear neutrinos inside of a white dwarf during this GW Vir stage, plasma-neutrinos represent the main energy loss mechanism, with the possibility of a considerable contribution of neutrino bremsstrahlung at later stages of the branch (Lamb & van Horn (1975)), noting that this last process implies a significant impact in the cooling of massive white dwarfs (Itoh et al. (1996)).

It is interesting to reflect on the fact that, while there's consensus in what concerns the prevalence of neutrino cooling during this stage of evolution of white dwarf stars, it is a difficult task to replicate and experimentally test this phenomena in the laboratory, mainly due to the small interaction cross section of these particles (Hansen et al. (2015)), which in turn, makes it hard to verify certain predictions regarding their impact on the overall behaviour of this cooling stage, whether it be at a structural or at a phenomenological level. On the other hand, asteroseismology has been a consistent tool in what concerns the study of an array of topics regarding stellar structure and evolution, and naturally encapsulates the main aspects to consider when trying to approach the subject of the impact of neutrino cooling, effectively working as a metaphorical laboratory that allows for the verification of this neutrino print.

It's also worth mentioning that calculation of neutrino emission rates in white dwarfs and pre-white dwarfs are based on the standard theory of leptonic interaction which contains several construction flaws, particularly in what concerns the inclusion of neutrinos, which are predicted to be left-handed particles with no renormalizable mass term Peskin & Schroeder (1995). This has since been proven incorrect with the introduction of neutrino flavor oscillation Maki et al. (1962). Nonetheless, stellar emission rates of these particles are computed making use of the interactions present in the standard electroweak Hamiltonian, being subject to the constraints established by this theory, and hence the measurement of the effects of altered neutrino rates and consequent neutrino interactions in these stars may represent an independent test of the coupling of neutrinos in the leptonic processes of the standard model.

3 MASSIVE WHITE DWARFS

An important consideration to take into account when studying white dwarfs is their mass distribution. These objects result from stars with masses up to $\approx 12 M_\odot$ (Doherty et al. (2014)), with resulting masses theoretically reaching up to the Chandrasekhar mass limit (Chandrasekhar & Milne (1931); Chandrasekhar (1935)), with a value of $1.45 M_\odot$ for a C/O core white dwarf. Recently, white dwarfs with masses reaching up to $1.33 M_\odot$ have been catalogued through the data acquired by the SDSS (Kepler et al. (2007)), and candidates with even higher masses (Gentile Fusillo et al. (2018); Jiménez-Esteban et al. (2018)), closing in on the limit were also identified after the Gaia Data Release (DR2) (Prusti et al. (2016)).

Recent studies resulting in mass distributions of select sets of white dwarfs (Liebert et al. (2005); Kleinman et al. (2013)) all seem to agree on a main peak of stars centered at around $\approx 0.6 M_\odot$, with existence of a secondary peak at higher mass values of around $\approx 0.8 M_\odot$ (Kepler et al. (2014)), and further analyzing isolated massive white dwarfs above this mass value reveals that a peak at $\approx 1.04 M_\odot$ (Nalezyty, M. & Madej, J. (2004)) is present. There seems to be indeed a significant number of massive white dwarfs with masses $> 0.8 M_\odot$, presenting fractions of around $\approx 8\%$ of all catalogued white dwarfs, either it be DA or DB (Kepler et al. (2007)).

It is clear to see that massive white dwarfs represent a considerable fraction of the total population of these kind of stars. Not only this, but several particularities characteristic of these massive objects make them interesting subjects of study. For instance, massive white dwarfs represent the only type of these objects where Debye cooling is present at observable luminosities, since crystallization of the core occurs at also high luminosities due to their higher densities (D'Antona & Mazzitelli (1990a); Althaus et al. (2010)), hence making it so that these objects cool faster than their less massive counterparts as the luminosities decrease. Another feature of these objects is the fact that the temperature of their progenitors is presumably high enough to achieve stable carbon burning, making it so that O/Ne cores are possible (Garcia-Berro et al. (1997)), which is a relevant point to consider when studying the cooling of these massive stars, since the diffusion of this ^{22}Ne in the core may be responsible for the release of a non-negligible amount of gravitational potential energy that may impact the cooling time of these objects (Deloye & Bildsten (2002)).

On the context of the cooling of these objects and on the topic of this article, it is important to mention the effect of neutrinos, which indeed influence the cooling times of white dwarfs, usually through the plasma-neutrino process (Haft et al. (1994)), but in the case of these massive stars, neutrino bremsstrahlung must also be taken into consideration (Itoh et al. (1996); Althaus et al. (2010)).This attribute, along with several other important factors, make massive white dwarfs great subjects of study in what concerns the influence of neutrino emission along their evolution. In particular, mass-radius relations for massive white dwarfs seem to show a notable dependence on the neutrino luminosity (Althaus et al. (2005)), and even beyond that, these stars seem to be the ones which exhibit a the most sensible temperature decay response to the neutrino luminosity in all the mass range of these kind of stars (Kantor & Gusakov (2007)).

4 WHITE DWARF ASTEROSEISMOLOGY

As mentioned prior, GW Vir stars present multiperiodic, low-amplitude g-mode pulsations, and hence, we will be focusing on the study of g-mode spectra of modelled pre-white dwarfs. These modes can be theoretically computed by solving the fourth-order set of equations concerning linear, nonradial and adiabatic pulsations given in (Unno et al. (1979)). It is easier to infer certain properties from these solutions making use of approximations such as the consideration of high radial order modes and also the Cowling ap-

proximation (Cowling (1941)), which make it so that these modes respect the following dispersion relation:

$$k_r^2 = \frac{1}{\sigma^2 c_s^2}\left(\sigma^2 - L_l^2\right)\left(\sigma^2 - N^2\right) \tag{1}$$

This relation contains two relevant quantities in what concerns the analysis of the pulsation modes of the star, the first being the Brunt-Väisälä frequency:

$$N^2 = g\left(\frac{1}{\Gamma_1}\frac{d}{dr}ln(p) - \frac{d}{dr}ln(\rho)\right) \tag{2}$$

Which governs the g-mode period spectrum (low frequency modes), as can be seen by the direct dependence on the local gravity acceleration g.

The second quantity is the Lamb frequency:

$$L_l^2 = l(l+1)\frac{c_s^2}{r^2} \tag{3}$$

Which defines the critical frequencies for p-modes (high frequency modes). These modes can be physically interpreted as radial displacements of the stellar fluid.

The relation defined by equation 1 allows for the mapping of the interior of the star in what concerns the propagation of modes, which is easily understandable when noting that pulsations only exist when the wavenumber is real. Considering the frequency σ of a certain mode, this can be achieved if $\sigma^2 > N^2, L_l^2$ which defines the resonant cavity where p-modes propagate, known as the p-region, or if $\sigma^2 < N^2, L_l^2$ which in turn defines the g-region.

When dealing with a g-mode spectrum, it is usual to study the evolution of the period of the pulsation modes, since these correspond to lower frequency modes which present periods whose timescales may correspond to values that are sensible enough so that they are prone to being measured. One of the main characteristics of the period spectrum of chemically homogeneous stellar structures is that in the asymptotic limit ($k >> l$), every consecutive radial order modes (k) with the same harmonic degree (l) have the same period spacing $\Delta\Pi_l^a$ (Tassoul (1980)):

$$\Delta\Pi_l^a = \Pi_{k+1l} - \Pi_{kl} = \frac{2\pi^2}{\sqrt{l(l+1)}}\left[\int_0^{R*}\frac{N(r)}{r}dr\right]^{-1} = constant \tag{4}$$

This is particularly interesting when considering the fact that typical models for GW Vir stars (and white dwarfs in general) present steep composition gradients which result in deviations from the behaviour established by equation 4. From a pictorial point of view, chemical interfaces work as reflecting boundaries inside of the star, making it so that if the length between boundaries matches the wavelength of a certain mode, it is possible to trap this mode as a standing wave, forcing it to oscillate with higher amplitudes in this trapping region. Trapped modes have their nodes confined to a smaller region, effectively making their periods seem shorter, and disabling the validity of a constant period separation value. The manifestation of mode trapping is then extremely dependent on the depth of the chemical transition regions inside of the star, as can be seen by the following analytical approximation, taken from (Kawaler & Bradley (1994)), which expresses the periods of trapped modes:

$$\Pi_i^2 = 4\pi^2\lambda_i^2\left[\left(1 - \frac{r_c}{R}\right)l(l+1)\frac{GM}{R^3}\right]^{-1} \tag{5}$$

This expression refers to the trapped mode that contains i nodes between the surface and the chemical transition radius r_c, with λ_i being constants related with the roots of Bessel functions.

An important flag in what concerns mode trapping is the behavior of the oscillation kinetic energy of modes, which can be written as the following (Córsico & Althaus (2006)):

$$E_k = \frac{1}{2}GM^*R^{*^2}\omega_k^2\int_0^1 x^2\rho\left[x^2y_1^2 + x^2\frac{l(l+1)}{(C_1\omega_k^2)^2}y_2^2\right]dx \tag{6}$$

In this expression, y_1, y_2, y_3 and y_4 are the dimensionless Dziembowski variables (Dziembowski (1971)), which are essentially eigenvalues, defined in order to solve the previously mentioned fourth-order set of equations that determine the pulsations. A^*, V_g and U are also dimensionless coefficients defined in order to further simplify the pulsation equations.

It's clear to see that, aside from the factors, this kinetic energy is proportional to the integral of some of the squared eigenfunctions defined as the Dziembowski variables, weighted by the density along the star. This then leads to the inference that modes propagating in deeper regions of the star, where the density is high, will have larger kinetic energy values, even when they are induced by small perturbations, while in turn, modes that are trapped in the outer layers of the star due to the steep He transition in the envelope will necessarily have small kinetic energy values. This makes it so that, similarly to the period spacing diagram, plots of the kinetic energy as a function o Π_k function as good indicators of trapped modes, since local minima of this function seems to indicate that a mode has less kinetic energy than it otherwise would have, were it not trapped,

Another interesting object that's worth looking into and may complement this period spectrum analysis is the weight function W_k of a mode with radial order k. Each mode runs through the star, presenting different amplitude values depending on the stellar structure and on how effective is the excitation mechanism. The relative values of weight functions serve as indicators on how the eigenvalues are settled along the star (Kawaler et al. (1985)), and they may provide information regarding which regions of the stellar interior most contribute to the determination of the modes' periods. We follow the expression defined in (Córsico & Althaus (2006)), given by:

$$W_k = (4\pi GR_*^2)\frac{r^2\rho^2}{R_*^2U^2}*\left[A^*y_1^2 + V_g(y_2 - y_3)^2 - \frac{1}{U}(l(l+1)y3 + y4)^2\right] \tag{7}$$

This expression, just like the kinetic energy, is also written as a function of the same dimensionless variables that were mentioned above.

5 EVOLUTIONARY INPUT PHYSICS AND PRE-WHITE DWARF TRACK

In order to study the signature of neutrino emission in massive white dwarfs, an appropriate model was used to replicate the evolution of said stars. This was done using the MESA code (Paxton et al. (2010)), version r10398, with evolutionary input closely following the description present in (Lauffer et al. (2018)), which details the evolution of both H and He atmosphere massive white dwarfs, starting from the ZAMS and reaching up to the oldest stages of cooling, where luminosity values are as low as $L/L_\odot \approx 4$.

Our models consist on different evolutionary tracks, concerning

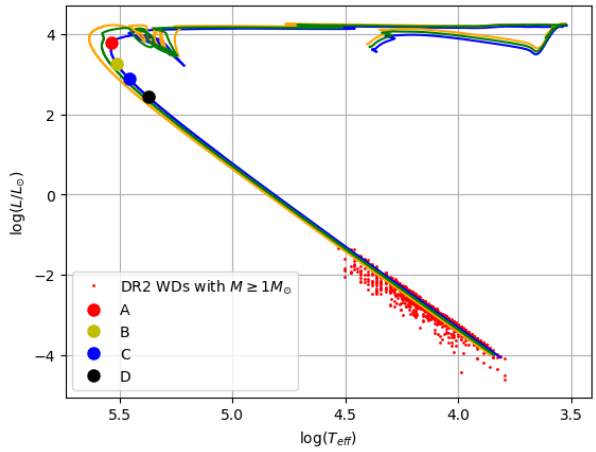

Figure 1. HR diagram containing the curves relative to the evolution of $9M_\odot$ (blue), $9.5M_\odot$ (green) and $10M_\odot$ (orange) initial mass stars from the ZAMS up to the white dwarf cooling sequence. Points A, B, C and D are benchmark evolutionary stages from the $9M_\odot$ initial mass star, chosen to study this region of evolution. Additionally, massive white dwarf candidates from GAIA (Jiménez-Esteban et al. (2018)) are shown at the end of the cooling sequences.

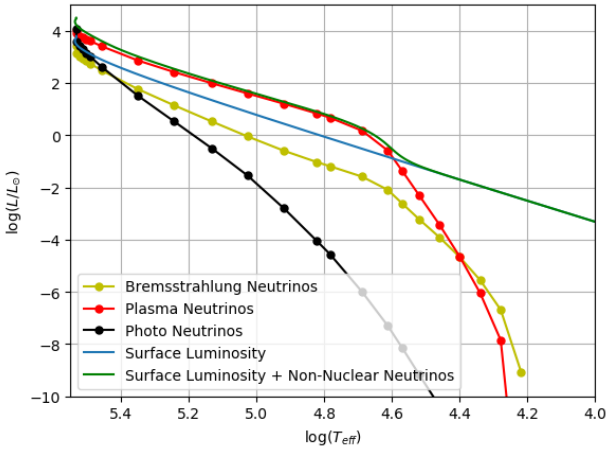

Figure 2. Weight of the several non-nuclear neutrino energy sinks for modelled $9M_\odot$ initial mass star, starting at the white dwarf cooling sequence.

stars beginning at the ZAMS with masses ranging from $9M_\odot$ to $11M_\odot$, resulting in white dwarfs with $1.02M_\odot$ to $1.22M_\odot$, chosen with the intent of covering a wide range in which typical massive white dwarfs are present. Regarding the evolutionary stage in which we will focus our study, this being the initial track of the white dwarf cooling sequence, corresponding to an age range of $\log t[yrs] \approx 7.435 - 7.440$, the main input considerations are, as described in (Lauffer et al. (2018)), the formulation of chemical diffusion and gravitational settling from (Burgers (1969)), the absence of convection due to numerical instabilities, which has no impact on the cooling times relative to when convection is left active, and particularly does not affect the study of stellar pulsations and neutrino emission at this stage of the evolution, since at this stage (GW Vir stage), convection is yet to set in and pulsations are mainly excited by the $\kappa-$mechanism (Saio, H. (2013)). Lastly, the emission rates for plasmon, brehmsstralung and several less important neutrino sources are taken from (Itoh et al. (1996)).

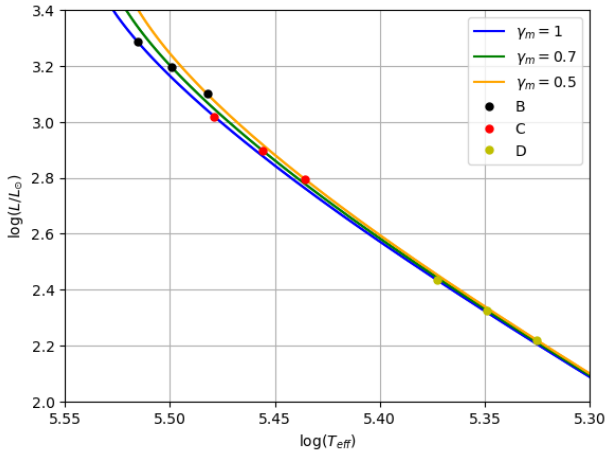

Figure 3. HR diagram containing the curves relative to the evolution of a $9M_\odot$ initial mass star, each with different initial neutrino emission rates, these being the unchanged rate of ϵ_ν (blue), $0.7\epsilon_\nu$ (green) and $0.5\epsilon_\nu$ (orange). Each curve contains their respective benchmark points A, B and C, where each set of points with the same color across all curves correspond to comparison evolutionary points.

Resulting HR diagrams from our models are shown in figure 1, as well as the benchmark profiles chosen for one of the models, to probe the region where neutrinos represent the largest energy loss mechanism. The selection of these profiles is based on the information conveyed in figure 2, which allows to compare the impact of several different energy loss mechanisms with the surface luminosity of the star as a function of T_{eff}.

Regarding the seismology component of this work, the pulsation eigenmodes of our models were obtained making use of the GYRE oscillation code (Townsend & Teitler (2013)), version 5.1, using the MESA models as direct input and using the formulation of (Christensen-Dalsgaard (2008)) in what concerns the boundary condition of the shooting method used in the search. An inverse frequency grid type (uniform in period) is also used in order to more easily scan for adiabatic g-modes.

6 NEUTRINO EMISSION RATES

The main purpose of this work is to study the impact that neutrino cooling has on the overall evolution of pre-white dwarf objects while neutrinos are still the most relevant energy sink. For this reason, and due to the numerical nature of the models, a similar prescription to that of O'Brien & Kawaler (2000) was used, in which the emission rates of non nuclear neutrinos was parameterized before the star enters the white dwarf cooling sequence. This parameterization takes the following form:

$$\epsilon_{\tilde{\nu}_m} = \gamma_m \epsilon_{\tilde{\nu}_0} \tag{8}$$

Where $\epsilon_{\tilde{\nu}_0}$ corresponds to the neutrino emission rate as predicted by standard leptonic theory. This then allows to compare models relative to the same star but with different neutrino emission rates and detect any changes which, as a result, will necessarily be a direct consequence of the neutrino effects on the cooling of the star.

Starting from the benchmark points shown in figure 1, we reproduce the same model, which in this case corresponds to the $9M_\odot$ initial mass model, up to the first of these points, this being profile

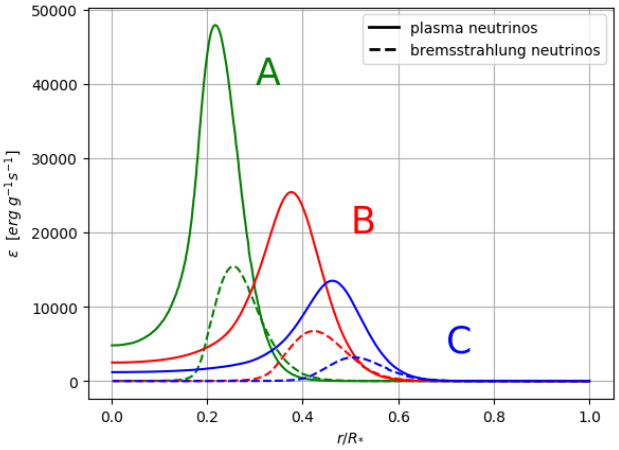

Figure 4. Neutrino emission rates relative to benchmark points A, B and C concerning the modelled $9M_{\odot}$ initial mass star with unchanged neutrino emission rates. Continuous lines refer to plasma neutrino emission rates while dashed lines refer to bremsstrahlung neutrino emission rates.

A, and at this point, we set the neutrino emission rate factor γ_m, making it so that the evolutionary track is slightly changed from this point on. Figure 3 shows how the evolutionary track is altered by considering situations where at point A, the neutrino emission rates are set to 50% and 70% of the original rate, these being represented in orange and green respectively, relative to the model with unaltered rates, represented in blue. As for the comparison points, which are also represented in the figure, where each set of points with the same color represent comparison points, these were selected such that the current neutrino rate of the unaltered model multiplied by the factor of the altered model, is equal to the current neutrino rate of the altered model, i.e., the neutrino emission rates of point B relative to the orange curve is, at that point, half of the neutrino emission rate of point B relative to the blue curve.

Furthermore, figure 4 shows how the main unaltered sources of neutrino emission change as the star evolves, both in terms of position in the star and intensity. As mentioned prior, plasma neutrinos are the dominant energy source during this pre-WD phase, and along with the energy due to bremsstrahlung neutrinos, which are also relevant when considering such high mass values, both make up for almost the totality of energy lost during this phase. From this figure, we notice how the production of these neutrinos moves outwards along the star as they decrease with time, and for this reason we don't extend the analysis to much later times relative to profile C, because it's clear to see that the neutrino emission rate dies off if we move ahead in time.

7 MODE PROPAGATION ANALYSIS

We now proceed with the analysis of the impact of altered neutrino rates on the structure and evolution of the model. We begin by discussing some of the properties that are usually relevant in typical spectra of massive (and overall) white dwarf pulsation. To this end, we can start by analyzing the evolution of propagation diagrams along the region in study.

The first row of Figure 5 shows exactly how this takes place, containing, from left to right, the corresponding diagrams relative to the profiles A, B and C present in Figure 1, concerning a $9M_{\odot}$ initial mass star and evolving into a $1.02M_{\odot}$ white dwarf. In this figure, both the propagation diagrams and the chemical profiles contain information regarding the star as it would normally evolve, and the case where neutrino emission rates were set to half (orange curve in figure 3), with this being represented with dashed lines. The situation corresponding to the rate reducing factor of 0.7 is not represented in these diagrams in order to keep the figure visually clear, but the shape of the lines concerning this case is evident, as this represents a midway point between the two cases that are shown.

Profile A, which is the common point between the cases, depicts the star right before T_{eff} achieves its maximum value, being at $T_{eff} = 341491K$ and with $\log(L/L_{\odot}) = 3.79$, and for this reason, it presents some similarities with typical red giants diagrams, which correspond to a previous stage of evolution in the lifetime of this star. In this regard, it can be seen that the central values of N^2 are comparable to the outer values, and some dips in this frequency structure allow for the presence of some mixed modes. This trait vanishes as the star keeps evolving through this neutrino phase, with N^2 increasing in value in the outer regions of the star, making it so that there is a wider gap between the G- and P-regions and no mixed modes seem to be possible. The propagation diagrams relative to profiles B and C clearly illustrate this point, with the correspondent chemical profiles revealing that this is accompanied with a settling of several layers in the star, with the outer carbon layer being the most evident. It is then interesting to compare the situation between the case where neutrinos are unaltered and the case where their rate is set to half. As seen in the figure, there's a clear agreement between the abundance curves at the inner regions of the star, but the outer layers seem to have a small departure from one another as the evolution goes on, as can be seen by the helium and carbon curves, indicating that the effects of gravitational settling are stronger when neutrino emission is halved, which is in agreement with the fact that the model with halved neutrino takes approximately double the time to reach point B when compared with the model where rates are unchanged.

As mentioned prior, GW Vir stars are known to pulsate with low amplitude g-modes, and for that reason, the focus of the seismologic analysis in this work is done according to the eigenmodes present in the G-region of the evolving propagation diagram of the star. We instill particular attention to the blue dashed line present in the propagation diagrams of B and C, which corresponds to the frequency of the mode g_{60} (radial order $n = 60$ and angular degree $l = 1$), which we choose as a reference mode due to the fact that it is one of the lowest radial order g-modes that is allowed to propagate up to the surface during most of the time range on which our study is focused on, and theoretically, would be one of the easiest to detect.

8 SENSITIVITY OF EIGENMODES TO NEUTRINO EMISSION

To further the study of this mode, we make use of the expression given in equation 7 to obtain the correspondent weight function, which is depicted in figure 6 at several stages of evolution of the star. Additionally, the first row in this figure represents the case where the neutrino emission rates are unchanged, with the letters A, B and C referring to the profiles to which these weight function applies. The second row refers to the case where the emission rate was set to half, and each lower panel corresponds to a profile of the altered star where the neutrino luminosity is half of the luminosity of the profile in the correspondent upper panel. The lines present in each panel correspond to the plasma (orange) and bremsstrahlung (green) neutrino emission rates associated to that profile, with all cases being normalized to the maximum value of the first panel of the correspondent row.

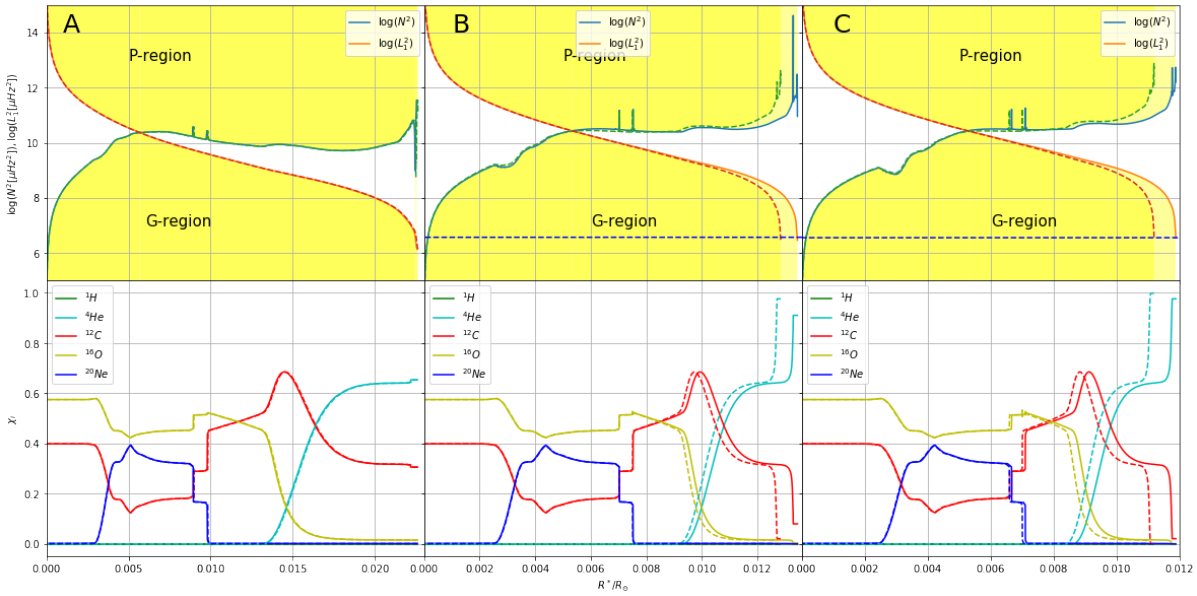

Figure 5. Propagation diagrams (first row) and chemical profiles (second row) of $9M_{\odot}$ initial mass star models. Continuous lines refer to the model where neutrino emission rates are unchanged and dashed lines refer to the case where neutrino emission rates are halved. A, B and C labels are representative of the benchmark points chosen for each model

One interesting characteristic of the weight function, regardless of the row that is being considered, is that its maximum value seems move from close to the core up to the surface as time goes by, which seems to be the case when considering lower mass white dwarfs, as seen in other works (Kawaler et al. (1985); Córsico & Althaus (2006)), meaning that the zone most contributing to the generation of this mode transitions outwards as the star cools. It is worth mentioning that all modes with $k > 10$ present a very similar behavior to this one, the only difference being the number of nodes, which evidently correspond to k itself, which means that the aforementioned statement regarding the region where the mode is most prevalent, as well as further analysis concerning this g_{60} mode also applies these lower order modes. This particular outward shifting effect that we just assessed is a consequence of a decrease in central condensation in the star, as described in (Schwank (1976)).

Perhaps the most interesting feature of this figure, which coincidentally also refers to an outward displacement, granted that this time we're referring to the well defined peak seen in each panel and not the overall maximum value, is how the normalized neutrino curve seems to resemble this prevalent peak in the weight function, both in shape and position, as they move outwards and decrease along this cooling period. Both these peaks seem to follow the small region just outside the C/O core where there's a drop in oxygen and carbon, and an increase in neon, which corresponds to the region where off-center carbon ignition occurred (Siess, L. (2006)), and hence represents the hottest region of the star during this neutrino dominated period. This attribute more or less explains why the neutrino emission rates are prevalent in this area, since it is the region that most easily excites the pair production from plasmons, but no evident connection between this neutrino production area and the peak in the weight function can be deducted.

In order to more or less quantify this apparent relation between these two quantities, we define a neutrino sensitivity function S_{ν_k}:

$$S_{\nu_k} = \frac{\int_0^r 4\pi r'^2 \rho(r')\epsilon_\nu(r')W_k(r')dr'}{L_\nu} \tag{9}$$

This function is taken at a certain temporal point of the evolution, with ϵ_ν being the rate of non-nuclear neutrinos along the star at this temporal point, W_k being the normalized weight function of the g_k mode also at this point, and $L_\nu = \int_0^{R*} 4\pi r^2 \rho(r)\epsilon_\nu(r)dr$ being the non-nuclear neutrino luminosity, which essentially corresponds to the integral in the numerator of equation 9 without the weight function, meaning that this sensitivity function will only present values between 0 and 1. This function is designed with the intent of verifying how sensible the g-modes are in what pertains to the decaying neutrino rates as the evolution proceeds, and hence why the numerator of this expression is chosen as a "weighted" version of the neutrino luminosity function, directly relating these two quantities across the entire stellar structure. Looking at the shape of both functions in each panel of figure 6, it is expected that this sensitivity assumes a similar behavior to that of a step function, with a very steep increase characterized by an inflexion point right where both peaks assume their maximum value, making it so that, as time progresses, this inflexion point moves outwards and the upper threshold decreases, assuming that the peak of the weight function ceases to be the overall highest value of this function as it happens in the first row of the figure.

It is of interest to analyze how the sensitivity function of different modes behave as the star evolves, and specially how it compares between the cases with different neutrino emission rates. Figure 7 contains several points concerning the maximum value (upper threshold) of the sensitivity function of different radial order g-modes at several stages of the neutrino cooling process as a function of the surface luminosity. Points connected by a continuous line represent modes concerning the model where neutrino rates are unaltered, while points connected by dashed lines represent modes concerning the model where rates were halved.

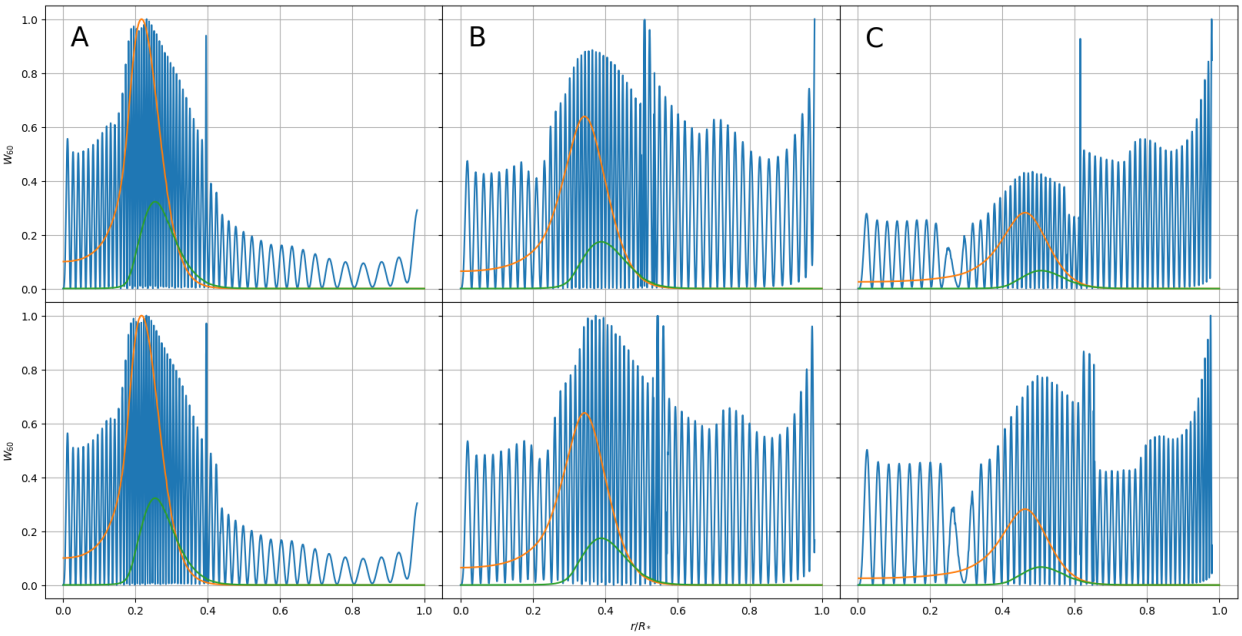

Figure 6. Weight functions of g_{60} mode at different evolutionary points of modelled $9M_\odot$ initial mass star with unchanged neutrino emission rates (first row) and halved neutrino emission rates (second row), as well as plasma (orange) and bremsstrahlung (green) neutrino emission rates normalized to highest value of correspondent row. Just as in figure 5, A, B and C labels are representative of the benchmark points chosen for the model with unchanged rates, while the correspondent comparison points for the model with halved rates are chosen such that at each column, the neutrino emission rate of the model of the lower panel is half of the rate correspondent to model with unchanged rates in the upper panel.

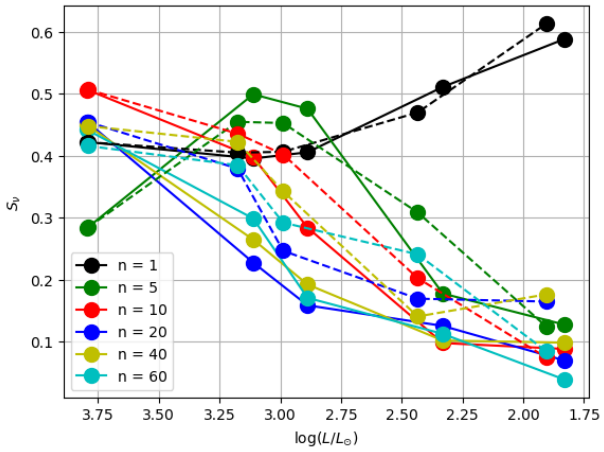

Figure 7. Evolution of the sensitivity function given in equation 9 for different radial order g-modes for modelled $9M_\odot$ initial mass star. Continuous lines refer to the model where neutrino emission rates are unchanged and dashed lines refer to the case where neutrino emission rates are halved.

It is clear to see that in most cases, regardless of the fact that the rates of neutrino emission were changed or not, there is a common behavior in which the sensitivity seems to decrease with time, which agrees with the fact that the peak of the weight function decreases with time relative to the absolute maximum of this function. This behavior however seems to only be established when we consider modes with $k \geq 10$, since modes such as g_1 and g_5 seem to respond in a different manner, presenting increasing sensibilities at certain stages. This seems to agree with the previously mentioned fact that modes with lower radial orders, specifically $k < 10$, have weight functions with a considerably different shape than the others, partly due to having a lesser amount of nodes, but mostly due to how their envelopes are more evenly distributed along the star, not showing many evident peaks as is the case with the envelopes of weight functions of higher radial order modes. Nonetheless, the existence of fewer nodes in the weight functions of these lower radial order modes makes it so that, if any of the peaks of this function fully encapsulates the peak of the neutrino emission rate, then the integral present in S_{ν_k} will increase relative to the case where a similar valued oscillatory weight function takes the same position. This trait explains the increases that might be present in the evolution of the sensitivity function of lower radial order modes.

Another interesting subject regarding this figure is how the functions concerning the altered and non-altered neutrino emission rates compare to each other. This, once again, seems to have a certain dependence on the radial order of the modes that are being considered, and while the number of points available should be increased in order to study this feature in more detail, it is more or less apparent that higher radial order modes seem to be the ones that are more sensible to changes in the rates of neutrino emission. Indeed when comparing the values of this function relative to a single mode in the case where neutrino rates are unchanged to the values of the function relative to this same mode but with the rates halved, it is indisputable that they do not match for any mode, even taking into account the small sampling size that is being used. However, it is also clear that this mismatch is much more evident as the radial order of the mode that is being considered increases, with a noticeable gap between the continuous and the dashed line forming at around $k = 10$ and seemingly increasing as we consider higher k values. This gap forms as a consequence of the fact that the sensitivity values are higher along the evolution of the star when the rates halved, which is something that can be understood by looking at figure 6 and noticing the differences between the weight functions present in the upper and lower panels

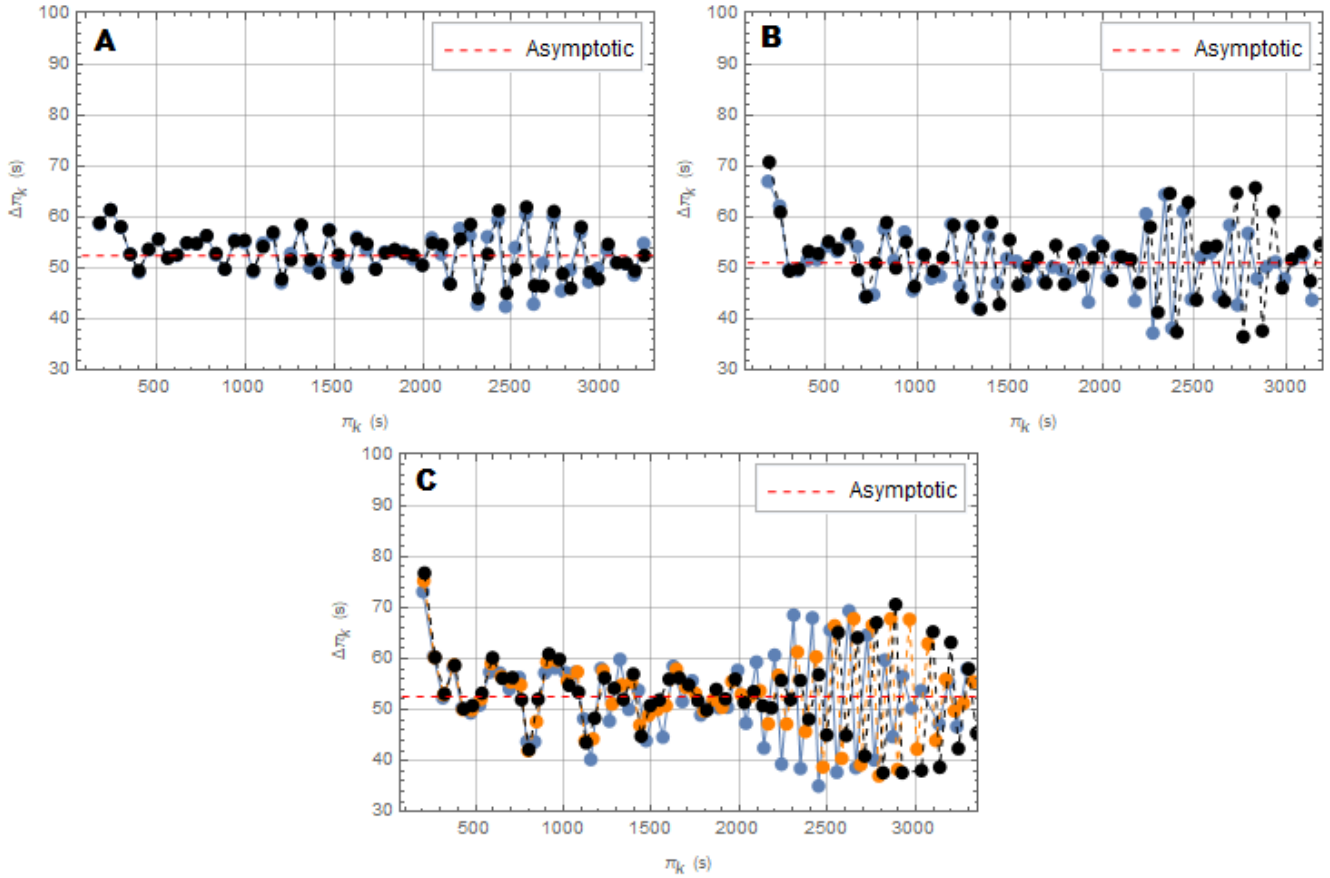

Figure 8. Evolution of the period separation $\Delta\Pi_l^a$ of the g-mode spectrum for modelled $9M_\odot$ initial mass star. Once again, continuous blue lines refer to the model where neutrino emission rates are unchanged, black dashed lines refer to the case where neutrino emission rates are halved, orange dashed lines refer to the case where neutrino emission rates were set to 70% and the A, B and C labels are representative of the benchmark points chosen for the models. The red, horizontal dashed line in each panel corresponds to the value of the period separation in the asymptotic limit given in equation 4 concerning the model with unchanged rates.

of the last two columns. In the case where neutrino production is halved, this being the second row, the maximum values of the peak's envelope that is being considered are considerably higher after normalization than those of the first row. As a consequence of this fact, the area below the smaller width peaks that are encapsulated by the envelope and also encapsulated by the neutrino emission peak, or in other words, the integral of the product of these two functions, is higher, which is easily understandable when noticing that these peaks "close" slower as they grow into their maximum value due to having a higher value to grow into when compared to the case where the rates are unchanged. This effect becomes more and more drastic as we increase the radial order of the mode, which indicates that the amplitudes of the weight functions of these modes are the most affected by changes in the rates of neutrino emission as the star cools.

9 ASTEROSEISMOLOGY DIAGNOSTIC: NEUTRINO INDUCED TRAPPING PHASE SHIFT

The analysis performed making use of the sensitivity function suggests that the rate of neutrino emission at a certain point of evolution of a pre-white dwarf has a direct or indirect influence on the pulsation modes of the star. This inference regarding the sensitivity of pulsation modes was done through a graphical analysis of a function that suggests, but does not imply correlation. It is then instructive to further extend the exploration of the impact of neutrino emission to defining and measurable properties of pulsation modes. To this end, we will study the evolution of the period separation pattern during this phase, which is shown in figure 8, where each panel corresponds to one of the previously mentioned profiles in what concerns the model where neutrino emission rates are unchanged. In this figure, points connected by a continuous (blue) line once again refer to this model, whereas points connected by a dashed (black) line correspond to the model where rates were halved. Additionally, the dashed, horizontal line (red) corresponds to the period spacing asymptotic limit, given by equation 4, concerning the model with unchanged rates, noting that while the asymptotic value relative to the model with halved rates is not represented, it practically matches the previous case.

At first glance, it is evident that neither of the patterns correspond to the behavior established by the asymptotic limit, which is to be expected due to the fact that our models contain several composition gradients that, as mentioned previously, may work as reflecting boundaries for certain modes, which makes it so that various resonant cavities may be identified throughout the star, these being evident by looking at the chemical profiles of figure 5. The direct consequences of these cavities is that modes with wavelengths identical to their sizes might get trapped inside, in return presenting

changes in their periods, which may then be mirrored onto the values of the period separation, since the distance relative to the periods of adjacent modes in radial order (which coincidentally, might also have their own periods altered due to this same effect) is altered as well. This creates a situation where $\Delta\Pi_l^a$ for a certain k mode becomes higher or smaller in value, and deviates from the expected behavior, hence creating the maxima and minima that can be observed in the period separation patterns of our figure. This trapping occurrence is of particular interest in what concerns predicting what modes might be impossible to measure even though they are excited, since they may be enclosed in the resonant cavities inside of the star, this being done with a correct identification of the extrema in the pattern and the respective mode and cavity that is causing them.

That being said, there is an interesting feature that can be identified in this figure once a comparison between the patterns generated by our two models is done, and that is the progressive shift of the rightmost part of the pattern corresponding to the model with halved neutrino emission rates relative to the model with unchanged rates, as both evolve. As can be seen on the first panel, both patterns seem to match entirely, which is expected since profile A correspond to the point of evolution where the rates of the second model were set to half, effectively working as the initial point of the cooling phase in study, but as we look further in time, there seems to be a slight localized displacement of the dashed pattern to the right, relative to the continuous pattern. This displacement begins to be noticeable at stages close to the temporal point where profile B is located, where from figure 4, plasma-neutrino rates are of around $\epsilon_{\nu_p} \approx 25000\ erg \cdot g^{-1} \cdot s^{-1}$, and half of that value in the case of the second model, and it seems to be completely established at the evolutionary point represented by profile C, where the rates are now close to half than the ones in B, and neutrinos start to become less and less relevant moving forward.

It is important to mention that this clear pattern that is being shifted contains several local minima and maxima of the period separation, which suggests that the modes relative to these points are being subject to trapping. This is further enhanced by noting that local minima in $\Delta\Pi_l^a$ correspond to local minima in the oscillation kinetic energy, which can be obtained with the use of equation 6. This can be seen in figure 9, where both these quantities, relative to the model with unchanged rates, are plotted in part of the period domain containing the pattern that is being shifted.

Another interesting trait from this result is that this displacement appears to occur only when considering higher period modes, starting at around $\Pi_k \approx 2000s$, which interestingly correspond to higher radial order modes, with $k \gtrapprox 30$, meaning that the direct or indirect effects of altering the neutrino rates of the star seem to have an impact on these modes while leaving lower order modes unaltered, which agrees with our previous assessment that higher radial order modes are more sensible to changes in the rates of neutrino emission.

This pattern shift seems to be a consequence of various factors in which neutrino emission seems to be a relevant factor, namely the propagation regions for g-modes inside the star, as well as the chemical profiles. Indeed when looking at figure 5, there is a clear displacement of the outer chemical transition interfaces between both models, which also seems to become more evident as time progresses. This feature makes us refer to equation 5, which shows the dependence between the periods of trapped modes and the radius of these transition regions r_c, with these being effectively different when looking at the outer layers of both models, but maintaining the same values when considering the inner regions. This in turn makes it so that the trapping effect occurring at the outer regions of the model with halved neutrino emission rates suffers a shift in what

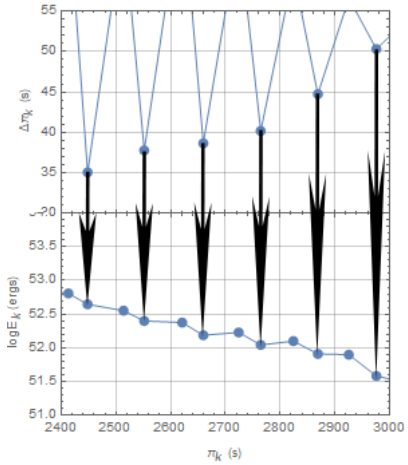

Figure 9. Segment of the evolution of the period separation $\Delta\Pi_l^a$ (upper panel) and oscillation kinetic energy E_{kin} (lower pannel) as a function of the pulsation periods relative to profile C of our modelled $9M_\odot$ initial mass star. Minima in each panel correspondent to the same period are connected by an arrow and represent to modes that are being subject to trapping.

concerns the periods of the modes that are being subject to this effect, relative to the model where neutrino emission rates are unchanged, while the periods of modes that are trapped in the innermost regions of the star are unaltered. We may quantitatively assess this effect by using equation 5 to write an appropriate expression that allows for the comparison of the periods of trapped modes in the case where neutrino emission rates are unchanged, which we label as Π_{100} with the periods relative to the case where rates are halved, labelled as Π_{50}:

$$\left(\frac{\Pi_{50}}{\Pi_{100}}\right) = \sqrt{\frac{\left[\left(1-\frac{r_{c_{100}}}{R^*_{100}}\right)\frac{M^*_{100}}{R^{*3}_{100}}\right]}{\left[\left(1-\frac{r_{c_{50}}}{R^*_{50}}\right)\frac{M^*_{50}}{R^{*3}_{50}}\right]}} \tag{10}$$

This expression eliminates the original dependence on λ_l since it intends to compare the modes that are subject to trapping as a consequence of a chemical interface r_c and contain the same amount of nodes between this interface and the surface, even though the interface is shifted between models.

It is now necessary to define the values of r_c relative to the interfaces that might be the reason for the trapping. As mentioned previously, this effect is a consequence of steep chemical interfaces in the interior of the star, such as the inner transitions from the core to outer layer, or even the steep transition to the He envelope. A useful diagnostic of what chemical interfaces might be relevant in what concerns this effect is the Brunt-Väisälä frequency N^2, since its dependence on dp/dr and $d\rho/dr$ will reveal some spikes in this structure as a consequence of discontinuities in pressure and density, which are typical traits of chemical transition regions. With this in mind, and focusing on profile C, three different transition regions were selected for each model with their r_c being represented by the colored dashed lines in figure 10.

Additionally, table 1 contains the values of all the r_c defined in figure 10, as well as the values given by equation 10 relative to these transition regions. Each of these values corresponds to ratio between the periods of modes trapped in the correspondent transition layer in the model where neutrino emission rates are halved and the

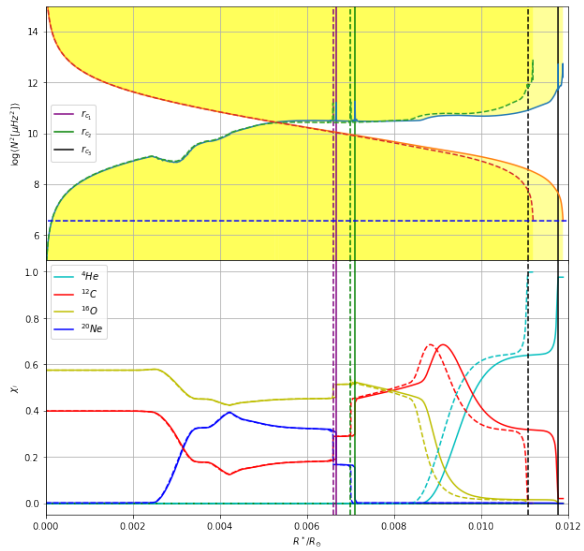

Figure 10. Propagation diagrams (first row) and chemical profiles (second row) relative to profile C of $9M_\odot$ initial mass star models. Continuous lines refer to the model where neutrino emission rates are unchanged and dashed lines refer to the case where neutrino emission rates are halved. A, B and C labels are representative of the benchmark points chosen for each model. The coloured vertical dashed lines correspond to the r_c of the steep chemical interfaces that might be responsible for mode trapping, and are identified according to the label in figure

[H]

Table 1. Values of all the r_c represented as dashed lines in figure 10 and correspondent values of equation 10 for these transition regions.

i	$r_{c_i;50}/R_\odot$	$r_{c_i;100}/R_\odot$	$(\Pi_{50}/\Pi_{100})_{r_{c_i}}$
1	0.0066	0.0067	0.945
2	0.0070	0.0071	0.946
3	0.1112	0.1175	1.194

model where these rates are unchanged. This seems to indicate that the shift of the rightmost pattern must be caused by the outermost transition region due to the He envelope, since the value for this ratio seems to correspond to the same ratio between the periods in which this pattern is present for each model. As for what modes are the ones being affected, the propagation diagrams seem to show that the region of the star in which g-modes propagate grows with increasing radial order, with modes starting at approximately $k \gtrapprox 30$ in radial order reaching this layer, meaning that this predicted shift of trapped modes' periods should only be noticeable for higher radial order modes, which agrees with the results shown in figure 8.

If we indeed shift the periods of the model with unchanged neutrino rates in which this pattern seems to occur (starting at $\Pi_{30} \approx 1700s$) by the equation 10 factor correspondent to this layer, we see that the patterns of both models almost coincide as can be seen in figure 11, which is a strong evidence to support the claims that indeed this trapping is being caused by the outer He layer, and that this trapping effect is dependent on neutrino emission rates of the star, which indirectly alter the periods of the modes that are being subject to this effect.

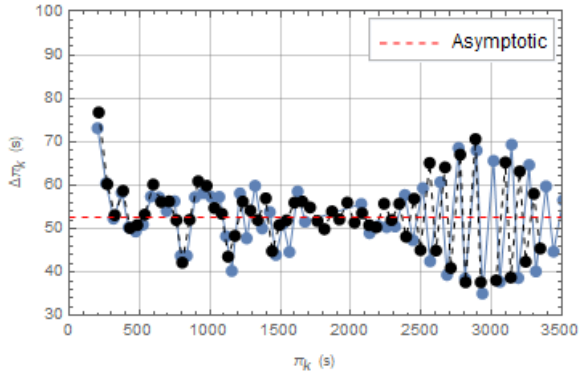

Figure 11. Evolution of the period separation $\Delta\Pi_l^a$ of the g-mode spectrum for modelled $9M_\odot$ initial mass star, with periods of trapping pattern relative to the model with unchanged rates corrected by the appropriate factor given by equation 10 for the He transition region. Continuous blue lines refer to the model where neutrino emission rates are unchanged and black dashed lines refer to the case where neutrino emission rates are halved.

10 CONCLUSIONS

The main intent of the work developed in this article was to verify that indeed the emission of non nuclear neutrinos has a significant impact on the pulsation spectrum of white dwarfs. To this point, not only did we verify the evolution of the star is sensitive to the emission rate of these particles at a structural level, as seen by the displacement of the outer chemical layers when comparing models with different emission rates, but most importantly, the part of the spectrum concerning higher radial order modes, specifically with $k \gtrapprox 30$, also shows a significant response in what concerns altering the emission rates of these particles.

We verified that the behavior of the modes in the interior of our model stars seems to follow a pattern in line with the emission rates, making use of the weight function of individual modes, and further noticed how altering these rates seems to impact the relative values of this weight function inside of the stars, with an evident discrepancy growing as the radial order grows, as quantified by our neutrino sensitivity function.

We further extended our study of the impact of neutrinos to typically measurable quantities of these kind of stars by comparing the period separation and kinetic energy of our distinct neutrino rates models, and verifying the onset of a displacement of the pattern of the period separation relative to higher radial order modes, with $k \gtrapprox 30$, in agreement with the assessment that may be inferred by our previous results that these are the modes most sensible to the emission rates of neutrinos. We verified that this pattern was being caused due to trapping of these modes, and concluded that the pattern shift was a consequence of the displacement of the He envelope transition layer between models with different rates, effectively presenting a method of deducing that this layer is responsible for the trapping of high order radial modes during this evolutionary stage, and most importantly establishing, as a complement of the analysis of the sensitivity function, that changing neutrino emission rates impact the propagation and overall behavior of these same modes.

It is important to mention that with the advent of mission PLATO Rauer et al. (2014), to be launched in 2025, the understanding of the underlying effects of certain phenomena on the measurable quantities of stars is of utmost importance, and hence, with neutrino emission being the controlling process in what concerns the cooling of stars at this stage of evolution, we intend with the work developed in this article to provide novel information that will contribute to the

increase in documentation of these kind of stars, particularly since "PLATO 2.0 will be the very first mission to bring WD seismology in the space era, (...)" Rauer et al. (2014).

REFERENCES

Althaus L. G., García-Berro E., Isern J., Córsico A. H., 2005, Astronomy & Astrophysics, 441, 689–694

Althaus L. G., Córsico A. H., Isern J., García-Berro E., 2010, The Astronomy and Astrophysics Review, 18, 471–566

Barkat Z., 1975, araa, 13, 45

Burgers J. M., 1969, Flow Equations for Composite Gases

Chandrasekhar S., 1935, Monthly Notices of the Royal Astronomical Society, 95, 207

Chandrasekhar S., Milne E. A., 1931, Monthly Notices of the Royal Astronomical Society, 91, 456

Christensen-Dalsgaard J., 2008, Astrophysics and Space Science, 316, 113–120

Cowling T. G., 1941, Monthly Notices of the Royal Astronomical Society, 101, 367

Córsico A. H., Althaus L. G., 2006, Asteroseismic inferences on GW Vir variable stars in the frame of new PG 1159 evolutionary models (arXiv:astro-ph/0603735)

D'Antona F., Mazzitelli I., 1990a, araa, 28, 139

D'Antona F., Mazzitelli I., 1990b, Annual Review of Astronomy and Astrophysics, 28, 139

Deloye C., Bildsten L., 2002, Astrophysical Journal - ASTROPHYS J, 580, 1077

Doherty C. L., Gil-Pons P., Siess L., Lattanzio J. C., Lau H. H. B., 2014, Monthly Notices of the Royal Astronomical Society, 446, 2599

Dziembowski W. A., 1971, Acta Astron., 21, 289

Eisenstein D. J., et al., 2006, The Astrophysical Journal Supplement Series, 167, 40

Garcia-Berro E., Isern J., Hernanz M., 1997, mnras, 289, 973

García–Berro E., Oswalt T. D., 2016, New Astronomy Reviews, 72-74, 1–22

Gentile Fusillo N. P., et al., 2018, Monthly Notices of the Royal Astronomical Society, 482, 4570–4591

Haft M., Raffelt G., Weiss A., 1994, The Astrophysical Journal, 425, 222

Hansen B. M., Liebert J., 2003, Annual Review of Astronomy and Astrophysics, 41, 465

Hansen B. M. S., Richer H., Kalirai J., Goldsbury R., Frewen S., Heyl J., 2015, The Astrophysical Journal, 809, 141

Harris H. C., et al., 2006, The Astronomical Journal, 131, 571

Holberg J. B., Bergeron P., 2006, The Astronomical Journal, 132, 1221

Isern J., Mochkovitch R., Garcia-Berro E., Hernanz M., 1997, The Astrophysical Journal, 485, 308

Itoh N., Hayashi H., Nishikawa A., Kohyama Y., 1996, apjs, 102, 411

Jiménez-Esteban F. M., Torres S., Rebassa-Mansergas A., Skorobogatov G., Solano E., Cantero C., Rodrigo C., 2018, Monthly Notices of the Royal Astronomical Society, 480, 4505

Jr I., MacDonald J., 1985, The Astrophysical Journal, 296, 540

Kantor E. M., Gusakov M. E., 2007, Monthly Notices of the Royal Astronomical Society, 381, 1702–1710

Kawaler S. D., Bradley P. A., 1994, ApJ, 427, 415

Kawaler S. D., Winget D. E., Hansen C. J., 1985, ApJ, 295, 547

Kepler S. O., Kleinman S. J., Nitta A., Koester D., Castanheira B. G., Giovannini O., Costa A. F. M., Althaus L., 2007, Monthly Notices of the Royal Astronomical Society, 375, 1315

Kepler S. O., et al., 2014, Monthly Notices of the Royal Astronomical Society, 446, 4078

Kleinman S. J., et al., 2013, apjs, 204, 5

Lamb D. Q., van Horn H. M., 1975, apj, 200, 306

Lauffer G. R., Romero A. D., Kepler S. O., 2018, Monthly Notices of the Royal Astronomical Society, 480, 1547–1562

Liebert J., Bergeron P., Holberg J. B., 2005, apjs, 156, 47

Maki Z., Nakagawa M., Sakata S., 1962, Progress of Theoretical Physics, 28, 870

Mendez R. A., Ruiz M. T., 2001, The Astrophysical Journal, 547, 252

Mestel L., 1952, Monthly Notices of the Royal Astronomical Society, 112, 583

Munakata H., Kohyama Y., Itoh N., 1985, apj, 296, 197

Nalezyty, M. Madej, J. 2004, A&A, 420, 507

Noh H.-R., Scalo J., 1990, apj, 352, 605

O'Brien M. S., Kawaler S. D., 2000, The Astrophysical Journal, 539, 372

Paxton B., Bildsten L., Dotter A., Herwig F., Lesaffre P., Timmes F., 2010, The Astrophysical Journal Supplement Series, 192, 3

Peskin M. E., Schroeder D. V., 1995, An introduction to quantum field theory. Westview, Boulder, CO, https://cds.cern.ch/record/257493

Prusti T., et al., 2016, Astronomy & Astrophysics, 595

Raffelt G., 1996, Stars as Laboratories for Fundamental Physics: The Astrophysics of Neutrinos, Axions, and Other Weakly Interacting Particles. Theoretical Astrophysics, University of Chicago Press, https://books.google.pt/books?id=6esnbt7BfIwC

Rauer H., et al., 2014, Experimental Astronomy, 38, 249–330

Saio, H. 2013, EPJ Web of Conferences, 43, 05005

Schwank D. C., 1976, Ap&SS, 43, 459

Siess, L. 2006, A&A, 448, 717

Tassoul M., 1980, The Astrophysical Journal Supplement Series, 43, 469

Townsend R. H. D., Teitler S. A., 2013, Monthly Notices of the Royal Astronomical Society, 435, 3406

Unno W., Osaki Y., Ando H., Shibahashi H., 1979, Nonradial oscillations of stars

Wood M. A., 1992, apj, 386, 539

This paper has been typeset from a TEX/LATEX file prepared by the author.